AFAPL-TR-72-10

QUASI AREA RULE FOR HEAT ADDITION IN TRANSONIC AND SUPERSONIC FLIGHT REGIMES

Dr. Allen E. Fuhs

Professor of Aeronautics

Naval Postgraduate School

TECHNICAL REPORT AFAPL-TR-72-10

August 1972

Air Force Aero Propulsion Laboratory
Air Force Systems Command
Wright-Patterson Air Force Base, Ohio

NOTICE

When Government drawings, specifications, or other data are used for any purpose other than in connection with a definitely related Government procurement operation, the United States Government thereby incurs no responsibility nor any obligation whatsoever; and the fact that the government may have formulated, furnished, or in any way supplied the said drawings, specifications, or other data, is not to be regarded by implication or otherwise as in any manner licensing the holder or any other person or corporation, or conveying any rights or permission to manufacture, use, or sell any patented invention that may in any way be related thereto.

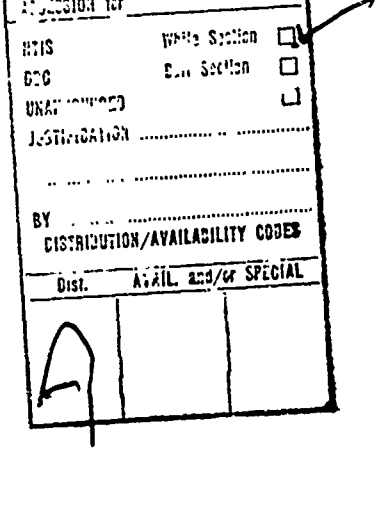

Copies of this report should not be returned unless return is required by security considerations, contractual obligations, or notice on a specific document.

UNCLASSIFIED
Security Classification

DOCUMENT CONTROL DATA - R & D

(Security classification of title, body of abstract and indexing annotation must be entered when the overall report is classified)

1 ORIGINATING ACTIVITY (Corporate author) Naval Postgraduate School Monterey, CA 93940	2a. REPORT SECURITY CLASSIFICATION UNCLASSIFIED 2b. GROUP N/A

3 REPORT TITLE

Quasi Area Rule for Heat Addition in Transonic and Supersonic Flight Regimes

4 DESCRIPTIVE NOTES (Type of report and inclusive dates)

Final, October 1970 to August 1971

5 AUTHOR(S) (First name, middle initial, last name)

Dr. Allen E. Fuhs

6 REPORT DATE August 1972	7a. TOTAL NO. OF PAGES 129	7b. NO. OF REFS 24
8a. CONTRACT OR GRANT NO. MIPR APO-71-007 b. PROJECT NO. 3066 c. Task 306603 d.	9a. ORIGINATOR'S REPORT NUMBER(S) None 9b. OTHER REPORT NO(S) (Any other numbers that may be assigned this report) AFAPL-TR-72-10	

10 DISTRIBUTION STATEMENT

Approved for public release; distribution unlimited.

11. SUPPLEMENTARY NOTES	12. SPONSORING MILITARY ACTIVITY Air Force Aero Propulsion Laboratory Wright-Patterson AFB, Ohio 45433

13. ABSTRACT

Body shapes, including axisymmetric and three dimensional, have been developed to minimize wave drag. The von Karman ogive and the area rule are examples. Similar work has not been accomplished for optimum shapes with propulsion. Propulsion can be divided into two categories--those devices with internal heat addition and those with external burning. For internal heat addition an analytical model is formulated which introduces the propulsive disc. Attention is shifted to external burning, which is examined for one dimensional and two dimensional linearized flow. Heat fronts and combustion fans are discussed as examples. Forces on a heat source in a uniform stream and adjacent to bodies are derived. Several possible applications are examined including base pressure augmentation by external burning, spin recovery using external burning, and transonic boattail drag alleviation. Previous work on base pressure augmentation has used a two dimensional planar model. A two dimensional axisymmetric model is examined.

DD FORM 1 NOV 68 1473 (PAGE 1)

S/N 0101-807-6811

UNCLASSIFIED
Security Classification

A-31408

14 KEY WORDS	LINK A		LINK B		LINK C	
	ROLE	WT	ROLE	WT	ROLE	WT
Area Rule						
Supersonic Aerodynamics						
Transonic Aerodynamics						
External Burning						
Propulsion Optimization						

AFAPL-TR-72-10

QUASI AREA RULE FOR HEAT ADDITION IN TRANSONIC AND SUPERSONIC FLIGHT REGIMES

Dr. Allen E. Fuhs

Professor of Aeronautics

Naval Postgraduate School

FOREWORD

This report describes work accomplished in the program "Quasi Area Rule for Heat Addition in Transonic and Supersonic Flight Regimes" conducted under USAF MIPR APO-71-007. The work was accomplished during the period 1 Oct 1970 through 31 Aug 1971 at the Naval Postgraduate School, Monterey, California, under the direction of Dr. Allen E. Fuhs. The report was submitted on 1 Nov 1971.

The program was sponsored by the Air Force Aero Propulsion Laboratory, Wright-Patterson Air Force Base, Ohio under Project 3066, Turbine Engine Propulsion, Task 306603, Advanced Component Research. Dr. Kervyn D. Mach, AFAPL/TBC, Turbine Engine Components Branch, was the project engineer.

Publication of this report does not constitute Air Force approval of the report's findings or conclusions. It is published only for the exchange and stimulation of ideas.

Ernest C. Simpson

ERNEST C. SIMPSON
Director, Turbine Engine Division

ABSTRACT

Body shapes, including axisymmetric and three dimensional, have been developed to minimize wave drag. The von Karman ogive and the area rule are examples. Similar work has not been accomplished for optimum shapes with propulsion. Propulsion can be divided into two categories--those devices with internal heat addition and those with external burning. For internal heat addition an analytical model is formulated which introduces the propulsive disc. Attention is shifted to external burning, which is examined for one dimensional and two dimensional linearized flow. Heat fronts and combustion fans are discussed as examples. Forces on a heat source in a uniform stream and adjacent to bodies are derived. Several possible applications are examined including base pressure augmentation by external burning, spin recovery using external burning, and transonic boattail drag alleviation. Previous work on base pressure augmentation has used a two dimensional planar model. A two dimensional axisymmetric model is examined.

TABLE OF CONTENTS

LIST OF FIGURES

LIST OF TABLES

LIST OF SYMBOLS

a	Speed of sound, ft/sec.
A	Area, ft^2.
c	Chord, ft.
c_p	Pressure coefficient, dimensionless. Specific heat capacity, BTU/slug ^oR.
C_D	Drag coefficient.
C	Compression wave.
D	Drag, lb_f.
e	Unit vector for cartesian coordinate system. Specific internal energy, BTU/slug ^oR.
E	Expansion wave.
F	Thrust, lb_f; stream thrust, lb_f.
g	Acceleration of gravity, 32.2 ft/sec^2.
h	Specific enthalpy, BTU/slug. Heat release rate, BTU/ft^2 sec.
H	Heat addition rate per unit span, BTU/ft sec.
$\mathcal{H}$	Heat addition rate, BTU/sec.
I	Impulse function.
K	Hypersonic similarity parameter, dimensionless.
ℓ	Length of an ogive, ft.
L	Length, ft; lift, lb_f.
m	Mass source strength, $slug/ft^3$ sec.
$\dot{m}$	Mass flow rate, slugs/sec.
M	Mach number, dimensionless.

n	Index in delta-function representation
NPR	Nozzle pressure ratio, dimensionless.
p	Pressure, lb_f/ft^2.
q	Dynamic pressure, lb_f/ft^2.
Q	Heat source strength, BTU/ft^3 sec.
r	Radius, ft.
R	Specific gas constant, $ft^2/sec^2\ ^oR$.
s	Specific entropy, BTU/slug ^oR. Distance along a characteristic, ft. Distance along a heat front, ft.
S	Base area, ft^2.
SFC	Specific fuel consumption, $(lb/hr)lb_f$.
T	Temperature, ^oR; thrust, lb_f.
u	Velocity, ft/sec.
U	Velocity of freestream, ft/sec.
v	Velocity, ft/sec.
V	Volume, ft^3.
$\dot{w}$	Weight flow rate, lb_f/sec.
α	Angle of perturbation velocity vector relative to freestream.
β	Equals $(M^2 - 1)^{1/2}$; coordinate in cylindrical coordinates.
γ	Ratio of specific heat capacities, dimensionless.
Γ	A function of γ; see equation (5), page 10. Circulation, ft^2/sec.
δ	Delta function.
η	Variable of integration.
θ	Angle of heat front relative to freestream. Angle of a streamline.
μ	Mach angle, arc sin (1/M).
ξ	Variable of integration; source coordinate.
π	Ratio of stagnation pressures, dimensionless
ρ	Density, $slugs/ft^3$.

τ	Ratio of stagnation temperatures, dimensionless.
ϕ	Potential function.
$( )'$	Perturbation quantity.

Subscripts

$( )_a$	Air.
$( )_b$	Burner or combustor.
$( )_B$	Base.
$( )_c$	Compressor.
$( )_d$	Design, downstream of a heat front.
$( )_E$	Exit.
$( )_f$	Fuel.
$( )_h$	Hub.
$( )_\ell$	Lip of inlet.
$( )_L$, $( )_R$ $( )_\ell$, $( )_r$	Left and right running waves.
$( )_n$	Normal component.
$( )_r$	Ram.
$( )_t$	Throat, turbine, tip.
$( )_T$	Stagnation or total conditions.
$( )_u$	Upstream of a heat front.
$( )_{WAVE}$	Values along Mach wave.
$( )_{WAKE}$, $( )_w$	Conditions in wake downstream of heat sources.
$( )_x$, $( )_y$, $( )_z$	Cartesian coordinates.
$( )_0$	Freestream values.

QUASI AREA RULE

FOR HEAT ADDITION IN TRANSONIC

AND SUPERSONIC FLIGHT REGIMES

Dr. Allen E. Fuhs
Professor of Aeronautics
Naval Postgraduate School

INTRODUCTION

In subsonic flow, drag can be attributed to viscous forces on the body surface and to the release of vorticity in the wake. The vorticity is associated with the generation of lift. In supersonic flow, there is a new phenomenon leading to drag; it is the radiation of waves from the body. These waves carry energy whose origin is the work done by drag and vehicle motion.

For almost every case of a body flying through a medium, drag is considered to be a degradation of performance. Consequently, considerable effort has been devoted to optimum shapes giving minimum drag.

One approach for optimizing a body shape is to represent the body by sources and sinks.(1) For a closed axisymmetric body, all sources and sinks are on the axis. It is found that for a nonlifting body, the slope of the cross sectional area curve equals the distribution of sources and sinks, $f(x)$. Distance along the axis is x. By means of the calculus of variations, one can arrive at shapes giving minimum wave drag. There are constraints on the body geometry, and the optimum shape depends on these constraints. Two examples are given in Table I. The shapes given in Table I are for minimum wave drag. Viscous effects are not included, and the bodies are nonlifting.

Table I. Optimum Shapes

Name of Body	Constraints	Wave Drag
Von Karman* Ogive[2]	Given length, ℓ, and base area, S	$\frac{4}{\pi} q \left(\frac{S^2}{\ell^2} \right)$
Sears**Ogive[3]	Given length, ℓ, and volume, V	$\frac{128}{\pi} q \left(\frac{V^2}{\ell^4} \right)$

*Used on Low Altitude Short Range Missile.

**Discovered by W. R. Sears of Cornell University.

It was discovered by Lomax and Heaslet[4] and by Whitcomb[5] that the optimum shape for an axisymmetric body applies to slender bodies with wings and rudders if one interprets the area distribution properly. It is the area cut by the Mach cone. If one uses this area distribution from a three-dimensional body to match the area distribution of an optimum axisymmetric body, then minimum wave drag occurs. This procedure is known as the area rule.

For a body with thrust, there are several new variables introduced. Thrust may be developed by adding heat to a flow internal to the body. Thrust also may be obtained by adding heat external to the body.

Consider external burning. Is there an area rule for a body with external heat addition analogous to the area rule involving body shape only? For this case, there are two functions to optimize. One is body shape, and the other is the distribution of heat addition. Table I gives some typical constraints; an additional constraint for the optimization could be specific fuel consumption.

Instead of finding minimum drag, the procedure should give the best thrust-minus-drag or zero thrust-minus-drag depending on the constraints. Since both the distribution of heat and cross sectional area are involved, an appropriate name is "quasi area rule."

When thrust is developed by adding heat to a flow internal to the body, the quasi area rule suggested in the previous paragraphs does not apply. For internal burning, the waves due to heat addition obviously do not occur as in the case of external burning. There is, however, a change in stagnation pressure and temperature between the inlet and nozzle. Also the velocity vector changes from inlet to exhaust. An energy disc can represent those changes. This report discusses aspects of the thrust-minus-drag problem for an airbreathing engine with confined heat addition. Figure 1 illustrates the various problems that can be studied with internal burning when the emphasis is on thrust-minus-drag. The analysis is linearized. Two-dimensional (2D) planar is the geometry of a propulsive wing. Axisymmetric 2D geometry is an isolated nacelle without fins or wings. Addition of fins or wings yields the 2D propulsion with 3D body. The connection between these two geometries is the area rule.

Figure 2 outlines the problems of interest for external burning. The analysis is linearized. For the 2D planar case, the heat and mass sources can be distributed over a surface or throughout a volume. Volume distributions must meet requirements for slender body theory. Axisymmetric 2D bodies are related to 3D bodies by the quasi area rule.

The linearized 2D planar flow with heat addition has been studied extensively. A solution to the 2D axisymmetric case does not appear in the scientific literature. Solutions for 3D bodies with heat addition have not, as yet, been

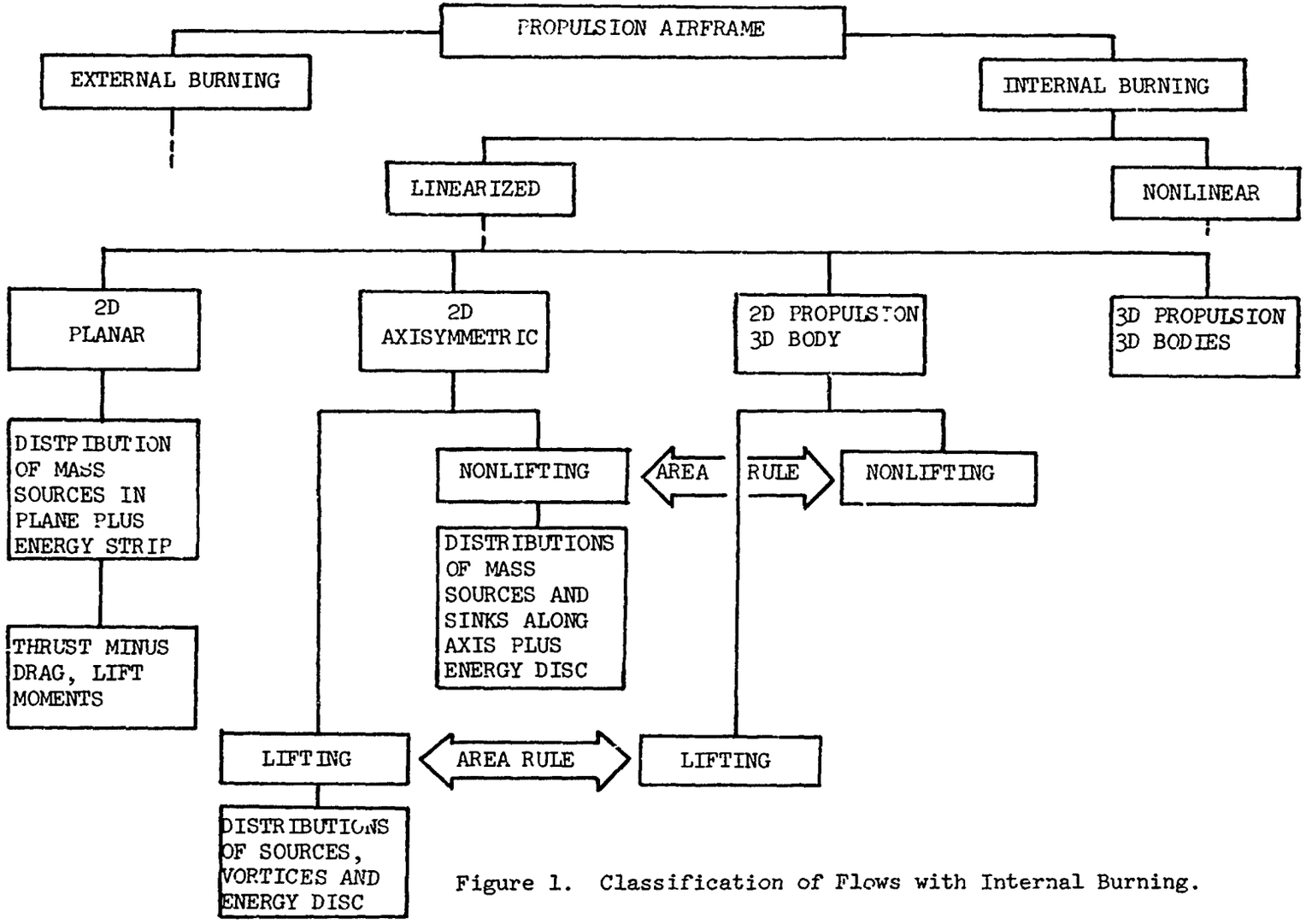

Figure 1. Classification of Flows with Internal Burning.

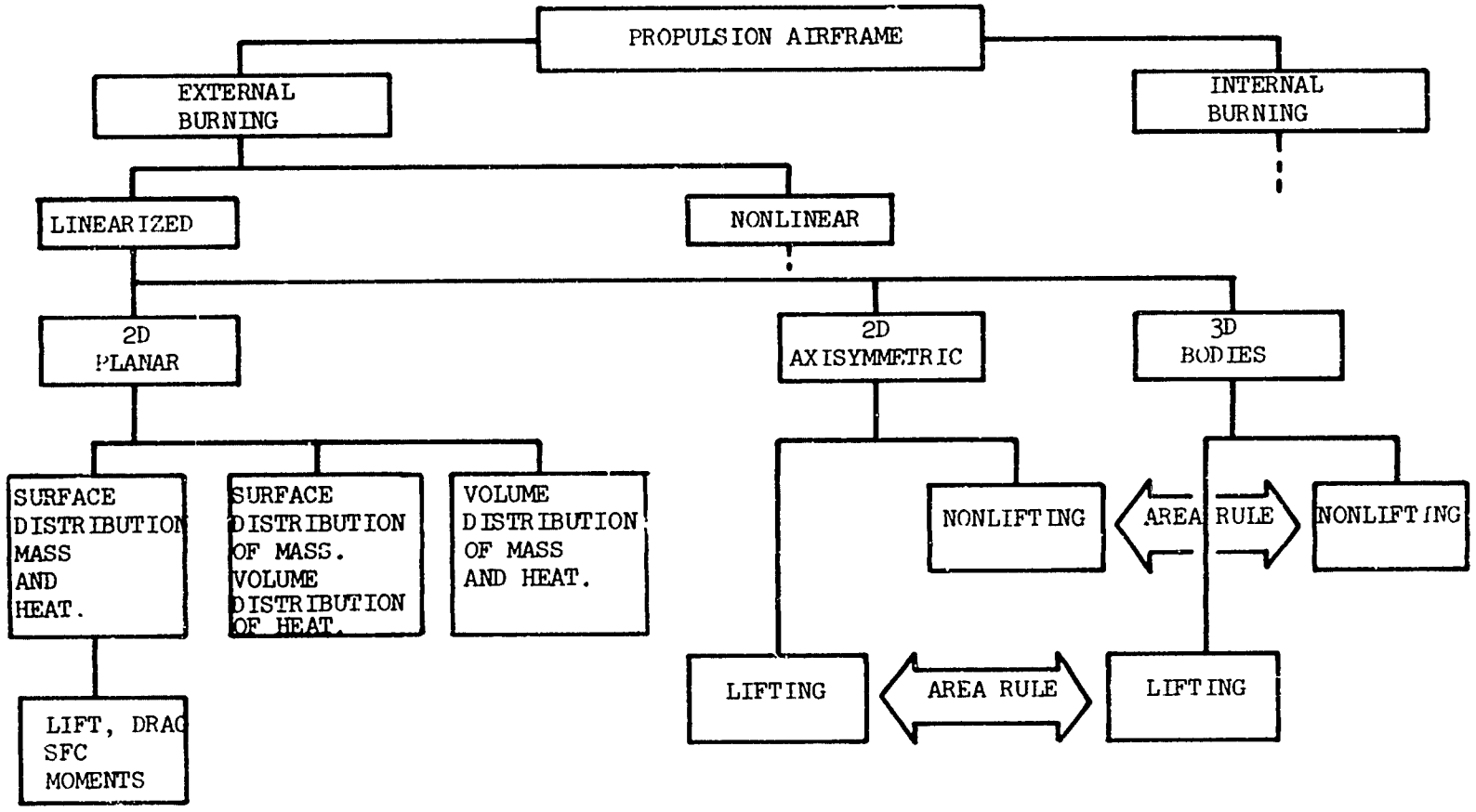

Figure 2. Classification of Flows with External Burning.

obtained. In order to develop the quasi area rule, these solutions are essential building blocks.

PROPULSION WITH INTERNAL HEAT ADDITION

Introduction

For a supersonic aircraft, the variation in nozzle pressure ratio (NPR) is very large. This requires a variable geometry nozzle. Under certain flight conditions, the nozzle setting and nozzle flow result in large base or boattail drag.

One motivation for treating the propulsion-airframe problem as a unit from the area rule point of view is to obtain new design approaches. First, the typical variation in NPR and nozzle geometry will be calculated for a Mach 2.5 aircraft. These results will be discussed to illustrate the problem. Second, the model for representation of a propulsion system with internal heat addition will be developed. Third, approaches to solution of the model will be outlined.

Exhaust Variation with Mach Number

The aim of this section is to calculate nozzle pressure ratio, nozzle area ratio, mass flow ratio, and thrust of an ideal turbojet as a function of Mach number. Knowledge of the trends is essential in understanding aircraft exhaust problems.

Consider an ideal turbojet with an ideal inlet. There is, however, a restriction on the Mach number, M_2, into the compressor. The thrust is given by

$$F = \left(\frac{F}{\dot{m}_a g}\right)\left(\frac{\dot{m}_a g}{\dot{m}_d g}\right)\dot{m}_d g \qquad (1)$$

where $\dot{m}_a$ is a mass flow of air, and $\dot{m}_d$ is mass flow of inlet at design conditions.

For the inlet, the various areas are illustrated in Figure 3(a). Station 0 is at a point in the freestream where p_0 is ambient pressure. Stations 1 and 2 are inlet throat and compressor face respectively. The mass flow ratio is

$$\frac{\dot{m}_a}{\dot{m}_d} = \frac{M_0}{M_{0d}} \frac{A_0}{A_t} \frac{A_t}{A_\ell} \tag{2}$$

where M_0 is flight Mach number, and M_{0d} is design flight Mach number. Areas A_0, A_t, and A_ℓ are identified in Figure 3(a). Both a fixed area and variable geometry inlet are considered. The ratio A_0/A_t is obtained from isentropic flow tables for given M_0 for the variable geometry inlet. For a fixed geometry inlet A_0/A_t comes from flow tables, entering the flow tables with the Mach number downstream of a normal shock at M_0. The mass flow ratios are shown in Figure 4 for both cases. A variable geometry operates supercritically and swallows more air. A variable geometry ramp or spike inlet may have superior mass handling capability at subsonic speeds.

The thrust per pound of air for an ideal turbojet is given by

$$\frac{F}{\dot{w}_a} = \frac{a_0 M_0}{g} \sqrt{\frac{1}{\tau_r - 1}\left[\tau^*\left(1 - \frac{1}{\tau_r \tau_c}\right) - \tau_r(\tau_c - 1)\right]} - 1 \tag{3}$$

where the symbols not previously defined have the following meaning:

a_0 = freestream speed of sound

$\tau_r = T_{T0}/T_0$ = ratio of stagnation to static freestream temperature

$\tau_c = T_{T3}/T_{T2}$ = stagnation temperature ratio across the compressor

The symbol τ^* deserves more discussion. It is

$$\tau^* = \tau_r \tau_c \tau_b = T_{T4}/T_0 \tag{4}$$

where $\tau_b = T_{T4}/T_{T3}$ = stagnation temperature ratio across the burner or combustor. The value of T_{T4} is limited and has a maximum value. Hence for a given engine and altitude, τ^* is fixed when the engine is at maximum power or maximum TIT.

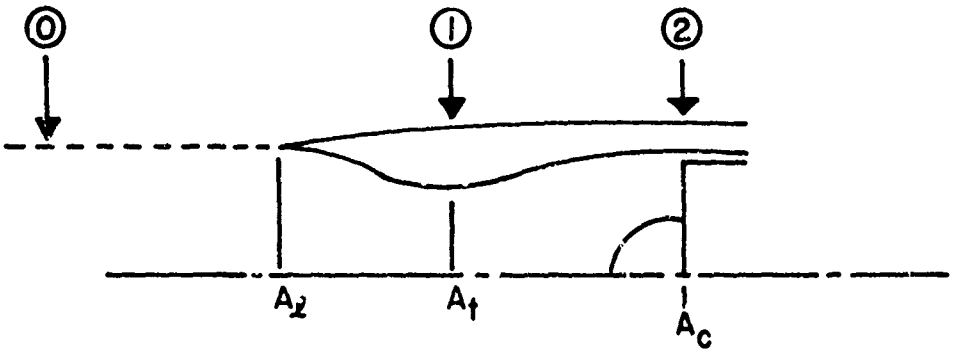

A_ℓ LIP AREA

A_t THROAT AREA

A_c COMPRESSOR FACE INLET

(a) AREAS FOR INLET

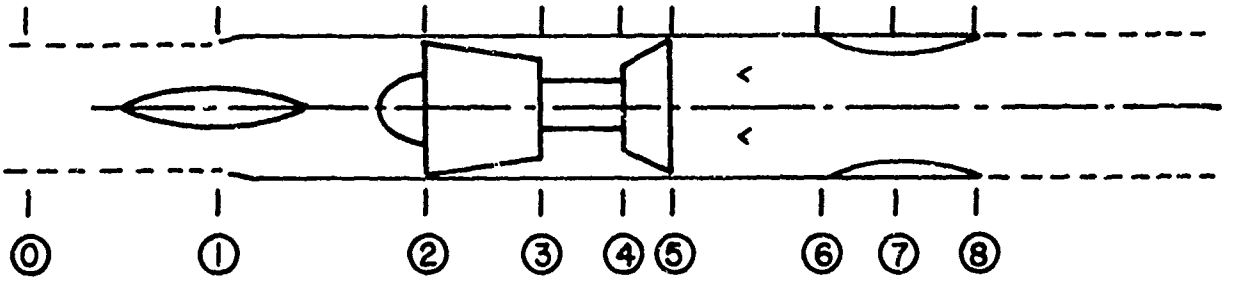

(b) STATION NUMBERING

FIGURE 3. NOTATION FOR TURBOJET CALCULATIONS.

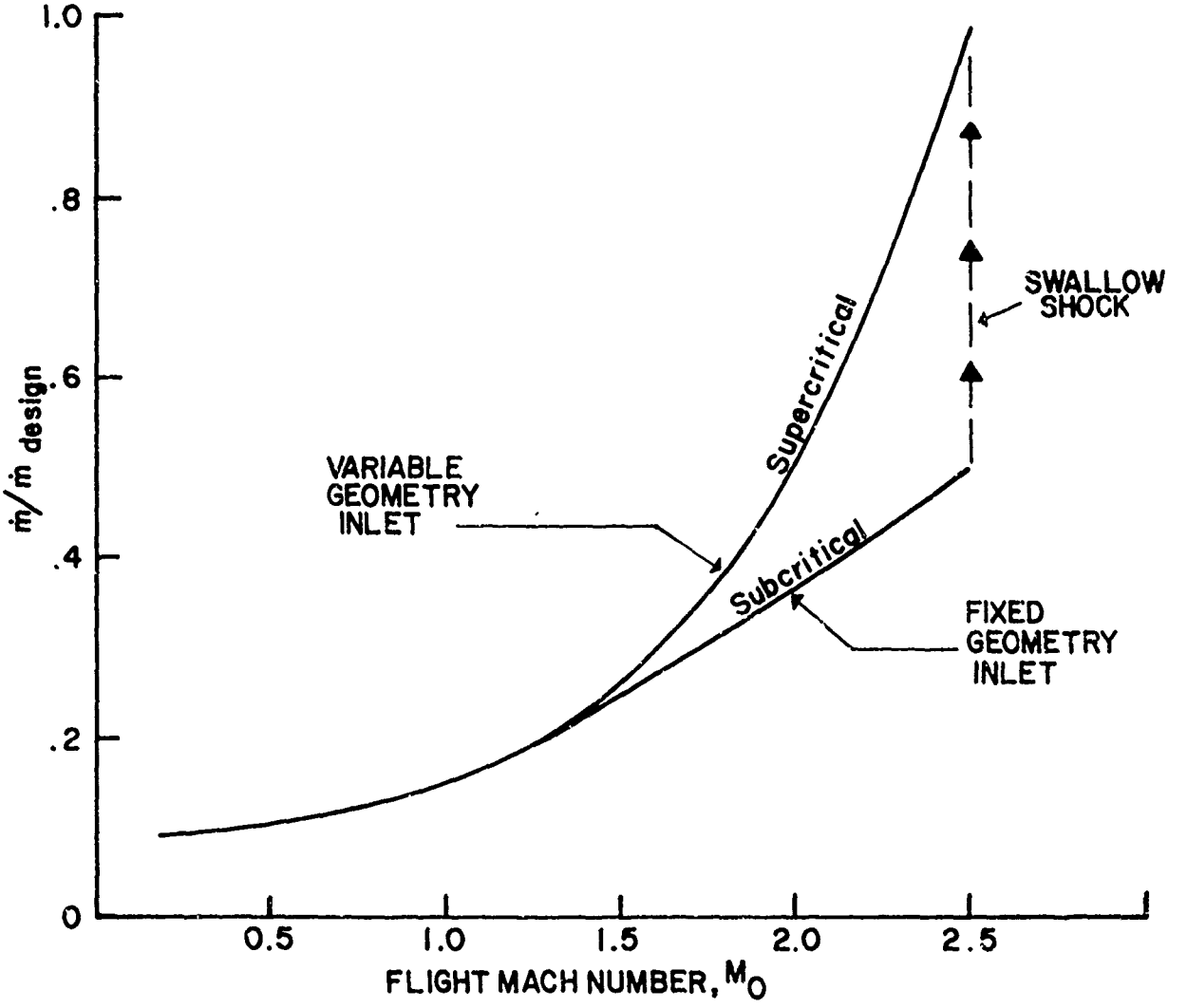

FIGURE 4. MASS FLOW OF AIR AS A FUNCTION OF FLIGHT MACH NUMBER.

The station numbering is shown in Figure 3(b). The throat area for the nozzle is

$$A_7 = \frac{\sqrt{RT_{T8}}\,\dot{m}_a}{\Gamma\ p_{T8}} \tag{5}$$

neglecting fuel addition. R is the gas constant. Γ is a function of the ratio of heat capacities, γ, and has a value of .683 for $\gamma = 1.4$. The nozzle pressure ratio, NPR, is p_{T8}/p_0. A ratio of A_7 to the design value is

$$\frac{A_7}{A_{7d}} = \frac{\dot{m}_a}{\dot{m}_d}\,\frac{NPR_d}{NPR}\sqrt{\frac{T_{T8}}{T_{T8d}}} \tag{6}$$

The area A_8 is obtained from NPR, isentropic flow tables, and the assumption $p_8 = p_0$. Two useful ratios are A_8/A_c and A_7/A_c, i.e., comparing nozzle areas with compressor face area.

Calculations were made for the values shown in Table II.

One of the results of the calculation is NPR which is shown in Figure 5. Some of the other results are summarized in Table III The symbols for the turbine ratios are $\tau_t = T_{T5}/T_{T4}$ and $\pi_t = p_{T5}/p_{T4}$.

Figure 6 illustrates the area variations required for a supersonic turbojet operating at maximum TIT for different M_0. Examination of Figure 6 and the data in Table III shows why turbojet nozzles usually operate underexpanded at design Mach number. The percentage variation in A_7 is 38 per cent based on design A_7. The percentage variation in A_8 is 77 per cent based on design A_8. NPR varies from 4 at low subsonic flight to more than 25 at design M_0 of 2.5.

Table II. Values for Calculation of Turbojet Quantities

Maximum turbine inlet temperature	T_{T4}	2000°F
Altitude		Sea Level
Freestream density	ρ_0	.002378 slugs/ft^3
Freestream speed of sound	a_0	1117 ft/sec
Compressor area	A_c	8.05 ft^2
Tip radius at face	r_t	2 ft
Hub radius at face	r_h	1.2 ft
Maximum Mach number at compressor	M_{2max}	0.65
Inlet throat area at design	A_{td}	7.1 ft^2
Design flight Mach number	M_{0d}	2.5
Compressor pressure ratio at 100 per cent corrected speed	π_c	8

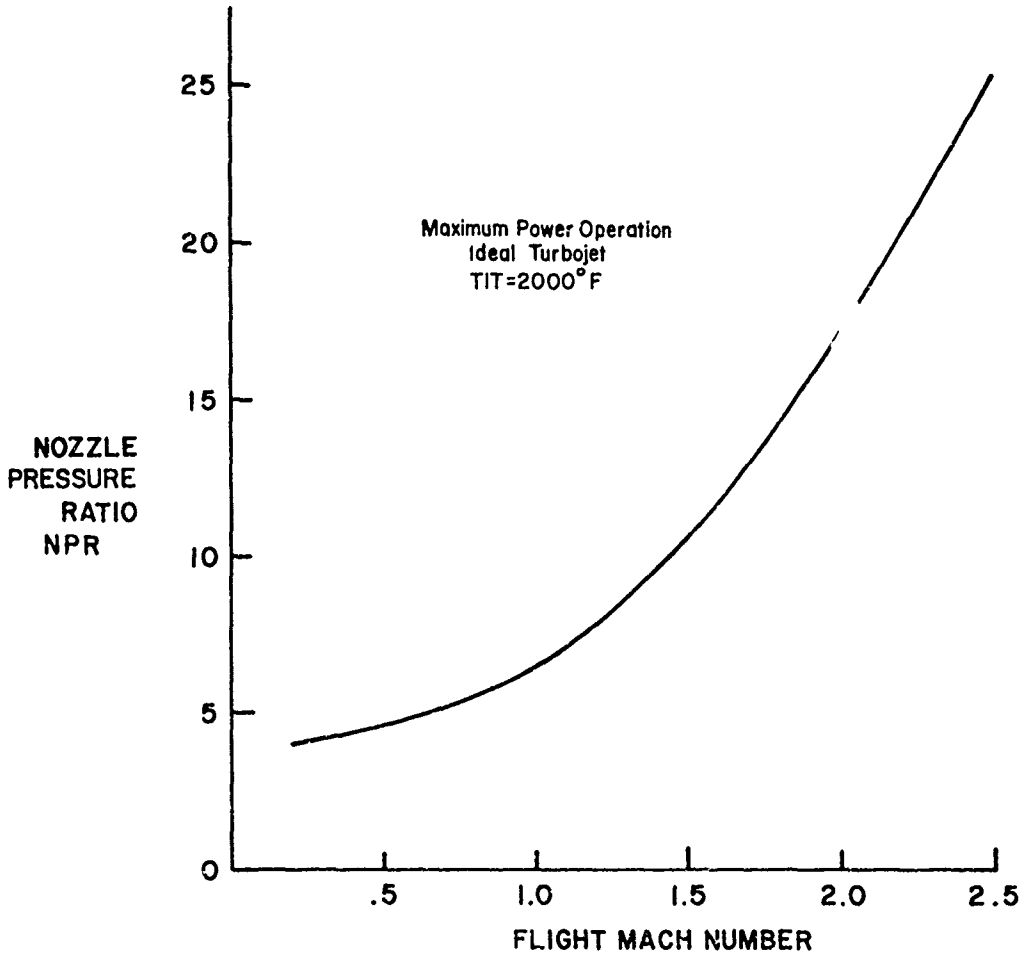

FIGURE 5. NOZZLE PRESSURE RATIO AS A FUNCTION OF MACH NUMBER.

Table III. Results of Calculation for Turbojet Performance and Areas

M_0	$\frac{NPR_d}{NPR}$	$\frac{A_7}{A_{7d}}$	$\frac{A_7}{A_c}$	$\frac{A_8}{A_c}$	τ_t	π_t
0.2	5.98	.625	.421	.526	.829	.518
0.4	5.63	.627	.423	.542	.825	.508
0.6	5.05	.628	.425	.574	.818	.495
0.8	4.42	.637	.427	.620	.808	.475
1.0	3.77	.650	.434	.677	.796	.45
1.2	3.15	.663	.443	.762	.780	.42
1.4	2.58	.702	.448	.860	.765	.391
1.6	2.14	.712	.477	1.02	.742	.352
1.8	1.77	.750	.503	1.20	.719	.315
2.0	1.47	.792	.537	1.42	.694	.278
2.2	1.24	.861	.582	1.72	.665	.240
2.4	1.07	.950	.642	2.07	.634	.203
2.5	1.00	1.00	.685	2.28	.616	.183

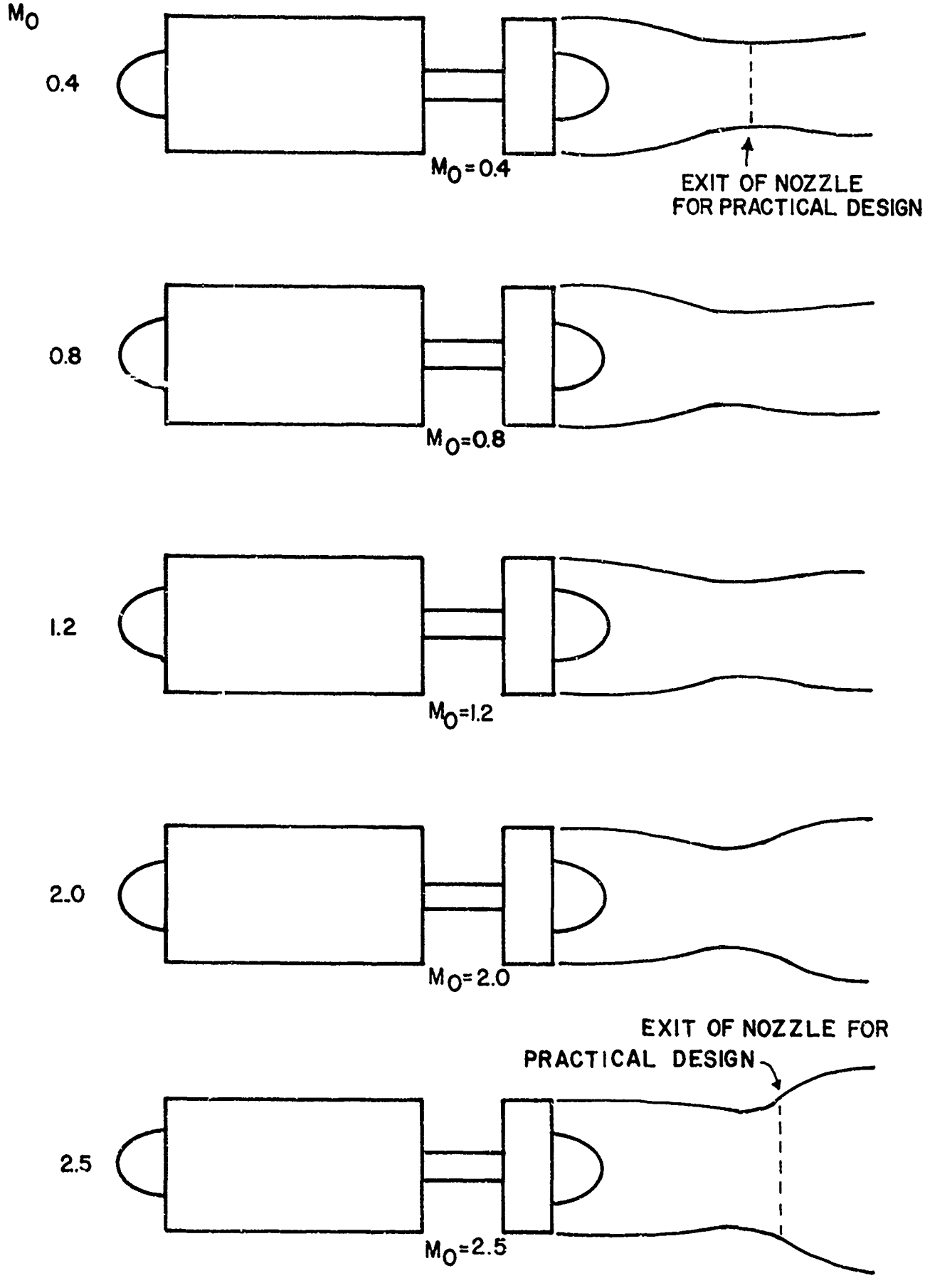

FIGURE 6. AREA VARIATIONS IN THE NOZZLE FOR DIFFERENT M_0.

As shown in Figure 6, to obtain ideal expansion the nozzle is converging-diverging for all M_0 illustrated. Usually the nozzle is a simple converging nozzle from subsonic through transonic range of M_0. This results in a large boattail area. At the design M_0 the exit area for ideal expansion significantly exceeds the maximum area of the propulsion system. The nozzle is cut off, relative to ideal, at some area appropriate to maximum engine area. The result is under-expansion and a ballooning plume. A shock wave may originate at the diverging streamlines of the plume, giving a drag increment.

Model for Propulsion with Internal Heat Addition

Consider a propulsion device as sketched in the top of Figure 7. To represent the wave drag of the inlet, it is necessary to duplicate streamline A-A. It does not matter what the details are of the inlet geometry internal to the streamtube bounded by A-A.

The inner body which generates a flow having streamline A-A is shown. Note that it is not the same shape as the inlet spike. A distribution of sources on the axis could generate the inner body as well as streamline A-A. Note that the spike shock wave does not have the same angle as the cowl shock wave.

If one applies the momentum relations to the control volume of Figure 7, the thrust minus drag is given by

$$\frac{T - D}{q_\infty} = \frac{1}{q_\infty} \int_A \rho_E u_E^2 dA + \frac{1}{q_\infty} \int (p_E - p)dA - \frac{D_B}{q_\infty} + 2 \int_{A_2} u_x u_r dA - \int_{A_4} (u_y^2 + u_r^2)dA \tag{7}$$

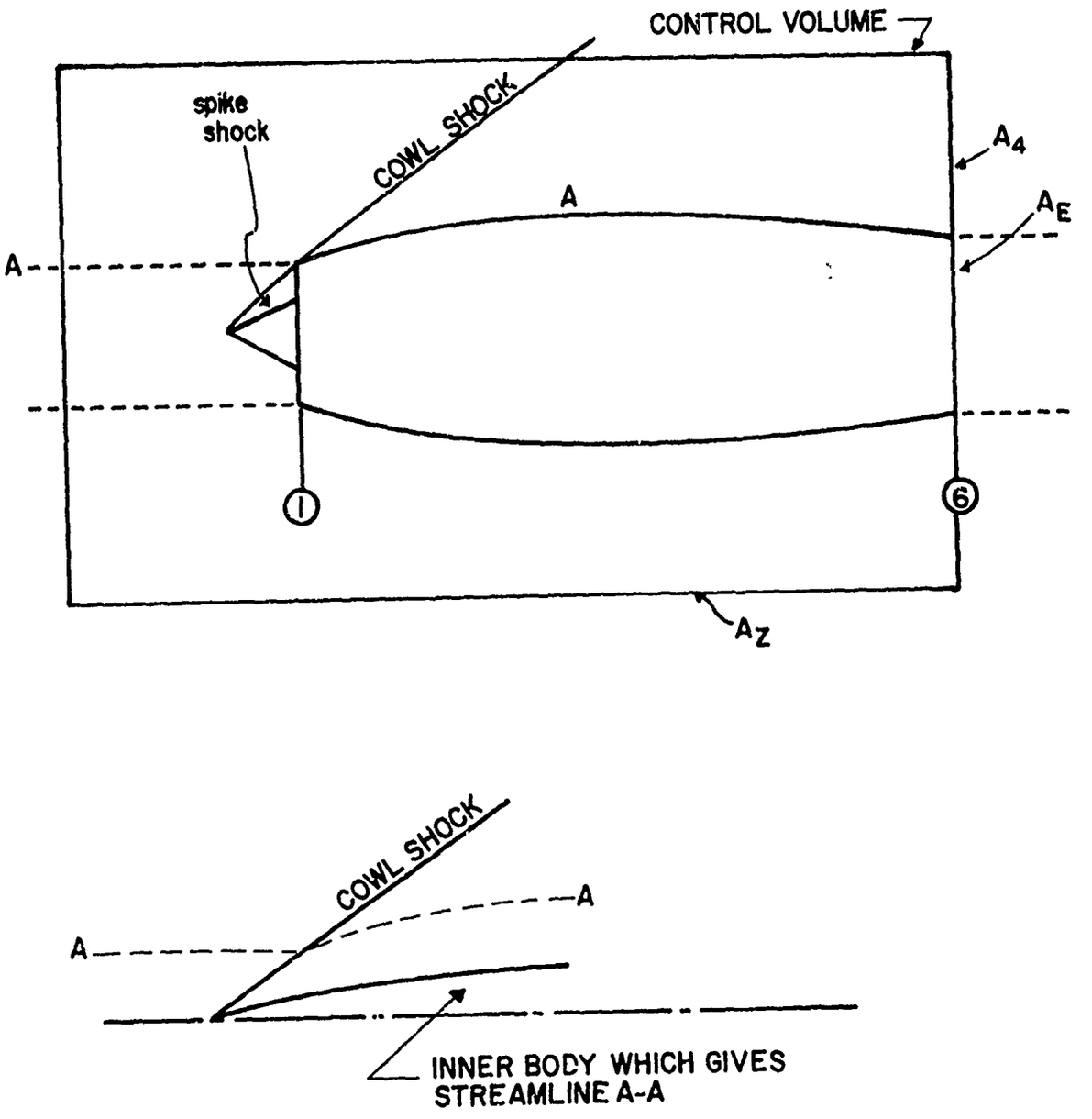

FIGURE 7. MODEL OF AN INLET USING SOURCES.

where u_x, u_r, and u_y are the dimensionless perturbation velocities arising from the nacelle. It is apparent that for the case where the exhaust exit defines a plane, as illustrated in Figure 7, the thrust and drag can be clearly separated. Waves generated by the exhaust plume do not influence T - D.

Following the analysis suggested by the model of Figure 7, one can obtain a nacelle of known wave drag. Figure 8 illustrates the concept. Start with an ogive of known shape. Plot the streamlines in the flow adjacent to the ogive. Pick the radii r_0 and r_B suitable for the nacelle. Insert the nacelle within the streamtube. The wave drag of the ogive and nacelle will be the same. The drag can be calculated using the potential function for the ogive. In the lower part of the figure, a nacelle with a spike inlet is shown.

Consider some thrust device inside a momentum control volume shown in Figure 9. How does one modify the variables so as to change conditions on the surface of control volume and improve T - D? What does one have available to change the wave drag? Available variables are: (a) number and location of nozzles, (b) velocity profile at nozzle exit, and (c) body geometry.

To obtain an optimum configuration, one must have a method to represent the body and exhaust analytically. The analytical representation can be subjected to the calculus of variations.

The body can be represented by sources and sinks. Changes in stagnation pressure, stagnation temperature, velocity vector, and other flow quantities make representation of exhaust more difficult.

Carrying the idea of Figure 7 further, let us look at an ideal ramjet. For an ideal ramjet, the following equalities hold true:

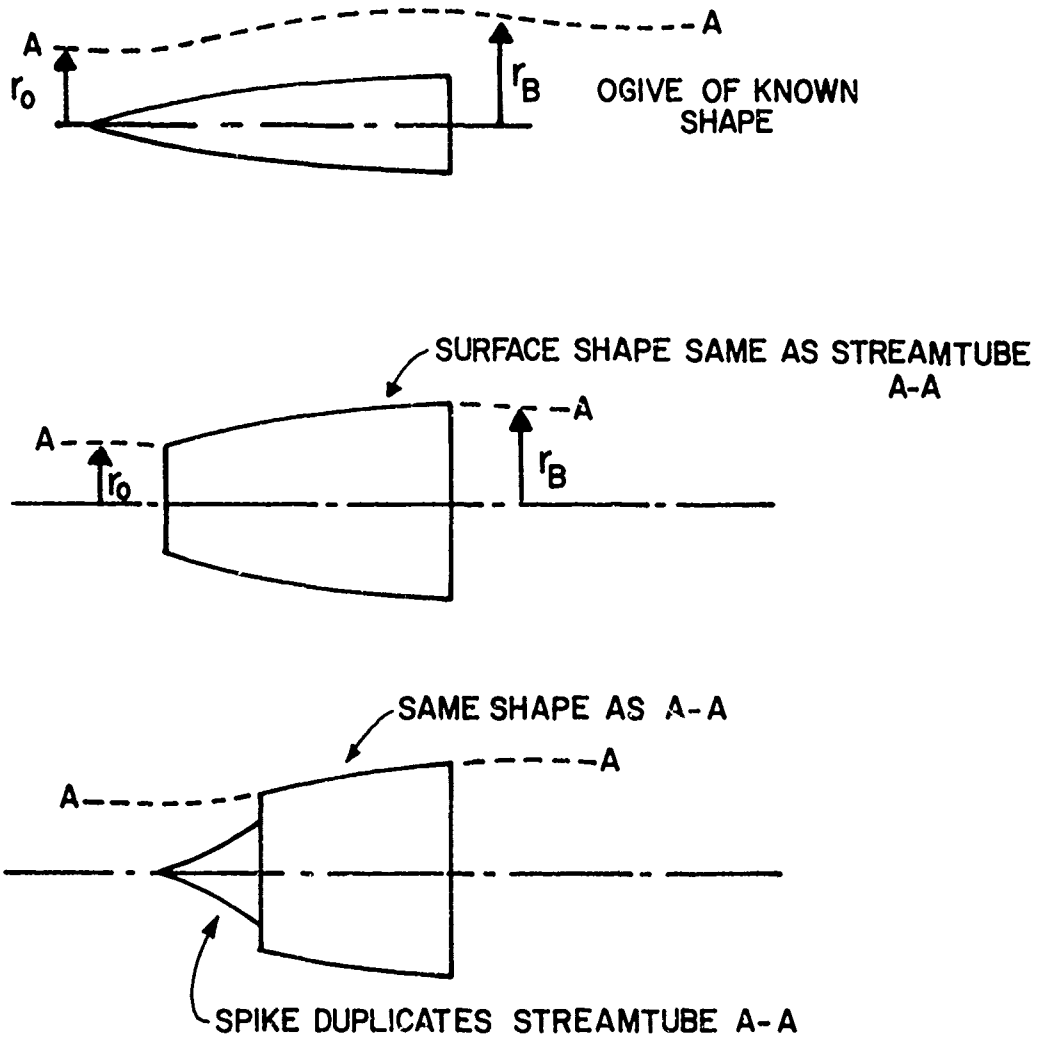

FIGURE 8. NACELLE OF KNOWN WAVE DRAG.

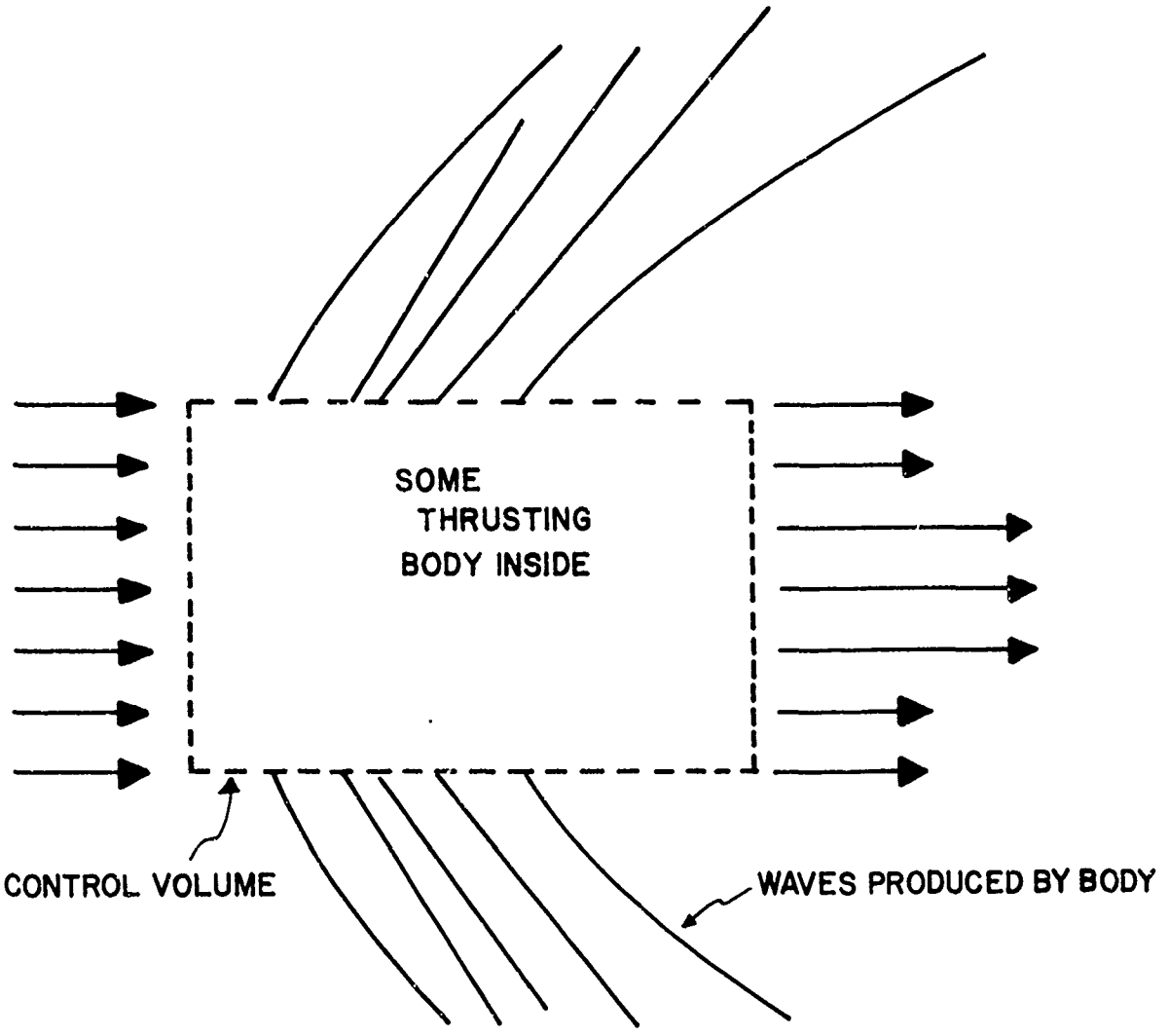

FIGURE 9. MOMENTUM CONTROL VOLUME FOR A THRUSTING BODY.

$$A_1 = A_6 \qquad \frac{\rho_6}{\rho_1} = \frac{T_{T1}}{T_{T6}}$$

$$p_{T6} = p_{T1} \qquad p_1 = p_6$$

$$\frac{v_6}{v_0} = \frac{T_{T6}}{T_{T1}}$$

For an ideal ramjet (or for any other propulsion device satisfying the above set of equalities), one can represent the flow by sources, sinks, and an "energy disc." This is illustrated in Figure 10; stations 1 and 6 are identified in Figure 10. The inner body duplicates streamline ABC. The inner body is formed from the source-sink distribution in the right-hand column of Figure 10. The change in density, velocity, and stagnation temperature is achieved by an "energy disc." In fact, that defines the energy disc. It changes the flow so that the equalities list above is correct. The sources, sinks, and energy disc shown in the bottom of the right column would have the same thrust and drag as the ideal ramjet sketched in the left-hand column.

This model looks as if it is satisfactory for an ideal ramjet, but it has some drawbacks:

1. The energy disc is not a heat front or other simple fluid flow.
2. When $A_1 \neq A_6$, it may be difficult to apply the energy disc.
3. For the case $p_{T6} \neq p_{T1}$, some means of changing p_T must be added.

The energy disc is bounded by a streamtube. Changing p_T within the disc gives a mismatch across the disc in regard to streamline shape.

A satisfactory way of specifying the conditions at station 6 is needed, and the energy disc has been suggested. One wants to retain sources and sinks for two reasons. Wave drag is readily calculated if you know the distribution function. The distribution function can be optimized to yield minimum wave drag.

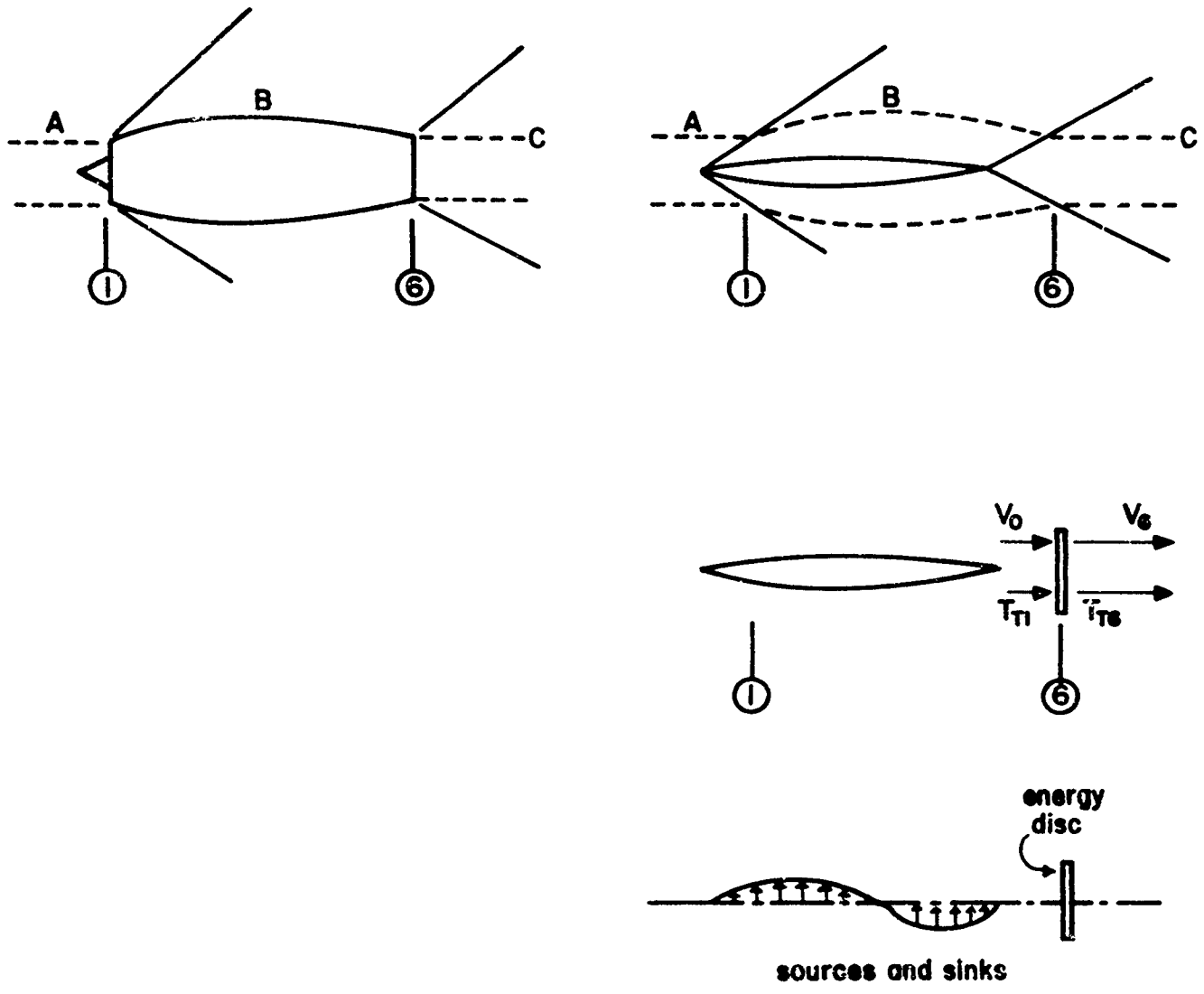

FIGURE 10. IDEAL RAMJET REPRESENTED BY SOURCES, SINKS, AND AN ENERGY DISC.

The energy disc represents the propulsion device. A particular engine generates changes in p_T, T_T, and velocity between the inlet and exhaust. For the case of a plane for an exit as shown at station 6 in Figure 10, one does not need the complexity of an energy disc. Equation (7) indicates that drag and thrust are separable for this case. When one varies quantities (a), (b), and (c) discussed previously as available, independent variables, then the energy disc may be an attractive model.

This section is closed by noting that a model has been proposed but has not been developed.

EXTERNAL BURNING; BASIC EQUATIONS AND SOLUTIONS

One-Dimensional Heat Addition

To provide a basis for comparison with subsequent sections, one-dimensional heat addition will be briefly reviewed.

There are several approaches to one-dimensional heat addition. For unsteady flow there is the self similar technique developed by Sedov.[6] We consider steady flow only here. There is the famous solution for constant area heat addition, i.e., the solution by Rayleigh. Rayleigh flow is discussed in most gas dynamics books.[7] When there is simultaneous variation of area and heat addition, the techniques outlined in the Princeton Series, Volume III, are applicable.[8]

The influence coefficients developed by Shapiro and Hawthorne[9] will be discussed here. Table IV summarizes the influence coefficients for heat addition and isentropic flow with area change. The influence functions relate a fractional change of a dependent variable, say M^2, to a fractional change of the independent variable, A or h_T. So far as heat addition is concerned, the

Table IV. Influence Coefficients for Area Change and Heat Addition

	$\frac{dA}{A}$	$\frac{dh_T}{c_p T}$
$\frac{dM^2}{M^2}$	$\frac{-2(1 + \frac{\gamma - 1}{2}M^2)}{1 - M^2}$	$\frac{1 + \gamma M^2}{1 - M^2}$
$\frac{du}{u}$	$-\frac{1}{1 - M^2}$	$\frac{1}{1 - M^2}$
$\frac{dT}{T}$	$\frac{(\gamma - 1)M^2}{1 - M^2}$	$\frac{1 - \gamma M^2}{1 - M^2}$
$\frac{d\rho}{\rho}$	$\frac{M^2}{1 - M^2}$	$-\frac{1}{1 - M^2}$
$\frac{dp}{p}$	$\frac{\gamma M^2}{1 - M^2}$	$-\frac{\gamma M^2}{1 - M^2}$
$\frac{dF}{F}$	$\frac{1}{1 + \gamma M^2}$	0
$\frac{ds}{c_p}$	0	1

velocity, u, and static pressure, p, change as they would flow into decreasing area. For u and p, heat addition and area variation produce the same result.

For unconfined flow with heat addition, there are some analogies between the flow due to a particular body shape and the flow due to a given distribution of heat addition. These analogies, which are limited in scope, will be pointed out as they arise in subsequent discussion. The fact that heat addition and a

body may influence the flow the same way may be understood using the du/u and dp/p influence coefficients.

The influence coefficients are the first terms in a Taylor series expansion of the dependent variables in terms of the independent variables. Many of the results of linearized heat addition in an unconfined flow can be related to influence coefficients. This statement is applicable, for examble, to heat fronts and combustion fans.

Linearized Equations for Combined Mass and Heat Addition

The equations of motion for steady flow with heat and mass addition are as follows:

Continuity $$\operatorname{div}(\rho\vec{u}) = m \tag{8}$$

Momentum $$\rho\frac{D\vec{u}}{Dt} + \vec{\nabla}p + m\vec{u} = 0 \tag{9}$$

Energy $$\operatorname{div}\ \rho\vec{u}\left(h + \frac{u^2}{2}\right) = Q \tag{10}$$

In the preceding equations, m is the rate at which mass is added per unit volume. Likewise Q is the rate at which heat is added per unit volume.

To linearize these equations, one introduces perturbation quantities which are defined as follows:

$$\begin{aligned} &\rho = \rho_\infty + \rho' \ ; \ p = p_\infty + p' \\ &\vec{u} = \vec{e}_x(U + u') + \vec{e}_y v' + \vec{e}_z w' \end{aligned} \tag{11}$$

When the perturbation quantities are introduced, the resulting equations are

Continuity $$\rho_\infty u_x' + \rho_\infty v_y' + U\rho_x' = m \tag{12}$$

Momentum $$\begin{cases} \rho_\infty U_\infty u_x' + p_x' = -mU_\infty \\ \rho_\infty U_\infty v_x' + p_y' = 0 \end{cases} \tag{13}$$

$$\text{Energy} \qquad \frac{p_\infty U_\infty}{\gamma - 1} \frac{\partial}{\partial x}\left(\frac{p'}{p_\infty} - \frac{\gamma \rho''}{\rho_\infty}\right) + \frac{a_\infty^2 m}{2}\left(\frac{2}{\gamma - 1} - M^2\right) = Q \tag{14}$$

We have formulated a 2D planar flow so that $w' = 0$. To avoid writing subscript ∞, we now drop it in subsequent equations. The notation with subscript x means partial differentiation with respect to x.

Starting with Equations (8) to (10), one could obtain the linearized equations appropriate for heat and mass addition in axisymmetric flow. The equations have been solved for mass addition (sources) but not for heat addition in axisymmetric flow.

The solution for a source in two-dimensional planar flow will now be obtained. Consider a row of point sources evenly distributed along the z-axis. Axis orientation relative to the flow is shown in Figure 11. For a point $P(x - x_1, y - y_1)$, only the sources within the Mach forecone influence point P as shown in Figure 11. To find the potential in two-dimensional flow, add up the sources along the z-axis from k to d. Points k and d are illustrated in Figure 11. From the geometry of Figure 11

$$z_d^2 = (x - x_1)^2 \tan^2 \mu - (y - y_1)^2 \tag{15}$$

Integration of a row of point sources yields the potential

$$\phi(x,y,0) = - \int_{-z_d}^{z_d} \frac{dz_1}{2\pi \sqrt{(x - x_1)^2 - \beta^2 z_1^2 - \beta^2 (y - y_1)^2}} \tag{16}$$

This integrates to

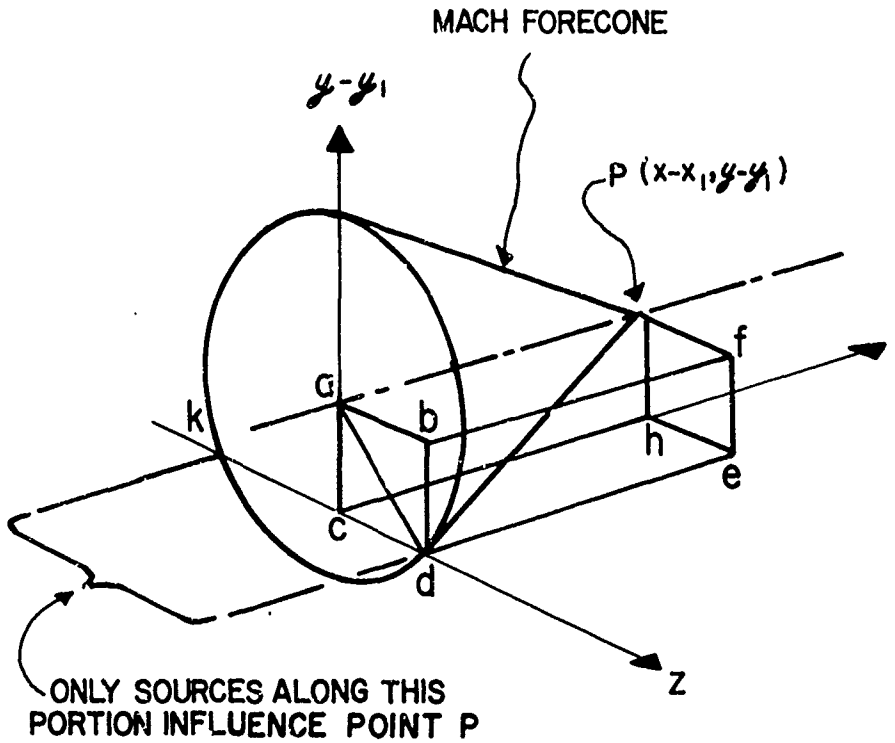

FIGURE II. POTENTIAL FOR A LINE SOURCE IN SUPERSONIC FLOW.

$$\phi(x,z) = -\frac{1}{\beta\pi} \sin^{-1} \frac{\beta z_1}{\sqrt{(x - x_1)^2 - \beta^2(y - y_1)^2}} \Bigg|_0^{z_d} \tag{17}$$

Inserting the limits gives

$$\phi(x,y) = \frac{1}{2\beta} \tag{18}$$

The potential is a constant. Think of a series of Mach cones with apex at the z-axis. Upstream of these cones, the potential is zero. Downstream of the envelope of Mach cones, it is constant. One can represent this by

$$\phi(x,y) = -\frac{1}{2\beta} I\left[(x - x_1) \pm \beta(y - y_1)\right] \tag{19}$$

where I is the unit function. The velocity components are, for a unit source strength,

$$u = \frac{\partial\phi}{\partial x} = -\frac{1}{2\beta}\delta\left[(x - x_1) \pm \beta(y - y_1)\right] \tag{20}$$

and

$$w = \frac{\partial\phi}{\partial y} = \mp\frac{1}{2}\delta\left[(x - x_1) \pm \beta(y - y_1)\right] \tag{21}$$

The (+) sign in front of β gives right-running waves, whereas the (-) sign gives left-running waves.

The solutions for a heat source in supersonic flow are[10]

$$u' = -\frac{(\gamma - 1)q}{2\gamma p\beta}\delta(x - \beta y) \tag{22}$$

$$v' = \frac{(\gamma - 1)q}{2\gamma p}\delta(x - \beta y) \tag{23}$$

$$p' = \frac{(\gamma - 1)Mq}{2a\beta}\delta(x - \beta y) \tag{24}$$

$$\rho' = \frac{(\gamma - 1)Mq}{2a^3\beta}\delta(x - \beta y) - \frac{(\gamma - 1)q}{a^2 U}\delta(y)I(x) \tag{25}$$

One can verify that there are the appropriate solutions when $m = 0$ and $Q \neq 0$ by substitution into Equations (12) to (14). The second term in Equation (25) is a wake. Pressure in the wake is the ambient value, and the velocity returns to freestream value. The solutions in Equations (22) to (25) are valid for all x and y including the source point $x = y = 0$. The symbol q, which has units heat/(length)(time), will be discussed shortly. The line heat source in a planar flow is illustrated in Figure 12.

Similar solutions can be written for the case of mass addition; these are:

$$u' = -\frac{m}{2\beta}\delta(x - \beta y) \tag{26}$$

$$v' = \frac{m}{2\beta}\delta(x - \beta y) \tag{27}$$

$$p' = \frac{\rho U m}{2\beta}\delta(x - \beta y) \tag{28}$$

$$\rho' = \frac{\rho m M^2}{2\beta U}\delta(x - \beta y) \tag{29}$$

Substitution of Equations (26) to (29) into Equations (12) to (14) indicate these are solutions except at the mass source point $x = y = 0$. With Equations (22) through (29), one has solution for volume distribution of heat and in regions where $m = 0$. This is adequate to describe planar bodies with adjacent heat addition zones.

Volume Heat Addition

Since the heat may be added throughout a volume rather than a line source (the z-axis in Figure 11), it is worthwhile to formulate heat as a volume release. Define, as in Equations (10) and (14)

$$Q = \frac{\text{heat}}{(\text{span})(\text{area})(\text{sec})}$$

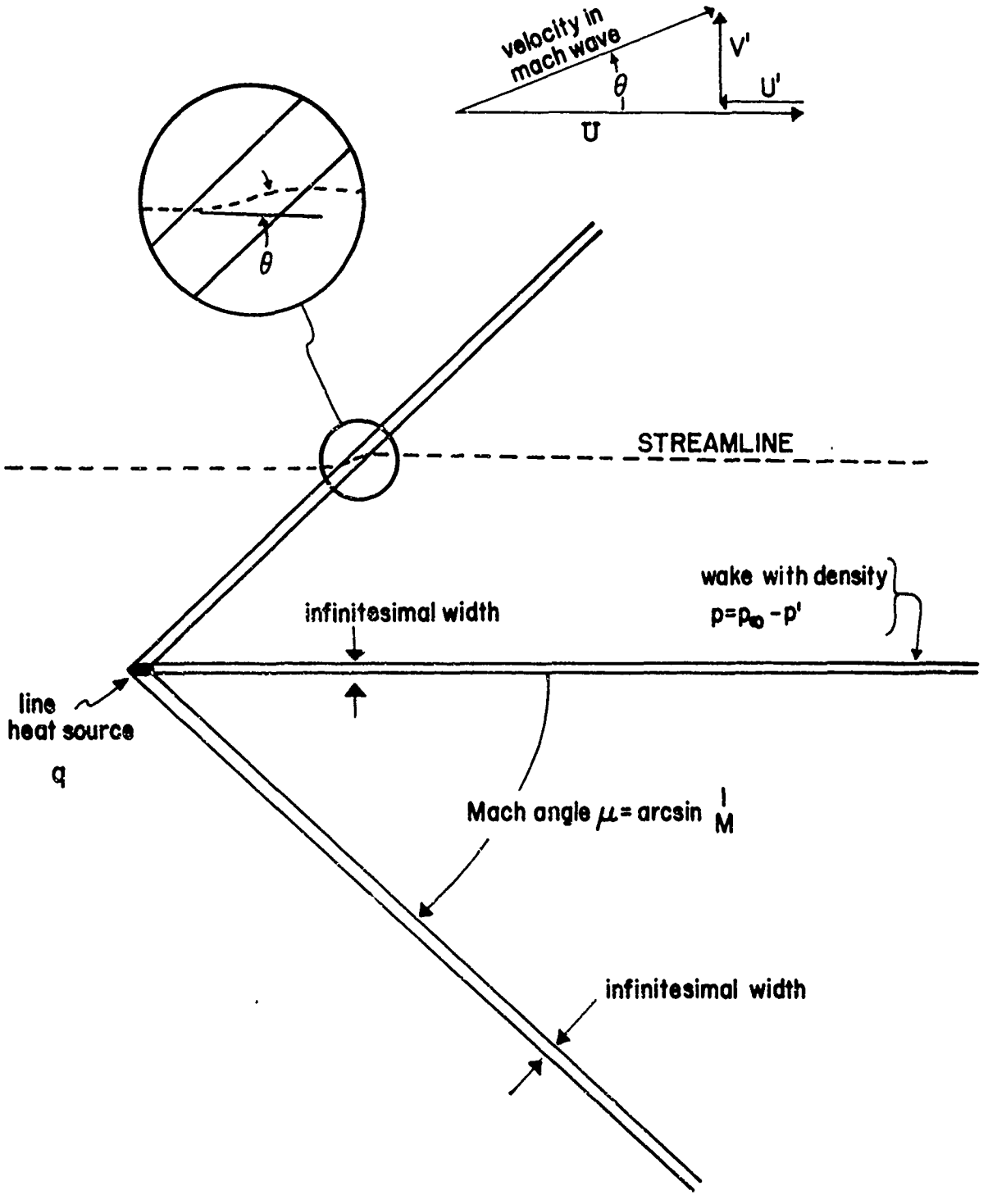

FIGURE 12. SMALL PERTURBATION HEAT SOURCE IN A SUPERSONIC FLOW.

Then we define

$$q = \frac{\text{heat}}{(\text{span})(\text{sec})}$$

$$q = Q dx dy$$

Another area element may be better than dxdy. Some element with its sides parallel to a Mach line is preferred. We think of $Q = Q(x,y)$. Figure 13 is a series of drawings illustrating the variables.

To get heat per unit span

$$H = \int_0^L \int_0^{\ell} Q dx dy = QL\ell \qquad \text{(30)}$$

(if Q = constant)

Heat released in the complete volume is $\mathcal{H} = Hs$.

$$\mathcal{H} = \frac{\text{heat}}{\text{sec}} \qquad H = \frac{\text{heat}}{(\text{span})(\text{time})}$$

Now to tie into the 2D flow equations, we use Equation (22) as an example,

$$u' = -\frac{(\gamma - 1)q}{2\gamma p\beta}\,\delta(x - \beta y) \qquad \text{(31)}$$

At a point on a characteristic, u' results from a source on that same characteristic. If there is more than one source on that characteristic, one adds the influence of each.

$$u' = \frac{(\gamma - 1)(q_1 + q_2)}{2\gamma p\beta}\,\delta(x - \beta y) \qquad \text{(32)}$$

For many heat sources, in fact n heat sources,

$$u' = -\frac{(\gamma - 1)}{2\gamma p\beta} \sum_{i=1}^{i=n} q_i\,\delta(x - \beta y) \qquad \text{(33)}$$

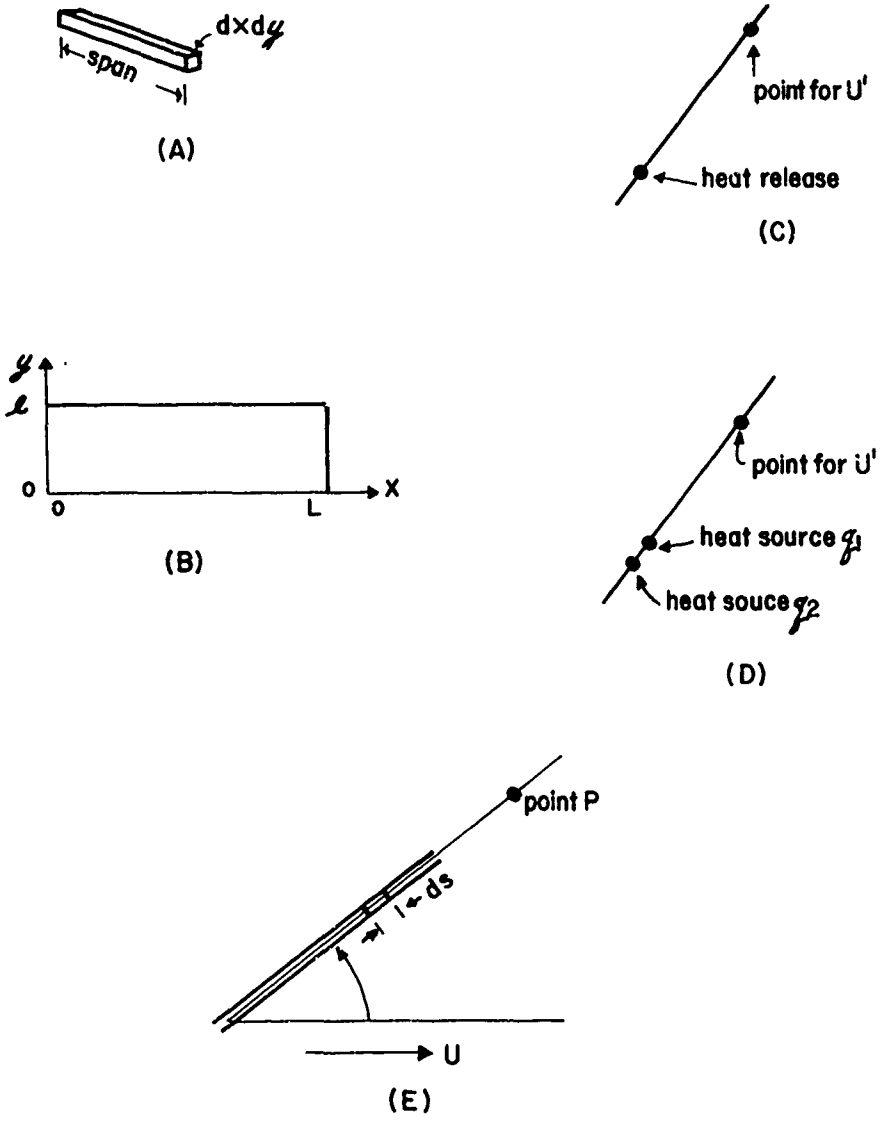

FIGURE 13.
ILLUSTRATION OF QUANTITIES RELATED TO SPECIFICATION OF HEAT RELEASE.

The equation for u' is correct if one thinks of

$$q_i = Q dy = \frac{\text{heat}}{(\text{span})(\text{length})(\text{sec})}$$

when the heat source is distributed in the volume. When heat sources are not discrete but are distributed, then one wants to integrate along a characteristic. Let s be distance along the characteristic. We express q_i in terms of Q and ds

$$q_i = Q \sin \mu \, ds = dq \tag{34}$$

The perturbation velocity is

$$u' = -\frac{(\gamma - 1)}{2\gamma p \beta} \int_0^s Q \sin \mu \, ds = -\frac{(\gamma - 1)}{2\gamma M p \beta} \int_0^s Q(x,y) ds \tag{35}$$

Since s,x,y are related quite simply

$$x = s \cos \mu, \qquad y = s \sin \mu, \qquad x = \beta y$$

one can integrate u' several ways:

$$\sin \mu \int_0^s Q\left[s \cos \mu, \; s \sin \mu\right] ds \quad \text{or} \quad \int_0^y Q(\beta y, y) dy$$

$$\text{or} \quad \int_0^x Q(x, x/\beta) dx/\beta \tag{36}$$

Referring to the region bounded by $0 < x < L$ and $0 < y < \ell$ in Figure 13(b) and for case Q = constant inside the region

$$\int_0^s \sin\mu\, Q\,ds = Q\ell = \int_0^y Q\,dy = Q\ell = \int_0^x Q(x,x/\beta)\frac{dx}{\beta} = (\tan\mu)\beta Q\ell = Q\ell \tag{37}$$

The pressure perturbation would be

$$p' = \frac{(\gamma - 1)MQ\ell}{2a\beta} \tag{38}$$

In terms of $Q(x,y)$, the perturbation quantities are

$$u' = -\frac{(\gamma - 1)}{2\gamma p\beta}\int_0^s Q(x,y)\sin\mu\, ds \tag{39}$$

$$v' = \frac{(\gamma - 1)}{2\gamma p}\int_0^s Q(x,y)\sin\mu\, ds \tag{40}$$

$$p' = \frac{(\gamma - 1)M}{2a\beta}\int_0^s Q(x,y)\sin\mu\, ds \tag{41}$$

$$\rho' = \frac{(\gamma - 1)M}{2a^3\beta}\int_0^s Q(x,y)\sin\mu\, ds - \frac{\gamma - 1}{a^2 U}\int_{x'}\int_{y'} Q(x',y')\delta(y - y')X \tag{42}$$

$$I(x - x')dx'dy'$$

The wake is given by the integral above; as an example for $x > x_i + L$

$$\rho'_{WAKE}(y) = -\frac{\gamma - 1}{a^2 u}\int_{x' = x_i}^{x' = x_i + L} Q(x',y)dx' \tag{43}$$

where the geometry is sketched in Figure 14.

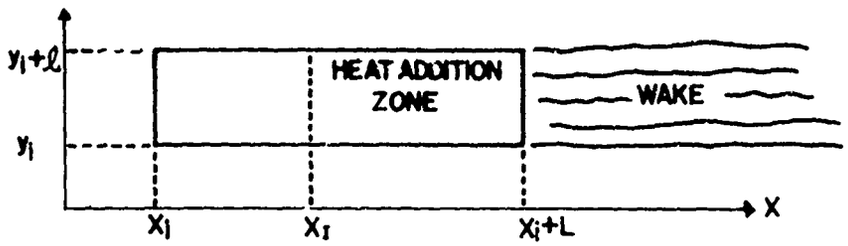

FIGURE 14. GEOMETRY OF WAKE DOWNSTREAM OF A HEAT ADDITION ZONE.

For a point inside the heat release region

$$\rho'_{WAKE}(x_I,y) = -\frac{\gamma-1}{a^2 u}\int_{x'=x_i}^{x'=x_I} Q(x',y)dx' \qquad (44)$$

The symbol x_I is defined in Figure 14.

Heat Addition at a Plane; A Heat Front

Consider a distribution of line sources which form a plane at angle θ to the flow, as illustrated by Figure 15. Terminology similar to that used in supersonic wing theory, i.e., subsonic and supersonic "leading edge," is employed to identify two cases, $\theta \gtrless \mu$ or $M_n \gtrless 1$. The normal Mach number M_n is M sin θ. Since sin $\mu = 1/M$, the normal Mach number is

$$M_n = \frac{\sin\theta}{\sin\mu} \qquad (45)$$

You can see from an examination of Figure 15 that the heat source can influence flow upstream if $M_n < 1$. However, if $M_n > 1$, the heat source does NOT influence flow upstream contrary to statements made by Tsien and Beilock.[10] Also it is apparent that point P is influenced only by right-running characteristics for $M_n < 1$, whereas P is influenced by both families of characteristics for $M_n > 1$.

The perturbation velocities for a heat front will now be obtained. Using Equation (22) and integrating along the heat front, the formula for u' is

$$u'(x,y) = -\frac{(\gamma-1)q}{2\gamma p\beta}\int_{-\infty}^{\infty}\delta\left[(x - s\cos\theta) - \beta(y - s\sin\theta)\right]ds \qquad (46)$$

where s is distance along the heat front. Consequently,

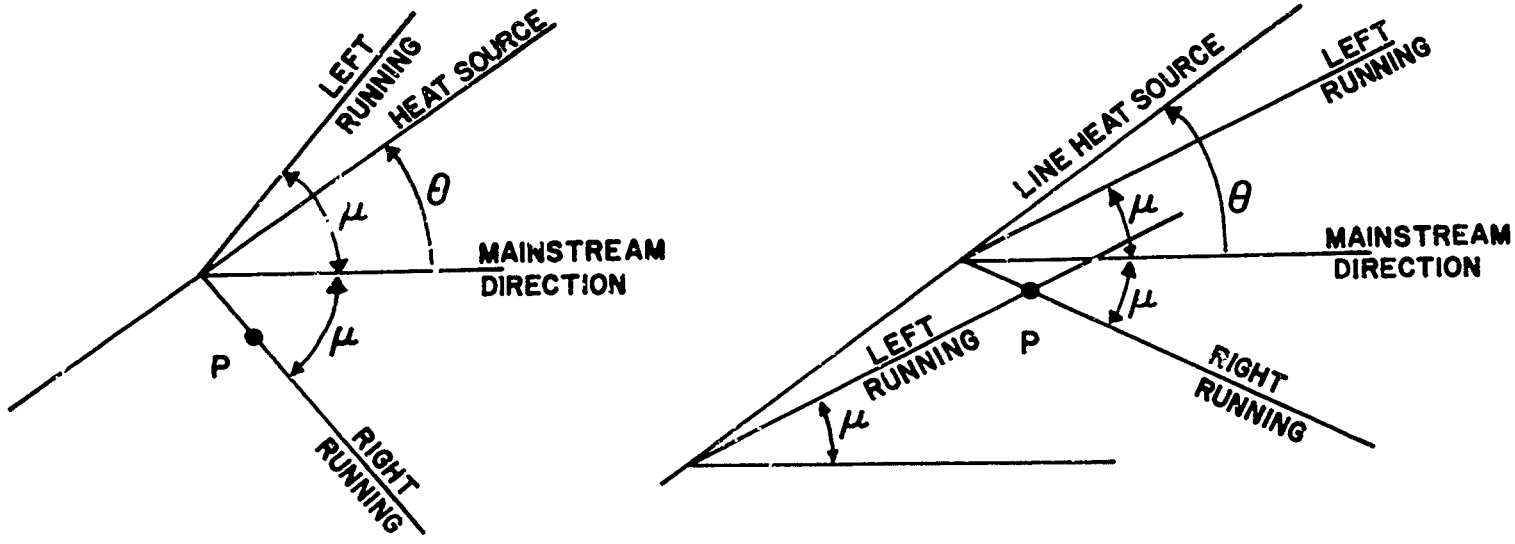

SUBSONIC "LEADING EDGE"

$M_n < 1$

SUPERSONIC "LEADING EDGE"

$M_n > 1$

FIGURE 15. LINE HEAT SOURCE AT ANGLE θ TO SUPERSONIC FLOW.

$$u' = \frac{(\gamma - 1)q}{2\gamma p\beta} \frac{-1}{\beta \sin\theta - \cos\theta} \int_{-\infty}^{\infty} \delta\left[s - \frac{x - \beta y}{\cos\theta - \beta \sin\theta}\right] ds =$$

$$- \frac{(\gamma - 1)q}{2\gamma p\beta(\beta \sin\theta - \cos\theta)} \tag{47}$$

Since $\beta = \sqrt{M^2 - 1}$, it is also true that $\beta = 1/\tan\mu$. Using this fact

$$u' = \frac{(\gamma - 1)q}{2\gamma p} \frac{\tan\mu \sin\mu}{\sin(\mu - \theta)} \tag{48}$$

For left-running waves, μ is positive; and for right-running waves, μ is negative. For a subsonic "leading edge," θ is less than μ. Downstream of the heat source for $M_n < 1$, Equation (48) indicates u'_d will be negative; upstream of the source u'_u will be positive. In addition

$$\left|u'_u\right| > \left|u'_d\right| \qquad \text{(for } M_n < 1\text{)}$$

where subscripts u and d indicate upstream and downstream respectively.

For a supersonic "leading edge," which is illustrated on the right-hand side of Figure 15, the left running Mach wave gives a u'_L which is negative. The right-running Mach wave gives a u'_R which is also negative but which is less in absolute value than u'_L. Subscripts L and R denote left- and right-running waves. Consequently,

$$u'_d = u'_L + u'_R < 0$$

Now let's look at v'; from Equation (23) one obtains for this case:

$$v'(x,y) = \frac{(\gamma - 1)q}{2\gamma p} \int_{-\infty}^{\infty} \delta\left[(x - s\cos\theta) - \beta(y - s\sin\theta)\right] ds \tag{49}$$

Integration of the δ-function yields

$$v' = \frac{(\gamma - 1)q}{2\gamma p} \frac{1}{\beta \sin \theta - \cos \theta} = \frac{(\gamma - 1)q}{2\gamma p} \frac{\sin \mu}{\sin (\theta - \mu)} \tag{50}$$

For the case $M_n < 1$, v_u' is negative, and v_d' is also negative. Furthermore

$$\left|v_u'\right| > \left|v_d'\right| \qquad \text{(for } M_n < 1\text{)}$$

For the case $M_n > 1$, v_L' is positive while v_R' is negative. In addition

$$v_d' = v_L' - \left|v_R'\right| > 0 \quad \text{(for } M_n > 1\text{)}$$

which means the flow is turned toward the line source much the same as an oblique shock wave. For $M_n < 1$, the flow turns away from the heat front.

A natural question is, "Is there any special direction to the perturbation velocity vector?" Let $\vec{v}_r$ be the resultant perturbation velocity vector. It is given by

$$\vec{v}_r = -\vec{e}_x C\left(\frac{\tan \mu \sin \mu}{\sin(\theta - \mu)} + \frac{\tan \mu \sin \mu}{\sin(\theta + \mu)}\right) + \vec{e}_y C\left(\frac{\sin \mu}{\sin(\theta - \mu)} - \frac{\sin \mu}{\sin(\theta + \mu)}\right) \tag{51}$$

The algebraic signs are correct for the case $M_n > 1$ which means $\theta > \mu$. The symbol C equals $(\gamma - 1)q/2\gamma p$. Let α be the angle of the perturbation velocity vector relative to freestream direction. Then

$$\tan \alpha = \frac{\dfrac{\sin \mu}{\sin(\theta - \mu)} \quad \dfrac{\sin \mu}{\sin(\theta + \mu)}}{\dfrac{\tan \mu \sin \mu}{\sin(\theta - \mu)} + \dfrac{\tan \mu \sin \mu}{\sin(\theta + \mu)}} \tag{52}$$

Manipulation of Equation (52) leads to

$$\tan \alpha = -\frac{1}{\tan \mu} \frac{\sin \mu}{\cos \mu} \frac{\cos \theta}{\sin \theta} = -\frac{1}{\tan \theta} \tag{53}$$

The conclusion from Equation (53) is that the velocity vector is normal to the planar heat source. Since this is so, one can transform the supersonic case of heat addition to an equivalent 1D problem. To do this, one uses

$$\frac{du}{u} = \frac{\sqrt{(u_L' + u_R')^2 + (v_L' + v_R')^2}}{u} \tag{54}$$

where $u = U \sin \Theta$. Proceeding by substitution of components from Equation (51) into Equation (54) gives

$$\frac{du}{U \sin \Theta} = \frac{1}{1 - M_n^2} \frac{h_T}{c_p T} \tag{55}$$

which is precisely the influence coefficient result when properly interpreted. See Table IV. For a subsonic "leading edge," the velocity increases. This means that the flow is turned away from the planar heat source for $M_n < 1$ (analogous to Prandtl Meyer expansion) and toward the planar heat source for $M_n > 1$ (analogous to oblique shock wave).

As has been demonstrated, one of the ways of adding heat which lends itself to analysis is by means of a heat front. The example chosen by Tsein and Beilock[10] was a heat front. Oswatitsch[11] considers other aspects of heat fronts.

Heat addition at a front is comparable in complexity to linearized heat addition. Combustion is a volume phenomenon. However, if the length of the heat release region is much less than a body length, a front is a reasonable approximation. Detonation is a heat front of a very special nature.[12]

A heat front with a subsonic leading edge located next to a wall will be preceded by an oblique shock. The oblique shock turns the flow away from the wall, and the heat front turns it back parallel to the wall. Recall that for a subsonic leading edge the heat front can influence the flow upstream. The corresponding changes in pressure are shown. The net change in pressure is positive although the heat front decreases pressure.

A heat front with a supersonic leading edge will be followed by an expansion fan if the front is adjacent to a straight wall. Once again the net pressure change is positive. The heat front turns the flow away from the wall, and the fan redirects it so as to be parallel to the wall.

Adding heat to a supersonic stream decreases the Mach number. When sufficient heat has been added, the normal component of the Mach number downstream of the heat front, M_{n2}, will become unity. The amount of heat required to make $M_{n2} = 1$ is known as "critical" amount of heat. With a heat front having a supersonic leading edge, heat can be added until $M_{n2} = 1$. If more heat is added, the flow illustrated in Figure16(b) changes to that shown in Figure 16(a). The oblique shock decreases the flow Mach number changing the leading edge of the heat front from supersonic to subsonic.

Adding heat to a subsonic flow or a heat front with a subsonic leading edge modifies the flow upstream. One cannot specify the flow immediately ahead of the front. Critical heat addition does not have the same impact in the subsonic case since the flow upstream will be modified to adjust to the large heat addition.

A detonation wave can be thought of as a shock wave followed by a combustion zone or heat front. In Figure.16(a) if the oblique shock and the heat front had the same angle, it would be an oblique detonation wave provided the Mach number and amount of heat released were correct.

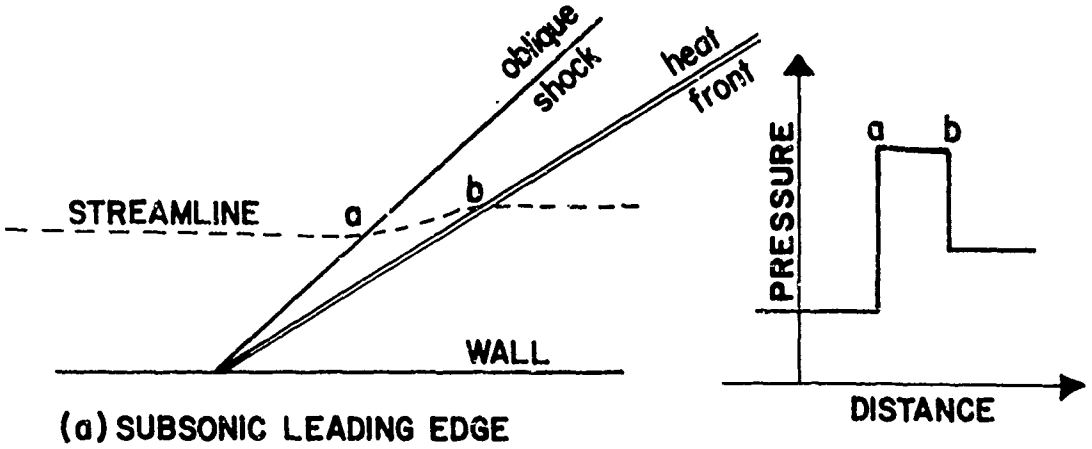

(a) SUBSONIC LEADING EDGE

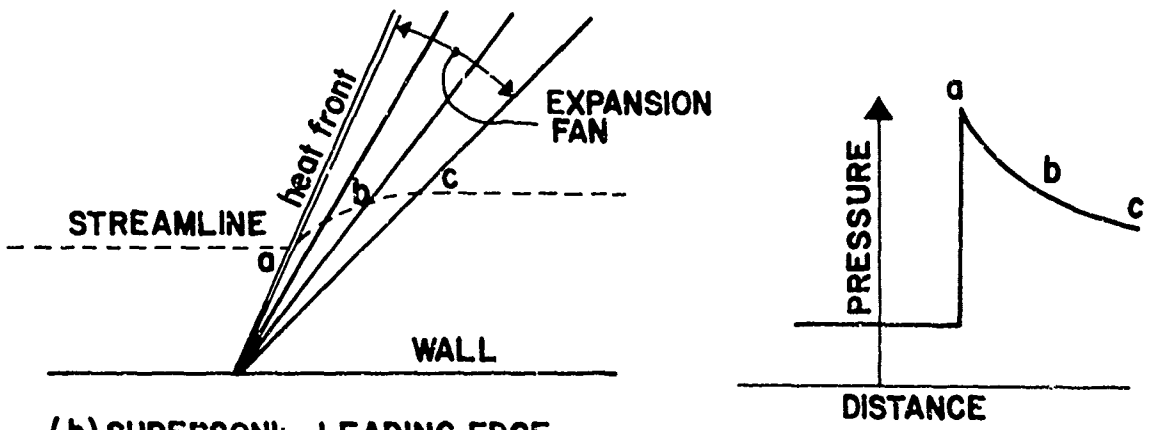

(b) SUPERSONIC LEADING EDGE

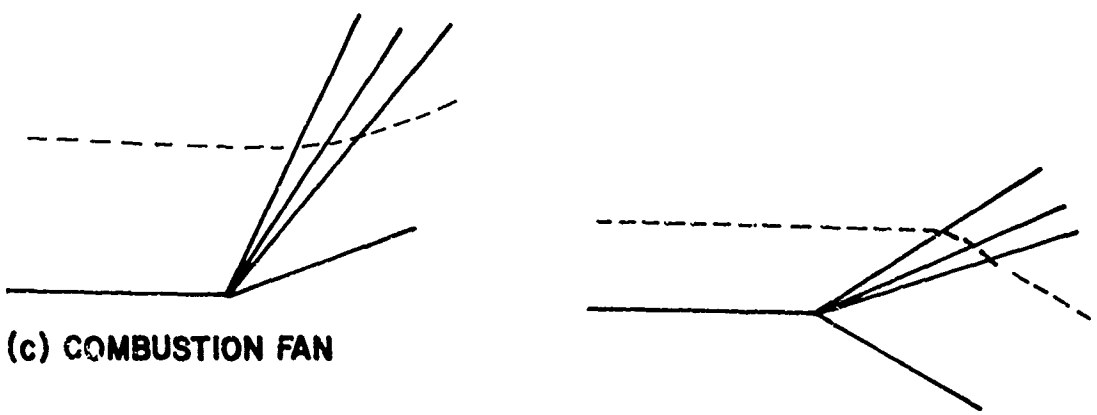

(c) COMBUSTION FAN

FIGURE 16. HEAT FRONTS AND COMBUSTION FANS.

In the Prandtl-Meyer expansion, conditions are constant along a characteristic. Centered combustion fans are possible with conditions constant along a ray. However, the ray is not a Mach line, and the normal component of Mach number need not be unity. Combustion fans could occur in subsonic as well as supersonic flow.

If M_n, the normal component of Mach number, exceeds unity, the fan will turn the flow away from the wall like a compression. This is illustrated in Figure 16(c) on the left-hand side. If M_n is less than unity, the flow would be turned downward as shown in Figure 16(c) on the right-hand side.

Starting with the continuity equation in cylindrical coordinates (r,β,z) and setting $\partial(\ )/\partial z = 0$ and $\partial(\ )/\partial r = 0$, one can derive the continuity equation for a combustion fan. It is

$$w_1 + \frac{dw_2}{d\beta} + w_2 \frac{d\ell n\rho}{d\beta} = 0 \tag{56}$$

The velocity components are illustrated in Figure 17. Heat addition does not cause an irrotational flow to become rotational. One additional equation is the condition for irrotational flow which is

$$\frac{dw_1}{d\beta} - w_2 = 0 \tag{57}$$

The rate of heat release controls $d\ell n\rho/d\beta$. One simple combustion fan occurs for $d\ell n\rho/d\beta$ = constant. For this case, Equations (56) and (57) can be readily integrated.

There is a particularly interesting expression that can be derived for the pressure coefficient associated with a heat front in hypersonic flow. Consider a heat front at angle θ relative to the main stream. The velocity components and angles are illustrated in Figure 18. The momentum equation is

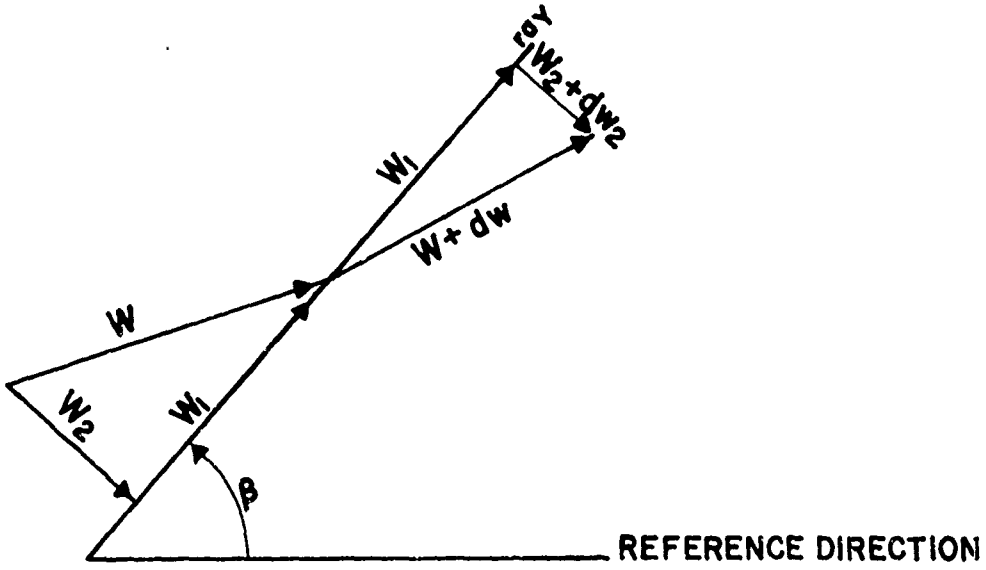

FIGURE 17. GEOMETRY FOR COMBUSTION FAN.

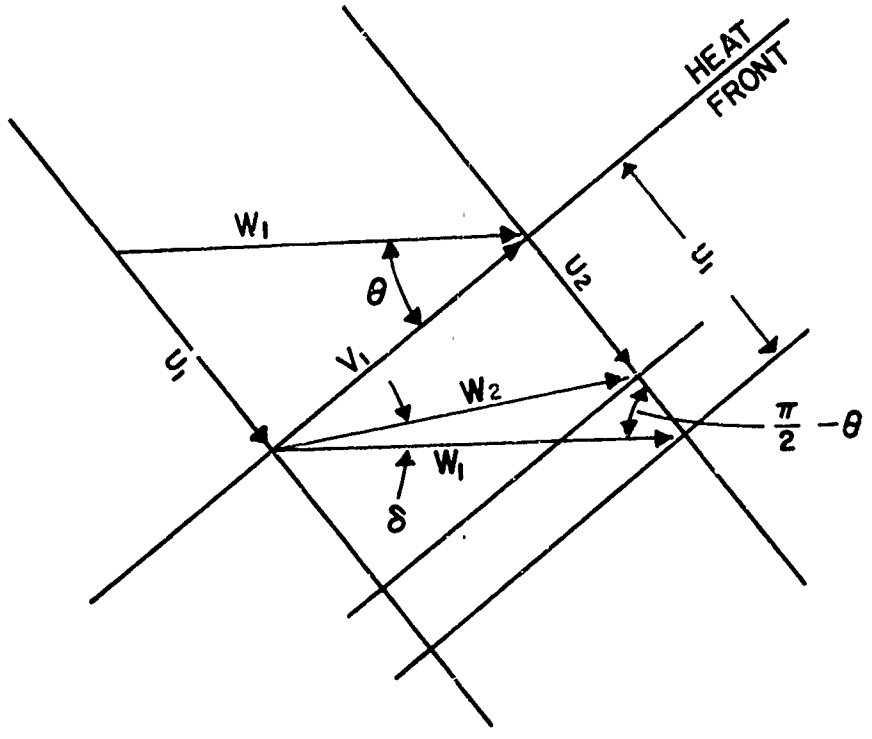

FIGURE 18. DEFINITION OF ANGLES AND VELOCITY COMPONENTS.

$$p_1 + \rho_1 u_1^2 = p_2 + \rho_2 u_2^2 \tag{58}$$

which can be rearranged, since from continuity $\rho_1 u_1 = \rho_2 u_2$

$$p_2 - p_1 = \rho_1 u_1^2 - \rho_2 u_2^2 = \rho_1 u_1 (u_1 - u_2) \tag{59}$$

From the geometry illustrated in Figure 18

$$\frac{w_2}{\sin\left(\frac{\pi}{2} - \theta\right)} = \frac{u_1 - u_2}{\sin\delta} \tag{60}$$

Noting that $U_1 = w_1 \sin\theta$ and combining Equations (59) and (60) leads to

$$p_2 - p_1 = \rho_1 w_1 w_2 \tan\theta \sin\delta \tag{61}$$

If $M_n^2 = M^2 \sin^2\theta \gg 1$, heat addition has little influence on w or ρ. Hence $w_1 \cong w_2$. For hypersonic flow Equation (61) becomes

$$p_2 - p_1 = 2\left(\frac{1}{2}\rho_1 w_1^2\right) \tan\theta \sin\delta$$

and the pressure coefficient is

$$c_p = 2 \tan\theta \sin\delta \tag{62}$$

This can be compared with the Newtonian expression which is

$$c_p = 2 \sin^2\delta \tag{63}$$

Equations (62) and (63) provide sufficient tools to explore the external burning ramjet shown in Figure 19. Angle δ is shown in the top figure and applies to Equation (63).

Heat Addition and Vorticity

In this section it is shown that heat addition does not change an initially irrotational flow to a rotational flow. The curl of the velocity vector should be zero. For subsonic flow, one uses the equations from Tsien

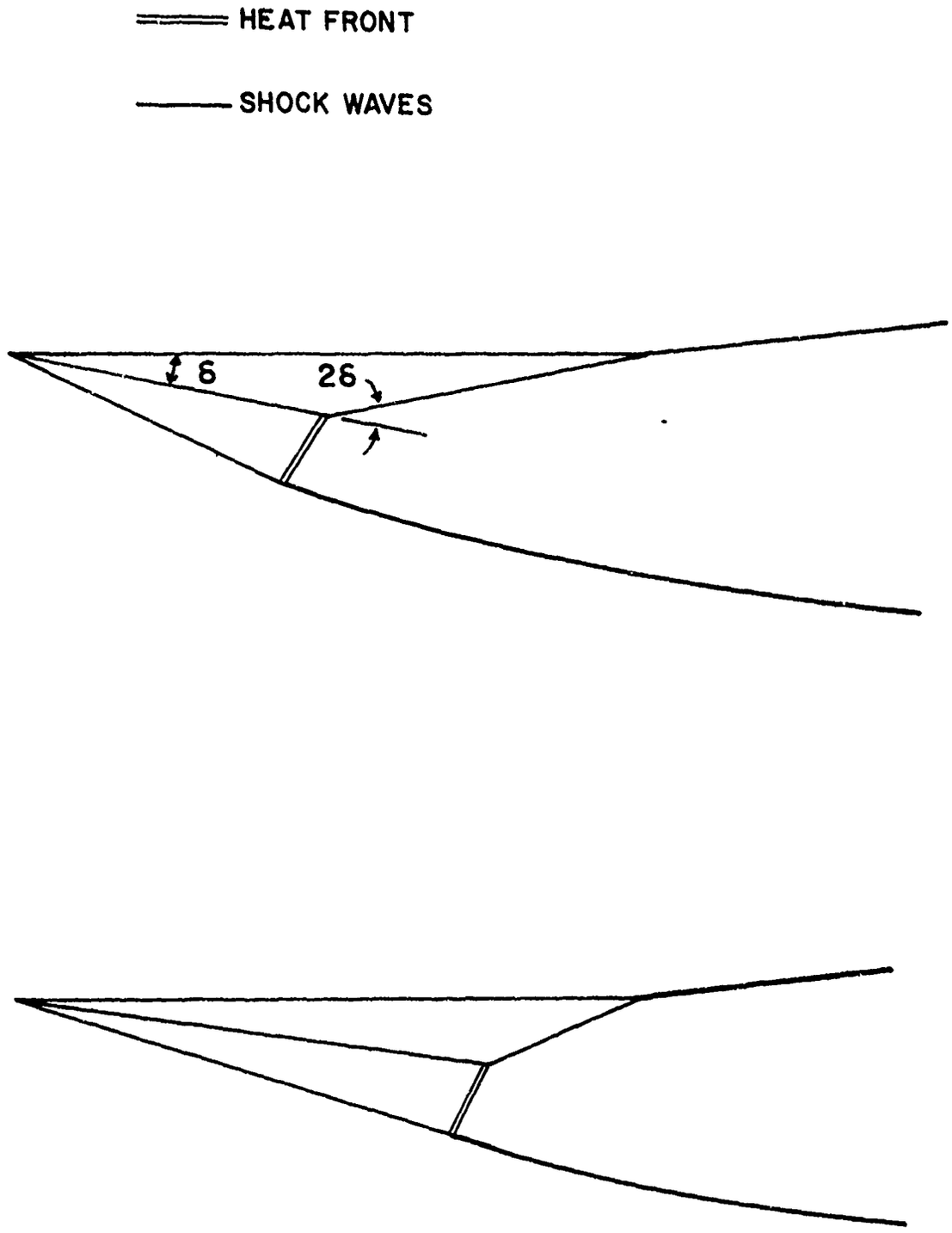

FIGURE 19. EXTERNAL BURNING SCRAMJET.

and Beilock[10]; and for supersonic flow, one uses Equations (22) and (23).

$$\text{curl } \vec{v} = \vec{e}_z\left(\frac{\partial v'}{\partial x} - \frac{\partial u'}{\partial y}\right) \tag{64}$$

Substituting Equations 22 and 23 into Equation (64) yields

$$\text{curl } \vec{v} = \vec{e}_z\left\{\frac{(\gamma - 1)Q}{2\gamma p}\left[-2n(x - \beta y)\,(x - \beta y)\right] + \frac{(\gamma - 1)Q}{2\gamma p\beta}\left[2n\beta(x - \beta y)\,(x - \beta y)\right]\right\} \tag{65}$$

Recall that $\beta^2 = M^2 - 1$. In the above analysis, δ has been represented by

$$\delta(x - \beta y) = \lim_{n\to\infty}\sqrt{\frac{n}{\pi}}\exp\left[-n(x - \beta y)^2\right] \tag{66}$$

Since curl $\vec{v}$ vanishes, one concludes that heat addition does not generate vorticity.

Mass Balance with Heat Addition

To gain additional insight to diabatic flows, it is worthwhile to examine some simple flows using familiar methods. One such case is a mass balance. Consider a heat addition region as shown in Figure 20 with a control volume. Half of the control volume can be used for the mass balance. This half has width w. Writing a continuity equation for mass flux across control volume yields

$$\rho_\infty u_\infty w = (\rho + \rho')v'(L - \beta\ell) + 2(\rho + \bar{\rho}')\bar{v}'\beta\ell + \rho_\infty u_\infty(w - \ell/2) + (\rho_\infty + \rho_w')u\,\ell/2 \tag{67}$$

where $\bar{\rho}'$ and $\bar{v}'$ are averages of perturbation quantities along $\beta\ell$ illustrated in Figure 20. The density perturbation in the wake is ρ_w'. Equation (67) reduces to

$$\rho v'L = -\rho_w' u_\infty \ell/2 \tag{68}$$

when second order terms (e.g., $\rho'v'$) are neglected. This can be rewritten as

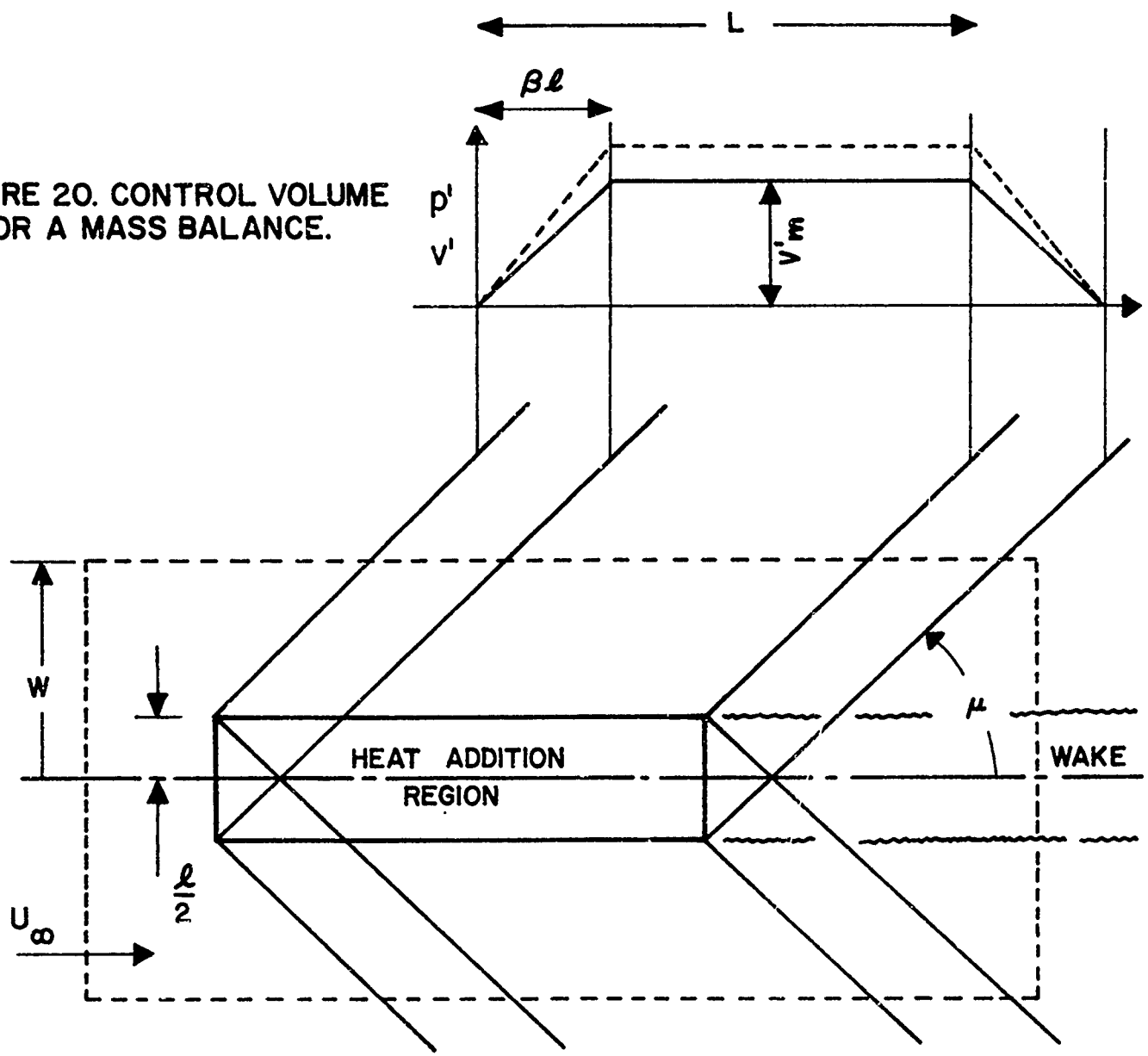

FIGURE 20. CONTROL VOLUME FOR A MASS BALANCE.

$$\frac{v'}{u_\infty} = -\frac{\rho_w'}{\rho}\frac{\ell}{2L} \qquad (69)$$

Substitution of Equations (40) and (42) in (69) gives an equality, as one expects.

EXTERNAL BURNING; THRUST MINUS DRAG

Drag--Subsonic and Supersonic

In subsonic flow of a perfect fluid around a body, there is no force on the body, either lift or drag. Motion of a body through a fluid would require work if there were a drag. This energy would appear in the fluid. For a perfect fluid, the perturbations in the fluid decay rapidly at large distances from the body. If the body has been moving for a long time and if there were drag, there should be significant motion of the fluid at large distances.

In supersonic flow, there is significant motion at large distances even in a perfect fluid. The waves caused by body motion move out from the body eventually decaying to sound waves. Far from the body, the flow consists of outgoing sound waves. These waves carry away energy. Work overcoming drag supplies the energy.

Relation Between Flux of Entropy and Drag

It is well known (See, for example, K. Oswatitsch.[13]) that the flux of entropy through a control surface can be related to drag of a body within the control surface. To get a feeling for the extent of the waves causing drag, a sample problem was worked. The results are shown in Figure 21.

Consider a 20° wedge at Mach 2, as shown in Figure 21. The wave geometry is shown and has been calculated using the method of finite waves. Width of

POINT	ℓ/b	PERCENTAGE DRAG
1	0	25.2
2	5.0	39.3
3	8.7	53.9
4	16.4	69.2
5	37.8	99.0
6	179.	

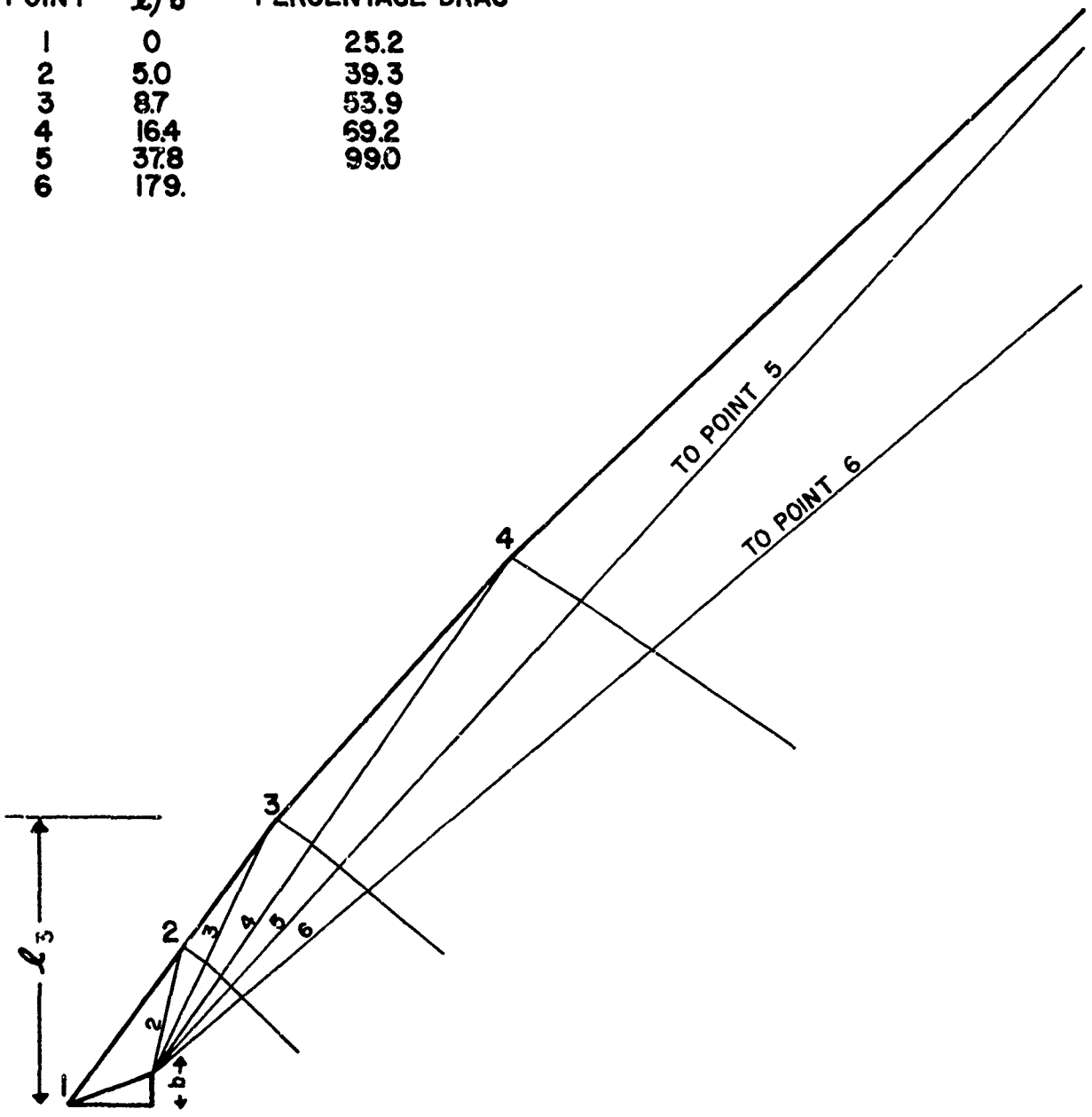

FIGURE 21. FLOW FIELD NEAR A WEDGE AT MACH 2.

the base of the wedge is b. The lateral distance to a point on the shock wave is ℓ. Distance ℓ_3 is illustrated. The flux of entropy in and out of the control volume (neglecting the wake) is equal to entropy jump across the shock wave times the mass flux. The first expansion wave intersects the shock wave at point 2. The wave between points 1 and 2 accounts for 25.2 per cent of wedge drag. The shock wave between points 1 and 3 accounts for 39.3 per cent of the wedge pressure drag. It is necessary to go out 179 base widths to obtain 99 per cent of the drag.

The conclusion from this little study is that the waves are important to great distances from the body. In axisymmetric flow, the bow wave would decay more rapidly.

Linearized Drag Due to Waves

A wave is a mechanism whereby energy can be propagated. The energy takes two forms in the linearized or acoustic case. These are flow work and kinetic energy. It can be shown[14] that an integral over space of the flow work equals the integral over space of kinetic energy. As an example, consider a half-diamond airfoil shown in Figure 22. The airfoil is moved exactly one chord length from position ABC to position DEA, and the undisturbed fluid is at rest. This motion does work Dc where D is the drag and c is the chord. The work appears as energy within the waves. Changes in the fluid motion occur normal to the waves. The disturbance originating at A now appears at A', B at B', C at C', etc. The motion within the wave below A'B'C' is due to earlier airfoil motion to the right of position ABC. The work done by drag moving one chord length appears within the volume, V, bounded by A'B'C'DEA. Consequently

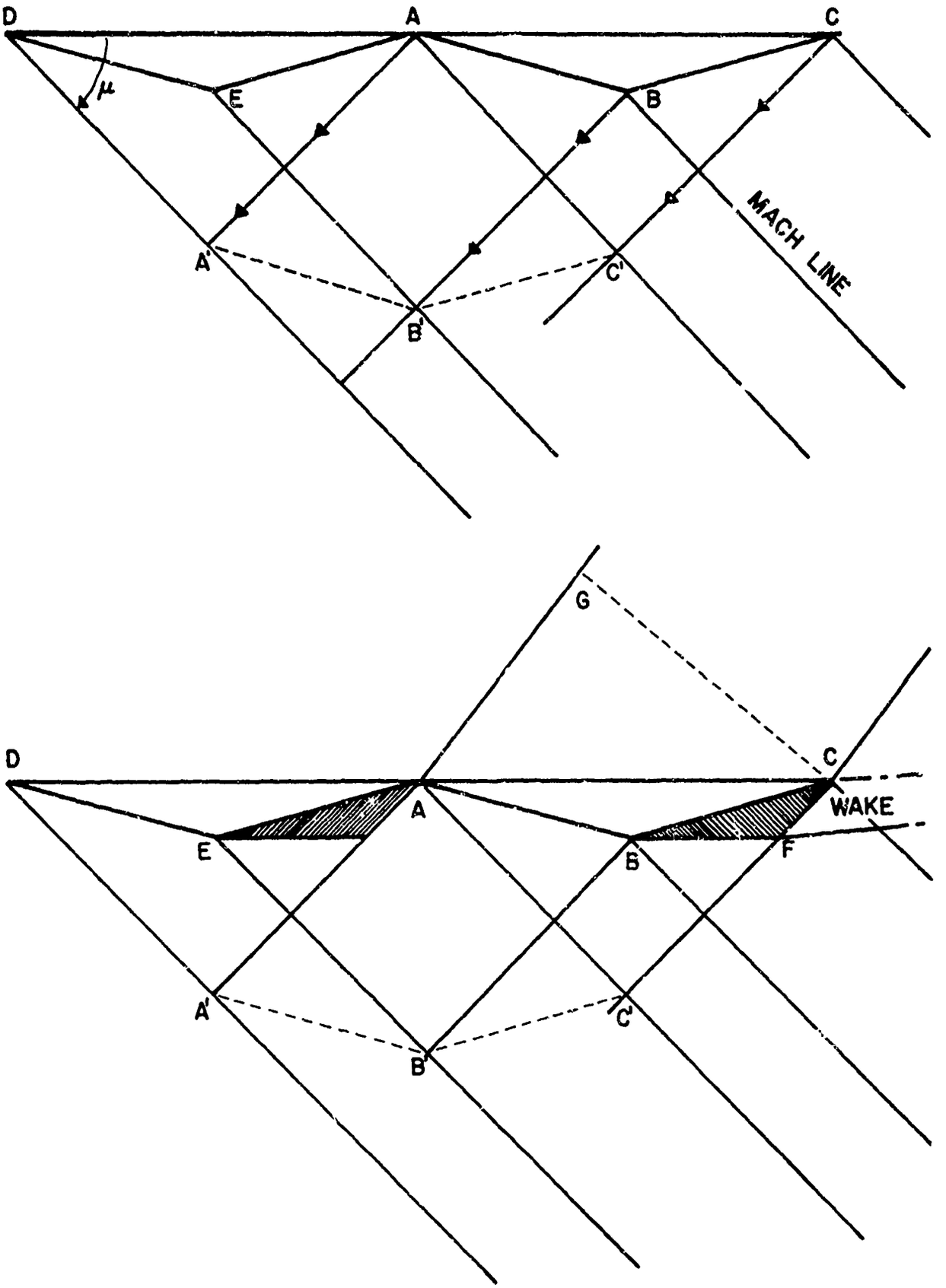

FIGURE 22. DRAG EVALUATION USING WAVE ENERGY.

$$Dc = \int_V \left[\rho\ (U + u)^2 + v^2\right] dV \tag{70}$$

where u and v are perturbation velocities. When there is heat addition, as illustrated in the lower part of Figure 22, Equation (70) changes. The force on the body is now thrust minus drag. Heat has been added. There is a left-running wave, AG, which moves into the fluid above the airfoil. Energy is added to the fluid bounded by ACG. Heat is added in a volume bounded by BFC. Downstream of this region there is a wake. Note that in the region EAC'B' the mass sinks cause u' and v' to be positive* whereas the heat sources cause u" and v" to be negative. In region AAC'B' the mass sinks decrease p whereas heat increases p. The energy equation associated with the waves now is

$$(T - D)c + (\text{heat added}) = \frac{1}{2} \int_V \rho\left[(U + u' + u'')^2 + (v' + v'')^2\right] dV$$

$$+ \int_V pd\left(\frac{1}{\rho}\right) + \int_{WAKE} (\text{energy})dV + \int_{AGC} (\text{energy})dV \tag{71}$$

Equation (71) is more conceptual than quantitative. There are some questions yet to be answered. Does the integral of flow work equal the integral of kinetic energy for waves caused by heat addition? Incorporating heat addition into the waves increases complexity. Can this method of drag and thrust ... ation lead to useful results and new insight? These questions will be

*We use the notation that mass sources cause perturbation velocities u' and v'; heat sources cause perturbation velocities u" and v".

considered in the section Wave Energy Due to Heat Addition which follows shortly.

Linearized Momentum Relations

In two dimensions, x and z, the drag formula in three dimensions is simplified. It becomes

$$D = -\int_C (p - p_\infty)dz - \int_C \rho(U + u)\left[(U + u)dz - wdx\right] \tag{72}$$

The corresponding lift equation is

$$L = \int_C (p - p_\infty)dx + \int_C \rho w\left[wdx - (U + u)dz\right] \tag{73}$$

where C denotes a closed contour surrounding the vehicle or wing. For small perturbations due to mass sources and sinks, the above equations become

$$D = \rho_\infty \int_C uwdx + \frac{1}{2}\rho_\infty \int_C \left[\beta^2 u^2 + w^2\right]dz \tag{74}$$

Note that drag is due to second order terms, i.e., uw, u^2, and w^2. First order terms drop out. For lift the small perturbation form is

$$L = -\rho_\infty U \int_C (udx + wdz) = \rho_\infty U \Gamma \tag{75}$$

In a following section the equivalent formulas for L and D will be derived for combined mass and heat addition. First, consider drag or thrust on a heat addition zone.

To illustrate the application of the heat addition equations, let us calculate the thrust of a line source of length, ℓ, oriented parallel and normal to the stream. Equation (76) is taken from Chapter 7 of Liepmann and Roshko;[15]

$$D = - \int_A (\rho u_1) n_k u_k dA - \int_A p n_1 dA \tag{76}$$

In their notation $x_1 = x$ and $x_2 = y$. The control volume is shown in Figure 23. If Equation (76) is negative, one gets a thrust. Using the numbers for surfaces in control volume:

$$D = - \int_{A_1} (\rho_\infty U)(- U) dA - \int_{A_3} (\rho_\infty - \rho'_{WAKE}) U^2 dA -$$

$$\int_{A_5} (U - u')(\rho_\infty - \rho'_{WAVE})(- 1)(- v') dA - \tag{77}$$

$$\int_{A_6} (U - u')(\rho_\infty - \rho'_{WAVE})(+ 1)(v') dA$$

The integral over A_1 can be integrated. The integral over A_3 can be split into two parts, and the part with ρ_∞ can be integrated. Equations (22) through (25) were derived dropping terms in second order in v'/U, etc. The integrands of A_5 and A_6 reduce to $\rho_\infty U v'$. Consequently, Equation (77) becomes:

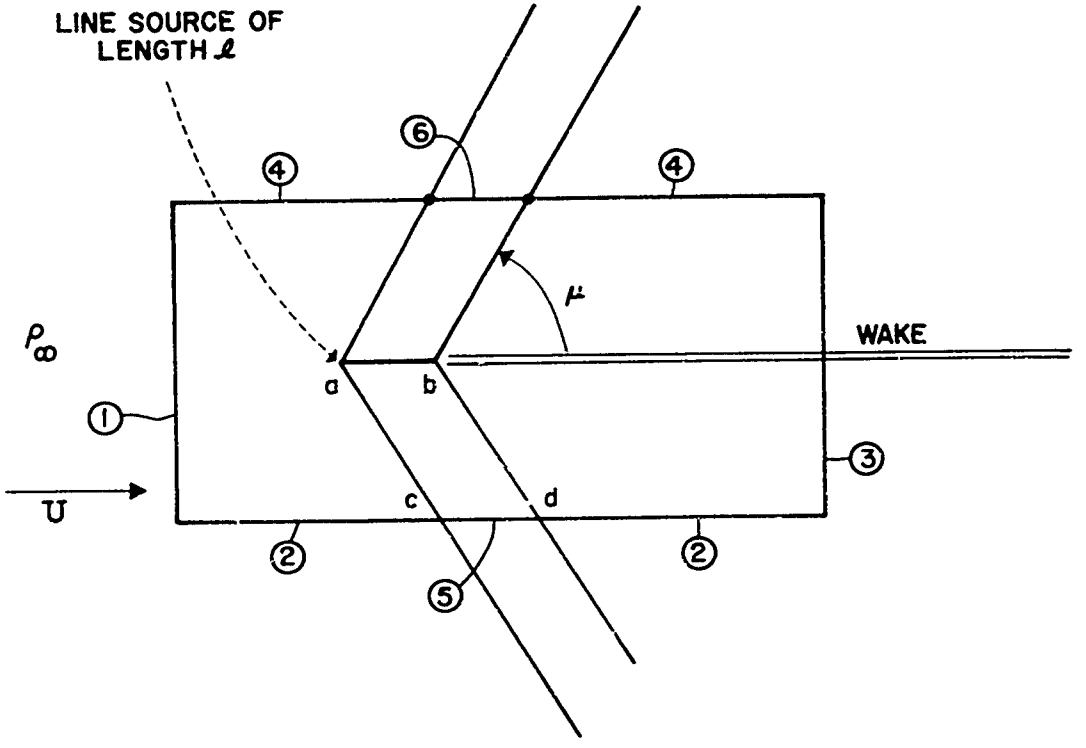

FIGURE 23. CONTROL VOLUME FOR CALCULATING THRUST OF A LINE HEAT SOURCE IN A SUPERSONIC FLOW.

$$D = -\rho_\infty U^2 A_1 + \rho_\infty U^2 A_3 + \int_{A_3} (\rho'_{WAKE}) U^2 dA - 2 \int_{A_5} \rho_\infty U v' dA \tag{78}$$

We now need expressions for ρ'_{WAKE} and v', which we obtain from Equations (25) and (23) respectively. Proceeding with ρ'

$$\rho'_{WAKE}(x,y) = \int_0^{\ell} \frac{(\gamma - 1)q}{a^2 U} \delta(y - y') I(x - x') ds \tag{79}$$

where s is distance along the source; x and y, the coordinates where you want to evaluate ρ'_{WAKE}; and x' and y', the coordinates of an element, ds, of heat source. When $x > x'$, $I = 1$; since we are evaluating A_3-integral, x will be greater than x'. Also $ds = dx'$ for the case at hand.

$$\rho'_{WAKE}(y) = \frac{(\gamma - 1)Q}{a^2 U} \delta(y - y') \int_0^{\ell} dx' = \frac{(\gamma - 1)q\ell}{a^2 U} \delta(y - y') \tag{80}$$

Substituting Equation (80) into A_3-integral of Equation (78), we get

$$\int_{A_3} \rho'_{WAKE} U^2 dA = \int_{A_3} \frac{(\gamma - 1)q\ell}{a^2 U} \delta(y - y') U^2 dy = \frac{(\gamma - 1)q\ell U}{a^2} \tag{81}$$

In a similar manner, an equation can be obtained for v' from Equation (23):

$$v'(x,y) = \int_0^{\ell} \frac{(\gamma - 1)q}{2\gamma p} \delta\left[(x - x') - \beta(y - y')\right] ds \tag{82}$$

Substituting Equation (82) in A_5-integral of Equation (78) yields

$$\int_{A_5} \int_0^{\ell} \rho_\infty U \frac{(\gamma - 1)q}{2\gamma p} \delta\left[(x - x') - \beta(y - y')\right] dx'dx \tag{83}$$

The coordinate system is chosen so that the heat source starts at $x' = 0$ and ends at $x' = \ell$. Also $y' = 0$. The coordinate of point c in Figure 23 is $(\beta y_5, y_5)$, and the coordinate of point d is $(\beta y_5 + \ell, y_5)$. Consequently, the limits of integration are as shown

$$\rho_\infty U \frac{(\gamma - 1)q}{2\gamma p} \int_{\beta y_5}^{\beta y_5 + \ell} \int_0^{\ell} \delta\left[(x - x') - \beta y_5\right] dx'dx \tag{84}$$

A change of variable helps evaluate the integral; let $z = x - \beta y_5$.

$$\rho_\infty U \frac{(\gamma - 1)q}{2\gamma p} \int_0^{\ell} \int_0^{\ell} \delta(z - x')dzdx' = \rho_\infty U \frac{(\gamma - 1)q\ell}{2ap} \tag{85}$$

The integral in Equation (19) is in the standard form as shown in the Appendix so that it is readily apparent that it has value ℓ. Now combine Equations (78), (81), and (85) to give

$$D = \frac{(\gamma - 1)q\ell U}{a^2} - 2\left(\rho_\infty U \frac{(\gamma - 1)q\ell}{2\gamma p}\right) \tag{86}$$

which vanishes since $a^2 = \gamma p/\rho$. Supersonic heat addition in an unconstrained (no walls) flow gives zero thrust or drag.

Now look at the case where the heat source is of length ℓ but normal to the streamlines. This is illustrated in Figure 24. Equations (78), (79), and (82) apply; however, ds is different as is the limit of integration. Put the origin of coordinates at the center of the heat source. Equation (79) becomes

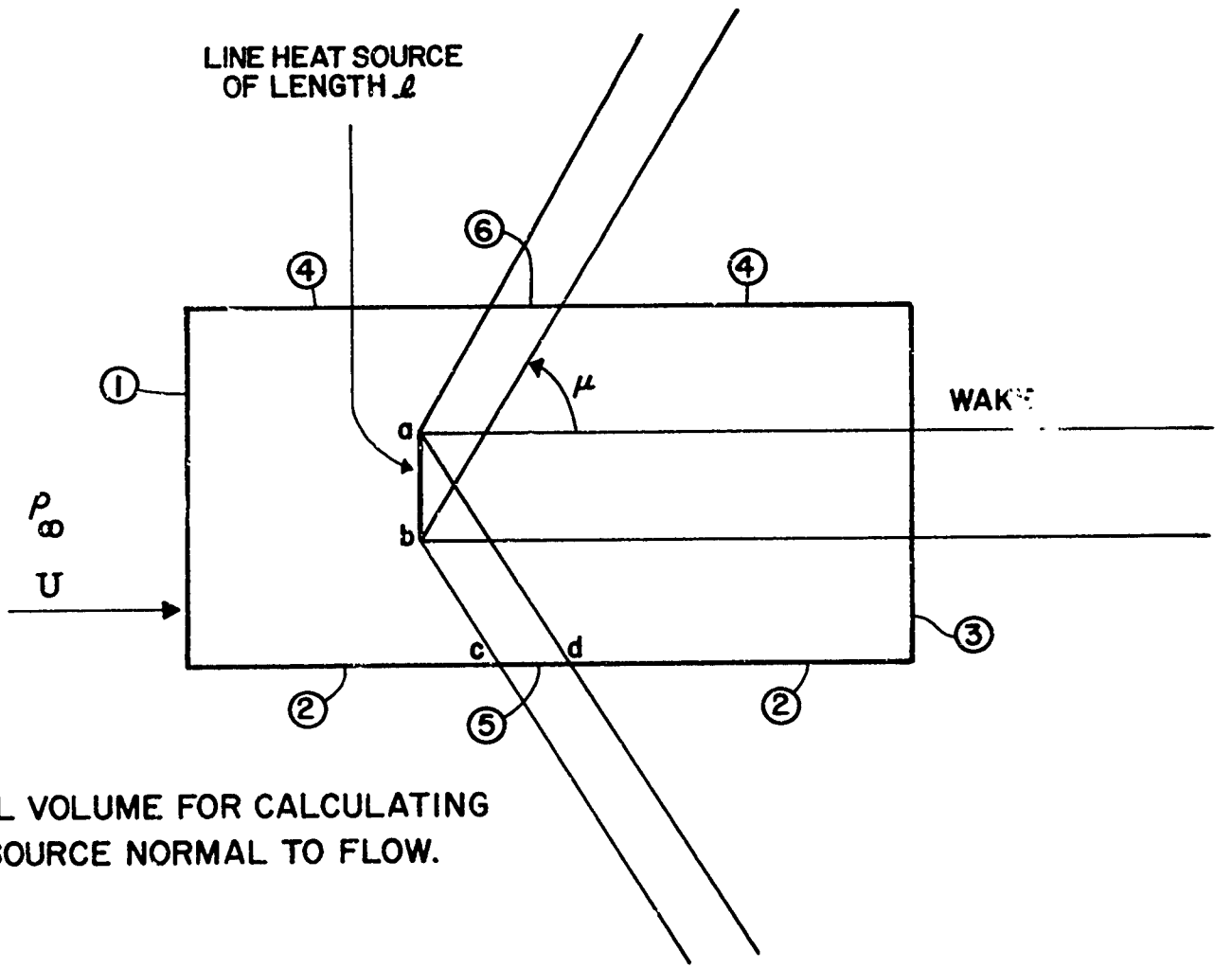

FIGURE 24. CONTROL VOLUME FOR CALCULATING THRUST OF A LINE SOURCE NORMAL TO FLOW.

$$\rho_{WAKE}(y) = \frac{(\gamma - 1)q}{a^2 U} \int_{-\ell/2}^{\ell/2} \delta(y - y')dy' \tag{87}$$

The A_3-integral in Equation (78) becomes

$$\int_{A_3} U^2 \frac{(\gamma - 1)q}{a^2 U} \int_{-\ell/2}^{\ell/2} \delta(y - y')dy'dy = \frac{(\gamma - 1)q\ell U}{a^2} \tag{88}$$

since the integrations over y' and y overlap over the region $-\ell/2$ to $\ell/2$.

For the perturbation velocity, the equation for v' becomes

$$v'(x,y) = \int_{-\ell/2}^{\ell/2} \frac{(\gamma - 1)q}{2\gamma p} \delta\left[x - \beta(y_5 - y')\right] dy' \tag{89}$$

where y_5 is the coordinate for plane A_5. The A_5-integral is

$$\int_{A_5} \rho_\infty U v'dy = \int_{A_5} \int_{-\ell/2}^{\ell/2} \frac{(\gamma - 1)q\rho_\infty U}{2\gamma p} \delta\left[x - \beta(y_5 - y')\right] dy'dx \tag{90}$$

The limits of integration for x are $\beta(y_5 - \ell/2)$ to $\beta(y_5 + \ell/2)$. To obtain a standard form for the integrand, we must eliminate β in the δ-function. This we do by letting $z = \beta(y_5 - y')$ and $dz = -\beta dy'$. Equation (90) is now

$$\rho_\infty U \frac{(\gamma - 1)q}{2\gamma p\beta} \iint \delta(x - z)dzdx = \rho_\infty U \frac{(\gamma - 1)q}{2\gamma p\beta} \left[\beta(y_5 + \frac{\ell}{2}) - \beta(y_5 - \frac{\ell}{2})\right] \tag{91}$$

The limits of integration for both z and x in Equation (91) are $\beta(y_5 - \ell/2)$ to $\beta(y_5 + \ell/2)$. Combining Equations (78), (88), and (91), one finds

$$D = \frac{(\gamma - 1)q\ell U}{a^2} - 2\left(\frac{(\gamma \quad)\eta\ell\rho_\infty U}{2\gamma p}\right) = 0 \tag{92}$$

which is what we expected.

It is interesting to draw the streamlines in the vicinity of the heat sources; see Figure 25. For the parallel heat source there is a conceptual difficulty which has a resolution. The "stagnation" streamline* C goes straight back since v' is an odd function and must be zero at y = 0. One can think of a streamtube bounded by streamlines B and D. Continuing, one can shrink this streamtube so that there is very little mass flow through it. Yet the streamtube diverges at angle θ. A finite amount of heat is added to an infinitesimal stream yielding a finite angle θ. Strange! One avoids this difficulty by using volume heat addition. The case of the heat source normal to the flow is more easily digested. Streamlines F and J are acted upon by characteristics of a single family. Streamline G passes through the heat source into a region where it is influenced by both left-running (gives + v') and right-running (gives - v') characteristics. In this region the streamline is not deviated from its original direction. Streamline G then moves into a region where only left-running characteristics act on it. It is deflected by an amount θ. Finally G moves into the wake where it accelerates and assumes its original direction. The speed along G is (U, U - 2u', U - u', U) as it moves from region to region. Streamline H is in the plane of symmetry; as a result, it does not deviate from freestream direction.

---

*A body will stagnate the flow; however a heat source does not do so.

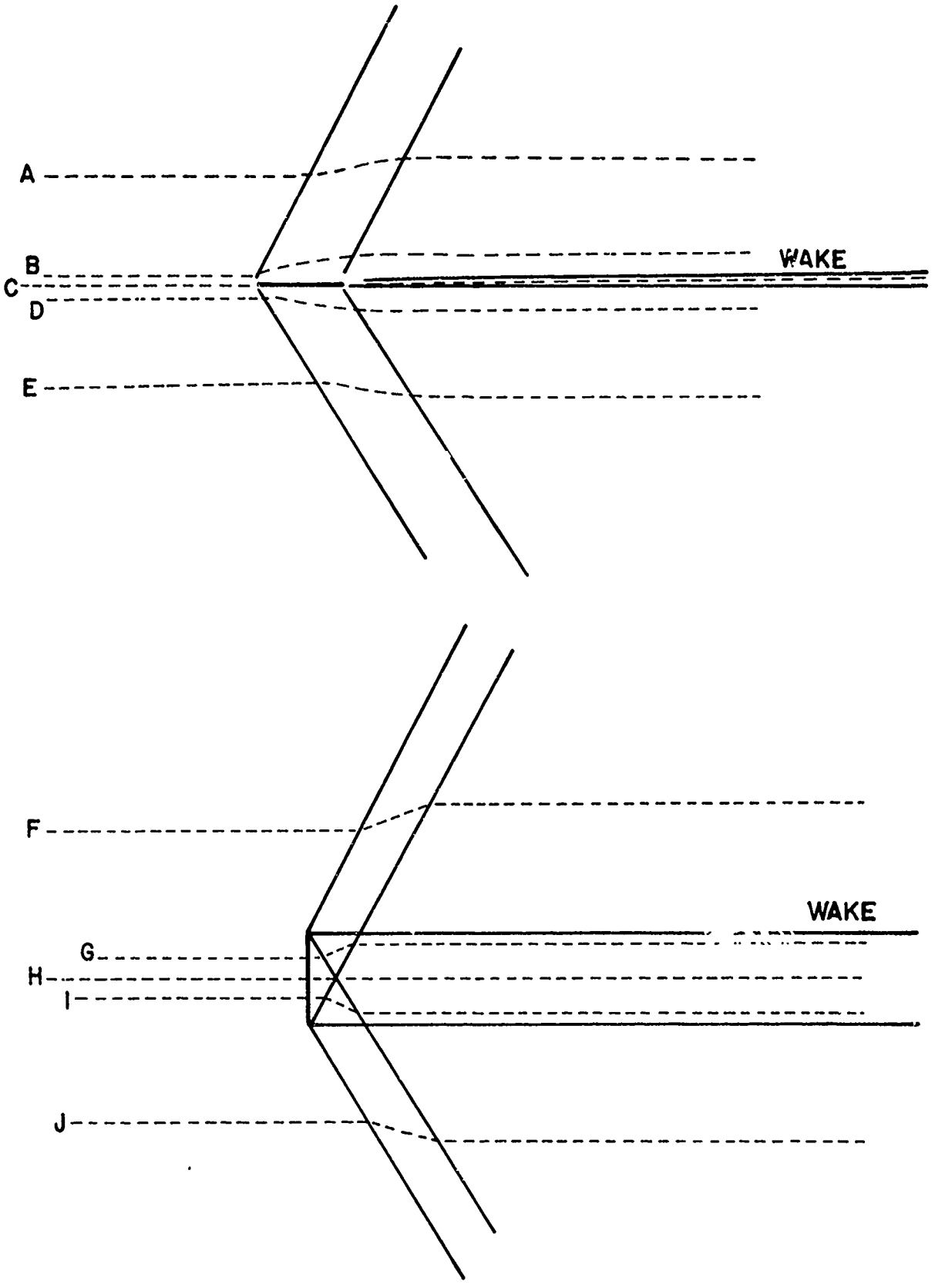

FIGURE 25. STREAMLINES IN VICINITY OF PARALLEL AND NORMAL LINE HEAT SOURCES.

Wave Energy Due to Heat Addition

The model for determining wave energy due to heat addition is shown in Figure 26. A heat addition zone EFGH is translated its own Length L in time L/u_∞. Its new position is AFEL. The heat released is $(h\ell L)(L/u_\infty)$. Since there is no force on the heat addition region, no work is done moving it from EFGH to AFEL. The question of forces on heat addition zones was discussed in the preceding section. All of the heat energy released must appear in the waves and in the wake.

In the time L/u_∞, the disturbance at J has moved to point K. The disturbance at F has moved to B. The dashed lines AC and BD would be streamlines if EFGH were stationary and the fluid moved by. The energy content of space bounded by ANCEL is the same as that inside FJMHE. Part of the energy added appears in the region ABDC. This is the wave energy. The remainder appears in the wake in the region EFGH. From B to P, work is done on the fluid to compress it. From K to D, work is done by the fluid as it expands. The flow work cancels. We are now ready to write the energy equation.

$$\frac{h\ell L^2}{u} = 2\left(\begin{array}{c}\text{kinetic energy}\\ \text{in ABDC}\end{array}\right) + \left(\begin{array}{c}\text{energy in}\\ \text{wake EFGH}\end{array}\right) \tag{93}$$

The factor 2 comes from the fact that waves go both up and down in Figure 26. The kinetic energy in ABDC is

$$\frac{1}{2}\rho_\infty \int_x \int_y u_n^2 dxdy = \frac{1}{2}\rho_\infty \int_0^L \int_0^{L\cos\mu} u_n^2 \sin\mu \, d\xi d\eta \tag{94}$$

where dx and dy have been replaced by a coordinate system $x = \xi$ and $y = \eta \sin\mu$. The symbol u_n represents the perturbation velocity normal to the wave. It is equal to

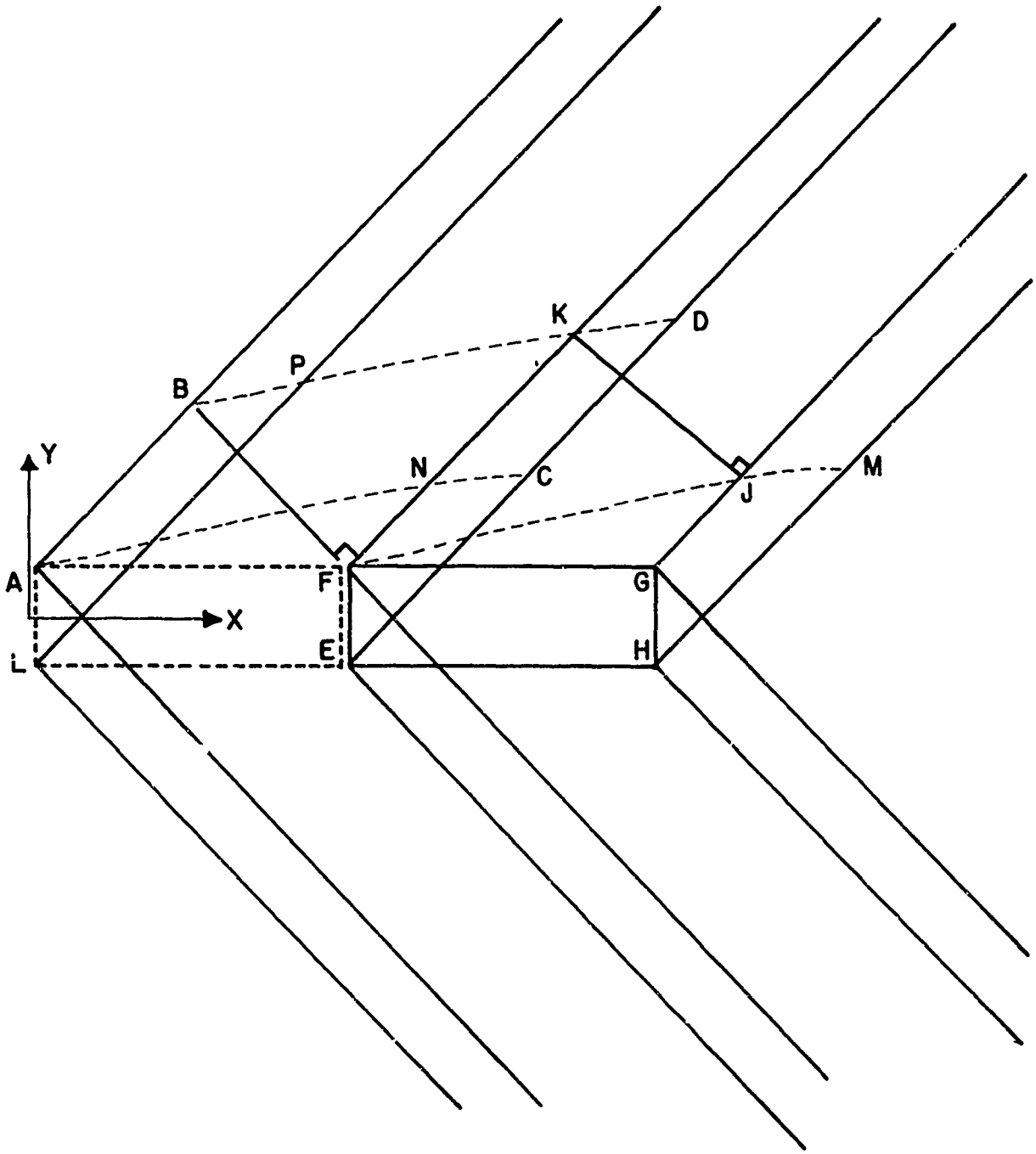

FIGURE 26. WAVE ENERGY DUE TO HEAT ADDITION.

$$u_n^2 = u'^2 + v'^2 \tag{95}$$

where u' and v' are given by Equations (39) and (40) respectively. The magnitude of v' has been plotted in the upper portion of Figure 20. Inserting Equation (95) into Equation (94) and recognizing the functional form of v' (and u') as shown in Figure 20, one arrives at

$$\left(\frac{\text{2KE in ABDC}}{L\rho_\infty \sin\mu\cos\mu}\right) = 2\int_0^{\beta\ell}\left[\left(\frac{u'_m}{\beta\ell}\right)^2 + \left(\frac{v'_m}{\beta\ell}\right)^2\right]\xi^2 d\xi + (u'^2_m + v'^2_m)\int_{\beta\ell}^{L} d\xi \tag{96}$$

The value of v'_m has been indicated in Figure 20. It is the maximum perturbation velocity. Integrating Equation (96) yields

$$\left(\frac{\text{2KE in ABDC}}{L\rho \sin\mu\cos\mu}\right) = \frac{2}{3}(u'^2_m + v'^2_m)\beta\ell + (u'^2_m + v'^2_m)(L - \beta\ell) = \tag{97}$$

$$= (u'^2_m + v'^2_m)\left(L - \frac{\beta\ell}{3}\right)$$

The energy in the wake is

$$\left(\begin{matrix}\text{energy in}\\ \text{wake EFGH}\end{matrix}\right) = \rho_\infty c_p L\ell(T_w - T_\infty) = \rho_\infty c_p T_\infty L\ell\frac{T'}{T_\infty} \tag{98}$$

The distance FG is the length L. According to small perturbation results, the wake has freestream velocity and pressure but reduced density and increased temperature. Knowing these facts and using $p = \rho RT$, Equation (98) becomes

$$\left(\begin{matrix}\text{energy in}\\ \text{wake EFGH}\end{matrix}\right) = c_p T_\infty L\ell\rho'_w \tag{99}$$

The density perturbation in the wake ρ'_w can be obtained from Equation (44).

Substituting Equations (39) and (40) into Equation (97), substituting Equation (44) into Equation (99), and combining the results in Equation (93) yields

$$\frac{Q\ell L^2}{u_\infty} = \frac{\rho_\infty L}{\beta}\left(L - \frac{\ell\beta}{3}\right)\left[\frac{(\gamma - 1)Q\ell}{2\gamma p}\right]^2 + c_p T_\infty L^2 \ell Q \frac{\gamma - 1}{a^2 u_\infty} \qquad (100)$$

WAVE ENERGY WAKE ENERGY

From Equation (100) it is apparent that the energy appearing in the waves is second order. The wave energy was based on $u_m'^2 + v_m'^2$ which is second order. The wake energy reduces to $Q\ell L^2/u_\infty$. If Equation (100) is to be an equation, the wave energy must be neglected.

There are some important conclusions from this exercise. First, the wave energy is second order. Second, most of the energy due to heat addition appears in the wake. Energy radiated away by waves is small compared to energy deposited in the wake.

If one examines the linearized momentum equations in two dimensions, as given in the section, Linearized Momentum Equations, one finds drag is related to an integral of second order terms. As shown in the discussion of Figure 21, drag can be related to the waves generated by motion of a body. A conclusion is that wave energy resulting from either drag or heat addition is second order in the perturbation quantities.

Control Volume Approach to Thrust Minus Drag with Heat Addition

As an example of a two-dimensional planar flow, examine Figure 27. A half diamond has a region of volume heat addition indicated as a shaded area. The dotted lines outline an image heat addition region above the shaded region. Part of a control volume boundary is shown as a dashed line. Mach lines are drawn from the body to the boundary of the control surface. Below the boundary are plotted the perturbation quantities for that location on the boundary. At the very bottom are the pressure, source strength, u' and v'. These are constant to mid chord and then switch to values opposite in sign.

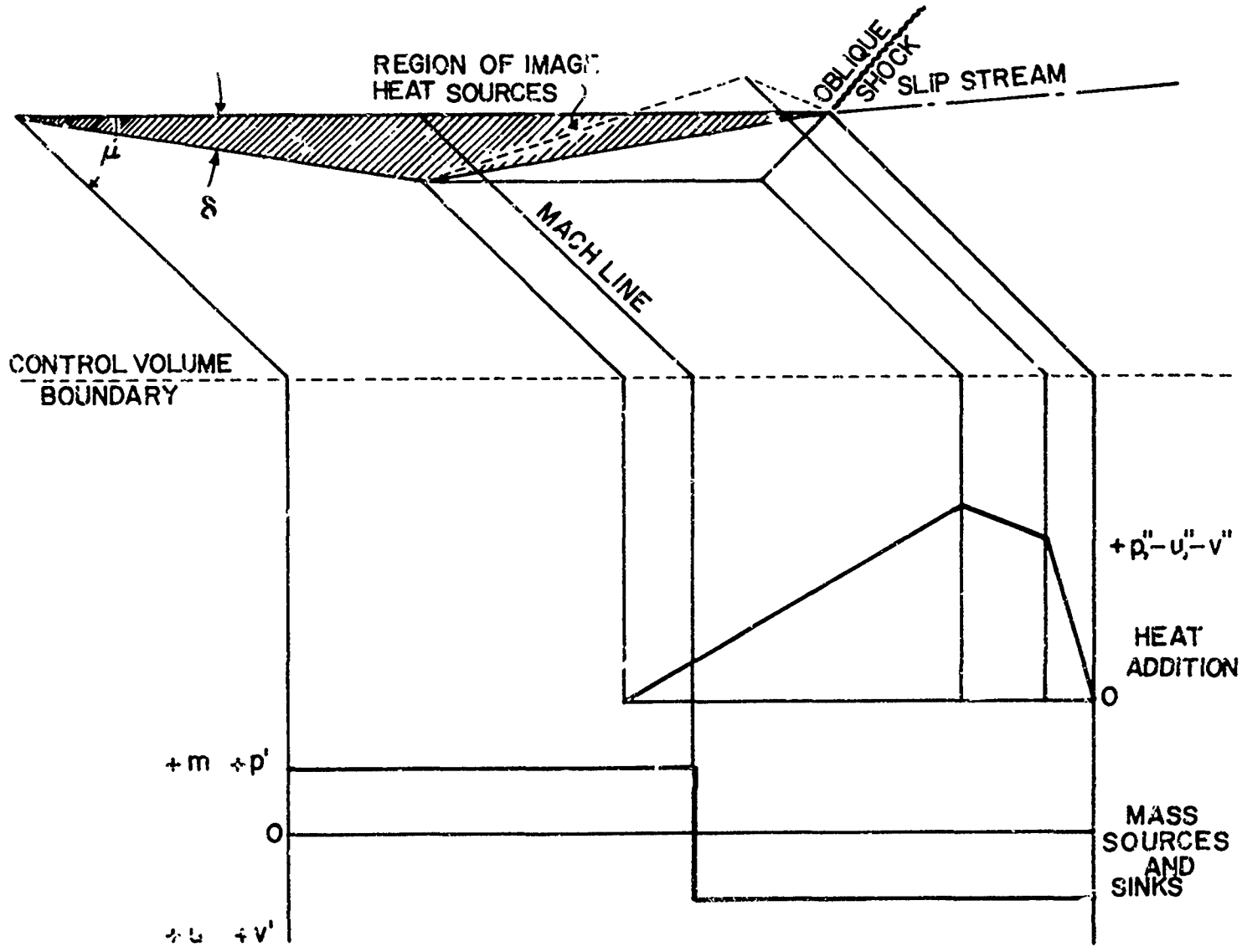

FIGURE 27. CONTROL VOLUME APPROACH TO DRAG AND THRUST.

The perturbation quantities due to heat addition are plotted about the right-hand side of mid-page. Heat addition increases pressure, slows the flow, and deflects it downward. If the two plots were to scale, the positive pressure increment due to heat addition would exceed the negative increment due to flow expansion (mass sinks). The body would have positive thrust minus drag.

The magnitudes of the perturbations due to heat addition are proportional to the length of the characteristic (Mach line) passing through the heat addition regions both real and image. Note that p', p", u', u", v', and v" are of opposite signs.

Let's look at drag and lift contributions due to the portion of control volume shown. In Equation (72) dz is zero. Hence the drag contribution

$$D = \int \rho(U + u' + u")(w' + w")dx \tag{101}$$

Multiplying the terms yields

$$D = \int \underset{1}{(\rho Uw')} + \underset{2}{\rho Uw"} + \underset{3}{\rho u'w'} + \underset{4}{\rho u'w"} + \underset{5}{\rho u"w'} + \underset{6}{\rho u"w"})dx \tag{102}$$

The following summary gives the contributions (+), 0, or (-).

Term	1	2	3	4	5	6
0 to c/2	(-)	0	(+)	0	0	0
c/2 to c	(+)	(-)	(+)	(-)	(-)	(+)

The integral of $\rho Uw'$ over a full chord gives zero; however, the integral of $\rho Uw"$ makes a large thrust contribution. Terms 3 and 6 give drag, whereas terms 2, 4, and 5 give thrust.

Lift is obtained from Equation (73). Once again for the segment of control volume illustrated, dz is zero. The lift contribution becomes

$$L = \underset{1}{\int}(p' + p'')dx + \underset{3}{\int}\rho(w'^2 + 2w'w'' + w''^2)dx \qquad (103)$$
$$\qquad\qquad 2 \qquad\qquad\quad 4 \quad 5$$

The following summary gives the contributions of the various terms.

Term	1	2	3	4	5
0 to c/2	(+)	0	(+)	0	0
c/2 to c	(-)	(+)	(+)	(-)	(+)

The pressure p' averages to zero, whereas p'' gives a lift. The cross term w'w'' reduces lift.

To optimize the heat addition, the airfoil shape must be expressed analytically. Heat addition also needs to be described by some function of x and z. Heat release need not necessarily be uniform.

Thrust from Cycle Point-of-View

The thrust due to a propulsion device is given by

$$F = \dot{m}(w - w_\infty) + A_e(p_e - p_\infty) \qquad (104)$$

If one evaluates the equation at the Trefftzplane, the pressure term may or may not drop out. This is one item which Oswatitsch[11] discusses. In Equation (104), F is thrust, and $\dot{m}$ is mass flow rate of fluid which receives a velocity increase $w - w_\infty$ over the freestream velocity w_∞.

Consider three flows as shown in Figure 28. Heat is added at stagnation conditions and at some Mach number other than zero. The pressures at the exhausts are all equal, i.e., $p_\infty = p_4 = p_2' = p_2''$. The Mollier Chart which depicts

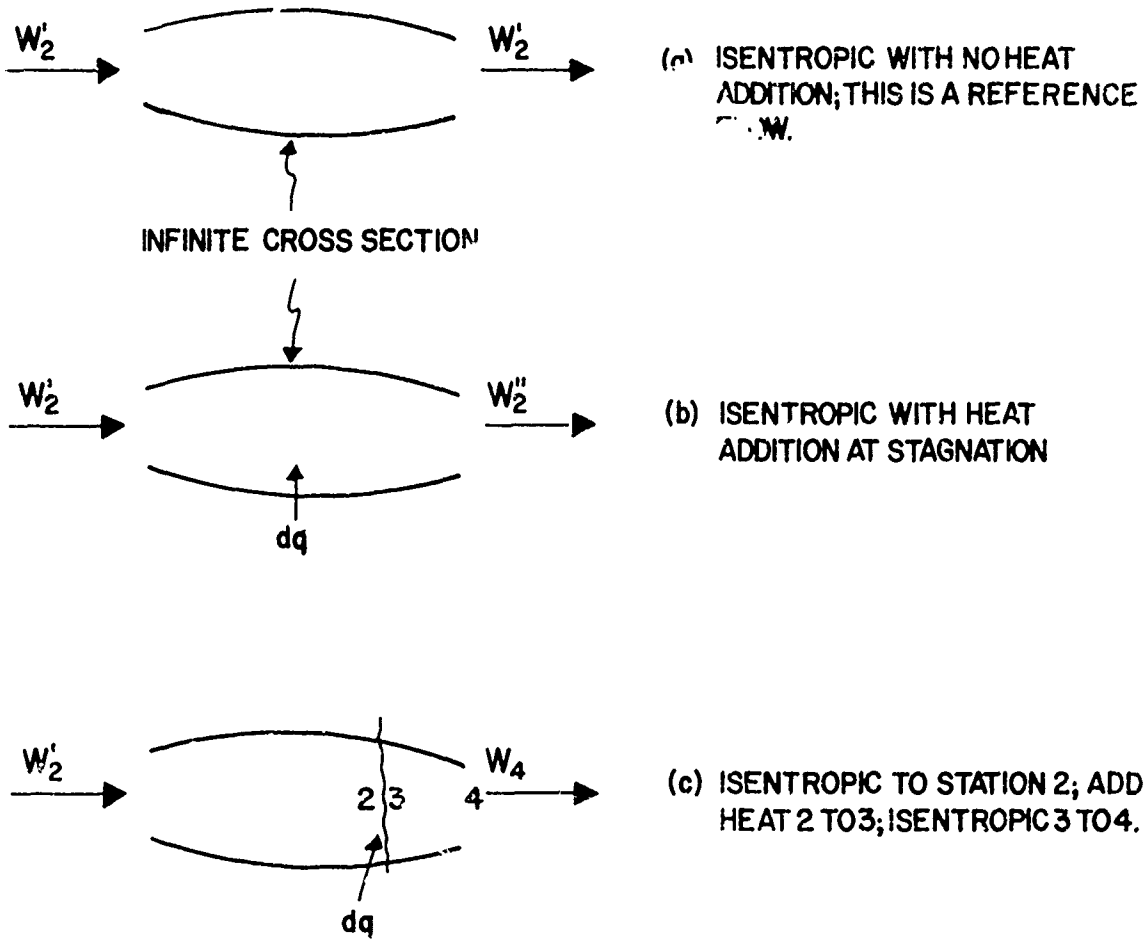

FIGURE 28. THREE FLOWS WITH TWO DIFFERENT WAYS OF ADDING HEAT.

the three flows is shown in Figure 29. It is apparent from energy considerations that

$$dq + \frac{1}{2}w_2'^2 = \frac{1}{2}w_4^2 + (h_4 - h_2') \tag{105}$$

Continuing

$$\frac{1}{2}(w_4^2 - w_2'^2) \cong wdw = dq - (h_4 - h_2') \tag{106}$$

Now

$$\left.\begin{array}{l} dw > 0 \\ w_4 > w_2' \end{array}\right\} \quad \text{if } dq > (h_4 - h_2') \cong dh \tag{107}$$

The slope of a p = constant curve is

$$\left.\frac{\partial h}{\partial s}\right|_p = T \tag{108}$$

Combining Equations (106) and (108) leads to

$$wdw = dq - dh = dq - \left.\frac{\partial h}{\partial s}\right|_p ds \tag{109}$$

The change in entropy of the flow is given by

$$ds = \frac{dq}{T_q} \tag{110}$$

A subscript q is used to indicate this is the temperature at which heat is added. Equations (109) and (110) yield

$$wdw = dq(1 - \frac{T}{T_q}) \tag{111}$$

If one compares flow (a) with flow (b) of Figure 28, then the temperature ratio in Equation (111) is T_2'/T_{T2}. If one compares flow (a) with flow (c), the temperature ratio is T_2'/T_2. To have $dw > 0$, one must have $T < T_q$.

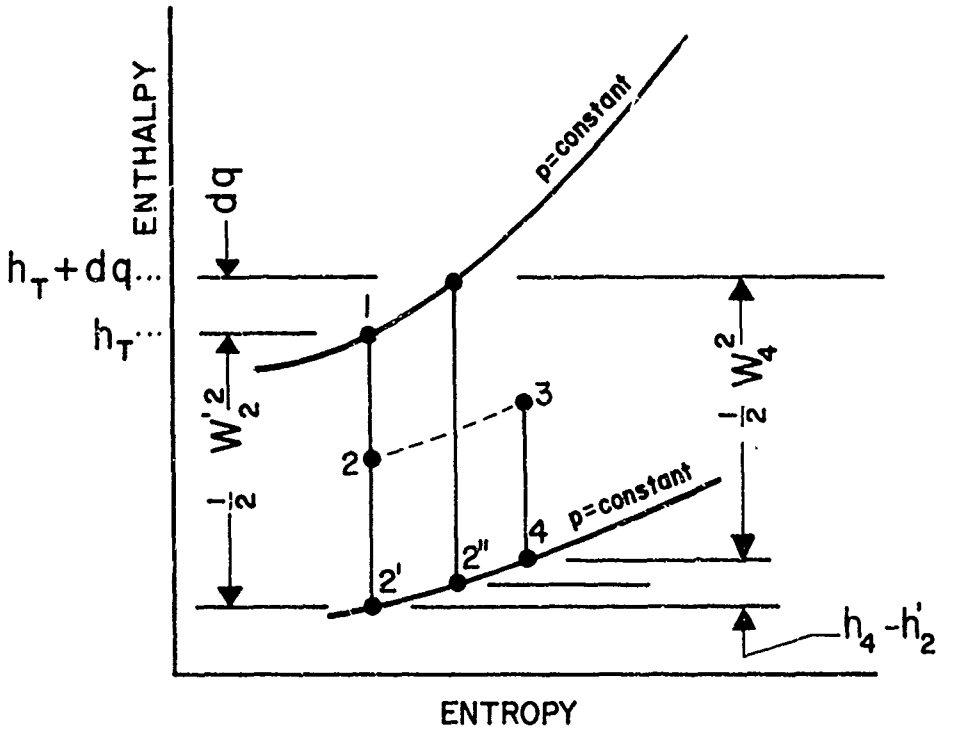

FIGURE 29. MOLLIER DIAGRAM FOR HEAT ADDITION.

As a numerical example, consider flight at M = 0.9. Heat is added at M = 0 in flow (b) and at M_2 = 0.5 in flow (c). Enough heat is added to accelerate the flow so that M_3 = 0.6. The same amount of heat is added in flow (b). The results are that $w_4/w_2' = 1.055$ and $w_2''/w_2' = 1.091$.

Equation (111) is not usually applicable to supersonic or hypersonic flow. The entropy change in the exhaust was attributed solely to heat addition. In supersonic flow, shock waves cause entropy changes. Furthermore heat addition may alter the shock wave geometry.

Thrust and Drag in Various Flow Regimes

For subsonic flow, the pressure term in Equation (104) is zero. For supersonic flow, the pressure term if evaluated in the Trefftzplane is not zero; however, it is extremely small. To see that the pressure is not zero, examine the flow illustrated in Figure 30. The entropy in the Trefftzplane is greater than ambient; $ds > 0$. If dp were zero, then $\rho w dw$ equals $-Tds$ so that $dw < 0$. Entropy is related to p and T by $Tds = c_p dT - dp/\rho = c_p dT$. Consequently $dT > 0$. From $p = \rho RT$, it follows $d\rho/\rho < 0$. The continuity equation ρwA must be satisfied. As shown in Figure 30, the streamtube area A does not change significantly. The changes in both ρ and w cannot be negative and still satisfy continuity. If $dp > 0$, then dw continues to be less than zero and $dT > 0$. Also $dp/p > dT/T$. Consequently $d\rho > 0$.

To account for the drag, the area A must be quite large. (See Figure 21.) The streamtube influenced by a propulsion system will be small as shown in Figure 30. It is an area of approximately A_e in Equation (104). The pressure at the Trefftzplane is due mainly to drag and is spread over area A, albeit not uniformly. The pressure term in the thrust equation is applicable to area A_e.

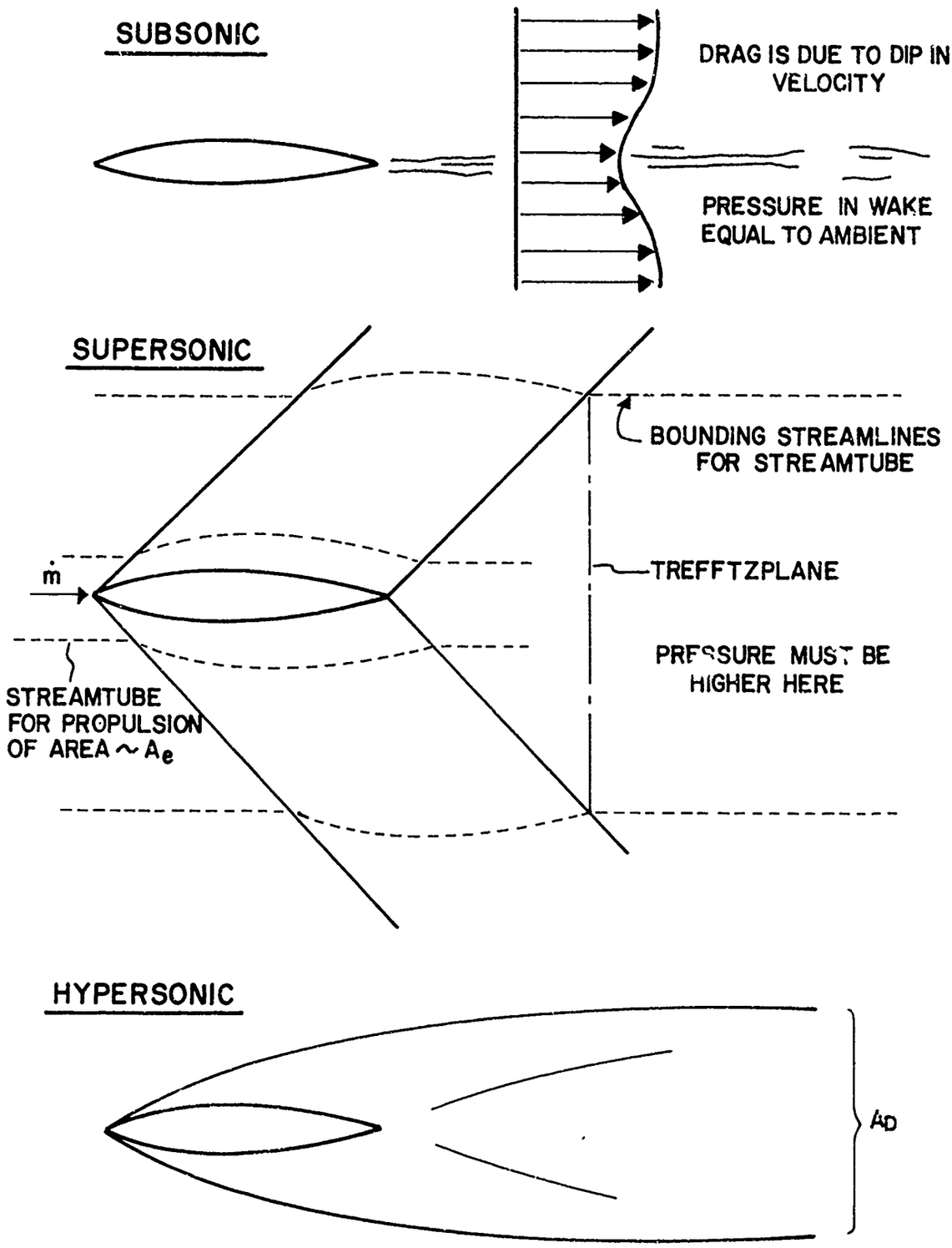

FIGURE 30. DRAG IN DIFFERENT FLIGHT REGIMES.

Since thrust equals drag, the pressure term will be of the order of A_e/A. It can be neglected for subsonic, transonic, and supersonic flow.

For slender bodies in hypersonic flow, dw/w is small. If the thickness ratio is τ = (thickness)/(body length), then dw/w is of the order τ^2. Heat addition also has little influence on dw/w, a fact that can be verified by examining Figure 7.3 in Volume I of A. H. Shapiro's The Dynamics and Thermodynamics of Compressible Fluid Flow.[7] In hypersonic flow, heat addition causes large changes in pressure and static temperature.

In hypersonic flow, the shock waves are close to the body. The drag is concentrated in a small area, A_D; see Figure 30. Thrust producing devices would influence an area comparable to A_D. Consequently, the pressure term in Equation (104) must be retained as a significant factor.

One can calculate forces on a body by suitable integration of pressure. Pressure in excess of ambient on forward-facing surfaces causes drag; define this as pressure drag, D_p. Pressure less than ambient on rearward-facing surfaces causes drag; define this as suction drag, D_s. The ratio D_s/D_p is shown in Figure 31 as a function of Mach number. Suction drag is very important in subsonic, transonic, and supersonic flow. However, as M becomes large and enters the hypersonic region, D_s becomes insignificant. In fact, Newtonian theory assumes ambient pressure p_∞ is zero with the result $D_s = 0$.

A propulsion device will increase pressure on rearward surfaces as shown in Figure 31. Heat addition must increase pressure so that the area under the curve labelled "with heat" equals the area under the curve, D_p. In supersonic flow, the thrust device simultaneously cancels a large D_s and balances D_p.

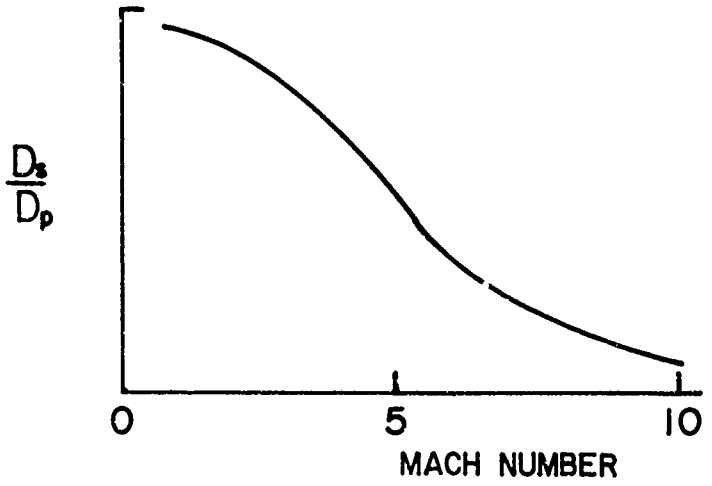

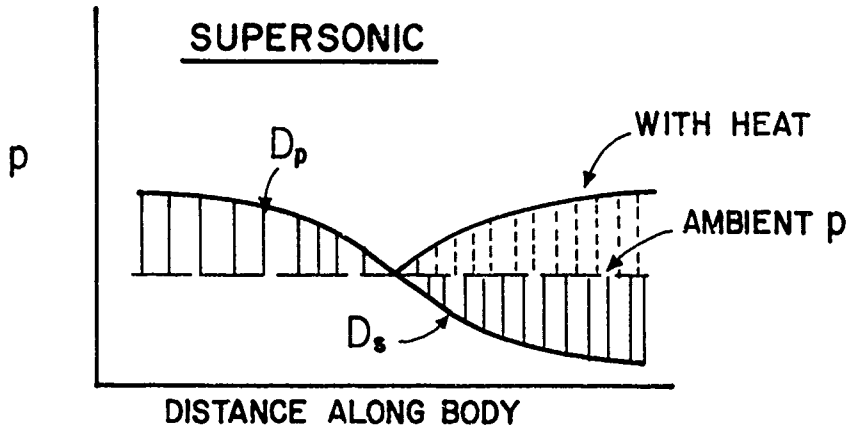

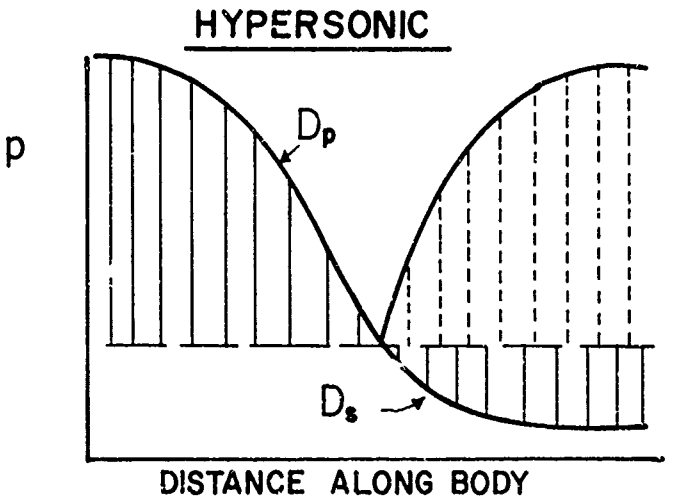

FIGURE 31 CONTRIBUTIONS TO DRAG AND THRUST.

In hypersonic flow, the thrust device does the same thing except that in hypersonic flow D_s is negligible. Heat addition in hypersonic flow balances D_p but counteracts only an insignificant D_s. This has implications concerning propulsion efficiency.

One more point is that in hypersonic flow D_p is the major drag contribution, and this can be related to the bow shock wave. In supersonic flow, D_d is important also so that the waves originating at the rear end of the body or at the rearward-facing surfaces are of equal importance to the bow shock wave in calculating drag.

Contrast in Thrust at Supersonic and Hypersonic Speeds

Consider a body immersed in a flow as shown in Figure 30. The force on the body in the direction of the freestream is

$$F = \int_A \left[(\rho u^2 - \rho_\infty u_\infty^2) + (p - p_\infty)\right] dydz \qquad (112)$$

If there is no energy addition and if A is the area of the large streamtube, F equals D. (It has been assumed that expansion waves have made pressure increments negligible along the streamline from a to b in Figure 30.) If there is energy addition to the stream and if A is, once again, the Trefftzplane in Figure 30, Equation (112) yields thrust minus drag. If one evaluates Equation (112) using the small streamtube in Figure 30 with flow $\dot{m}$, then F is approximately thrust.*

*It is not, of course, possible to separate out the thrust accurately using Equation (112). If it were possible, how much more simple the propulsion integration problem would be.

The continuity equation is, neglecting fuel added,

$$0 = \int_A (\rho u - \rho_\infty u_\infty) dydz \tag{113}$$

The energy equation in integral form is

$$0 = \int_A \left[\rho u \left(h + \frac{u^2 + v^2}{2} \right) - \rho_\infty u_\infty \left(h_\infty + \frac{u_\infty^2}{2} + q \right) \right] dydz \tag{114}$$

In Equation (114), q is the heat added per unit mass, and v is the component of velocity normal to the freestream. By combining the preceding equations in the following way

$$(u_\infty \times \text{thrust}) + \left(h_\infty + q - \frac{u_\infty}{2}\right) \times \text{continuity} - \text{energy} = u_\infty F$$

one obtains

$$u_\infty F = \int_A \left[\rho u (h_\infty - h + q) + u_\infty (p - p_\infty) - \rho u \frac{(u - u_\infty)^2 + v^2}{2} \right] dydz \tag{115}$$

Substituting $h = e + p/\rho$ into Equation (115) yields

$$u_\infty F = \int_A \left\{ \rho u \left[q - (e - e_\infty) \right] - p(u - u_\infty) - \rho u \frac{(u - u_\infty)^2 + v^2}{} \right\} dydz \tag{116}$$

There are three terms in the integrand of Equation (116). The term $\rho u(e - e_\infty)$ is the flux of energy thrown away in the jet. The term $\rho u\left[q - (e - e_\infty)\right]$ is the energy converted to work or jet kinetic energy. The term $p(u - u_\infty)$ is the flow work, and the last term in the integrand is the flux of kinetic energy of the

jet relative to the stationary surroundings. The left-hand side is the rate at which the thrust does work in overcoming drag.

For transonic and supersonic flow, all terms are important. In hypersonic flow, $(u - u_\infty)/u_\infty$, $v/u_\infty \ll 1$. Changes in velocity due either to shock waves or heat addition are small. However $\Delta p/p_\infty$, $\Delta T/T_\infty$, or $\Delta\rho/\rho_\infty$ are of the order of unity or larger. Based on these comments, one can neglect the jet kinetic energy in hypersonic flow. In hypersonic flow, the term $p(u - u_\infty)$ varies as $1/M^2$ as will now be demonstrated. Rewriting the term as

$$p(u - u_\infty) = p_\infty u_\infty \left(1 + \frac{\Delta p}{p_\infty}\right)\left(\frac{u}{u_\infty} - 1\right)$$

one can introduce the Mach number dependence. In hypersonic flow, $\Delta p/p_\infty \sim K^2$ where K is the hypersonic similarity parameter τM. The velocity perturbation varies as τ^2 as discussed previously. Substitution of these quantities into the flow work term yields

$$p(u - u_\infty) = \frac{p_\infty u_\infty}{M^2}(1 + K^2)(K^2) \tag{117}$$

Compared to the heat addition term in Equation (116), the term $p(u - u_\infty)$ is small for $M \gg 1$ and $K = O(1)$.* Equation (116) reduces to

$$F = \int_A \rho\left[q - (e - e_\infty)\right]dydz \tag{118}$$

which is valid for $M >> 1$ and $K = O(1)$. In hypersonic flow, Equation (118) tells us that the thrust is simply due to the heat added less the amount of internal energy thrown away in the exhaust. In supersonic flow, it is more complex; see Equation (116).

---

*Requiring $K = O(1)$ is not a severe restriction.

APPLICATIONS OF EXTERNAL BURNING

In the preceding sections some of the analytical tools for understanding external burning have been discussed. It is worthwhile to look at some possible applications of external burning. Four applications will be examined briefly in the following section; these are forces on a planar airfoil due to heat addition, transonic boattail and base pressure alleviation, base pressure modification in both the planar and axisymmetric cases, and spin recovery of aircraft.

Before discussing the applications, a model for pressure rise due to heat addition near a flat plat will be discussed. This model uses some of the results from EXTERNAL BURNING; BASIC EQUATIONS AND SOLUTIONS and from EXTERNAL BURNING; THRUST MINUS DRAG. The model is a refinement of a similar model by Billig.[16]

Model for Heat Addition Adjacent to a Flat Plate

Figure 32 illustrates the geometry. There are three zones. Zone I is the freestream which is supersonic. Zone II is the heat addition region separated from Zone I by a heat front. Zone II is bounded by the wall, heat front, and streamline c Zone III is downstream of the oblique shock comprising the region below streamline c. The heat addition turns the flow by an angle θ. The streamline deflection angles and static pressures in regions II and III must be equal along streamline c. In the following development, terms in θ^2 are dropped as being negligible.

The deflection angle is approximately:

$$\theta = \frac{y_3 - y_1}{x} \tag{119}$$

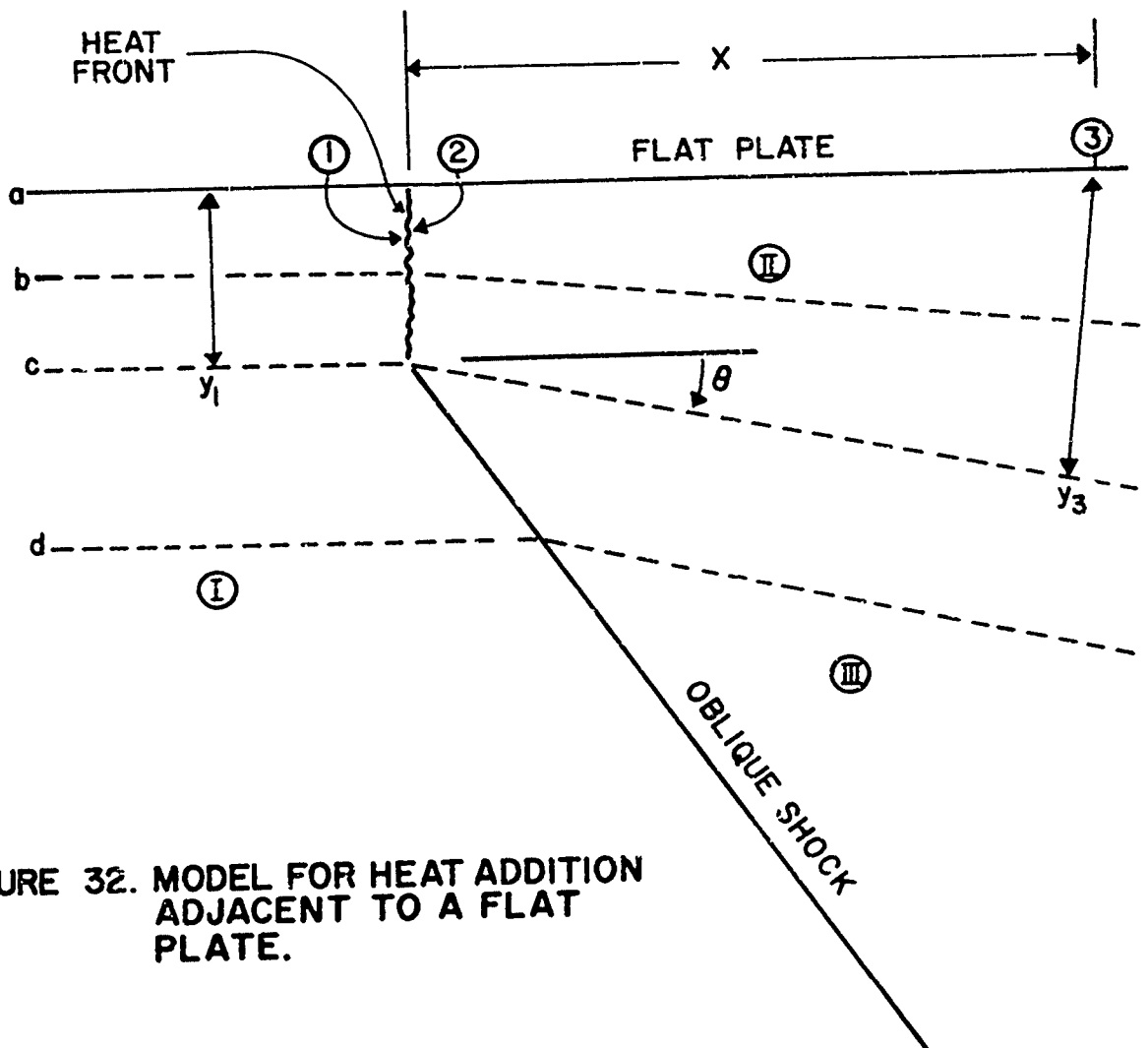

FIGURE 32. MODEL FOR HEAT ADDITION ADJACENT TO A FLAT PLATE.

The continuity equation is

$$\rho_1 u_1 y_1 - \rho_3 u_3 y_3 = \rho_3 u_3 (y_1 + \theta x) = \rho_2 u_2 y_2 \tag{120}$$

Across the oblique shock there is a pressure increase equal to

$$\frac{p_2 - p_1}{p_1} = \frac{\gamma M_1^2 \theta}{\sqrt{M_1^2 - 1}} = \frac{\gamma M_1^2 \theta}{\beta} \tag{121}$$

Equation (121) defines β. Define Q' as the heat addition per unit mass of air flowing in the streamtube defined by streamlines a and c. The energy equation is

$$c_p T_{T1} + Q'_{13} = c_p T_{T3} \tag{122}$$

or as

$$c_p T_{T2} + Q'_{23} = c_p T_{T3} \tag{122}$$

Using Equation (7.14) from Liepmann and Roshko,[15] one can derive the following momentum equation

$$- \rho_2 u_2^2 y_2 + \rho_3 u_3^2 y_3 - p_2 y_2 + p_3 y_3 - p_2 \theta x = 0 \tag{123}$$

Combining equations (119), (120), and (123) yields

$$\rho_2 u_2 y_2 (u_3 - u_2) + (p_3 - p_2)(y_2 + \theta x) = 0 \tag{124}$$

A solution exists for $u_3 = u_2$ and $p_3 = p_2$. Let's examine the consequences of that solution. From the continuity equation and equation of state

$$\frac{p_2 u_2 y_2}{T_2} = \frac{p_3 u_3 y_3}{T_3} \tag{125}$$

Since $u_3 = u_2$ and $p_3 = p_2$, this reduces to

$$\frac{T_3}{T_2} = \frac{y_3}{y_2} \tag{126}$$

The energy equation becomes

$$c_p T_2 + \frac{1}{2}u_2^2 + Q'_{23} = c_p T_3 + \frac{1}{2}u_3^2$$

or (127)

$$c_p T_2 + Q'_{23} = c_p T_3$$

since $u_3 = u_2$. From Equations (126) and (127)

$$\frac{y_3 - y_2}{y_2} = \frac{Q'_{23}}{c_p T_2} \tag{128}$$

In the notation of the influence coefficients of Table IV, Equation (128) can be rewritten as

$$\frac{dA}{A} = \frac{dh_T}{c_p T} \tag{129}$$

In view of the equality expressed by Equation (129), the influence coefficients give the result $dp/p = 0$ and $du/u = 0$.

The heat added by the heat front must increase pressure in the streamtube a-c by an amount equal to pressure rise across the oblique shock. Using this fact

$$\frac{dp}{p} = \frac{\gamma M_1^2 \theta}{\beta} = \frac{\gamma M_1^2 Q'_{12}}{\beta c_p T_1} \tag{130}$$

Combining Equations (119) and (128), the heat added in Zone II is

$$Q'_{23} = c_p T_2 \theta x / y_1 \tag{131}$$

The difference between T_2/T_1 and 1 is the order of θ. Hence

$$Q'_{23} = c_p T_1 \theta x / y_1 \tag{132}$$

Total heat added to turn the flow by an angle θ is

$$Q'_{31} = Q'_{12} + Q'_{23} = \theta\left(1 + \frac{x}{y_1}\right) \tag{133}$$

The heat addition Q'_{13} turns the flow by an angle θ and increases pressure by the amount given by Equation (130).

Forces on a Planar Airfoil in Supersonic Flight Due to Heat Addition

A problem which has been studied by several investigators is external burning near a two-dimensional wing. One such study is that of Mager.[17] Mager uses the linearized heat addition formulas, Equations (22) to (25), to find the forces on an airfoil in supersonic flight with heat addition in adjacent streamtubes.

Consider an area bounded by x_i and x_f in the x-direction and by a surface and a parallel side at distance h_i. See Figure 33. Within this area, add heat Q. From Equation (41) the pressure at the surface is

$$\frac{p'_w}{p} = 2\left(\frac{\gamma - 1}{2}\frac{QM}{a\beta p}\right)\int \sin\mu \, ds = \frac{(\gamma - 1)QMh}{a\beta p} \tag{134}$$

Where does the factor 2 come from? There must be an image heat source above the surface; otherwise, there would be a v with flow through the wall. Combining Equation (134) and the definition of H [H is defined in the paragraph preceding Equation (31).] gives

$$\frac{p'_w}{p} = \frac{(\gamma - 1)HhM}{h_i(x_f - x_i)a\beta p} \tag{135}$$

In Equation (135) the quantity h varies from 0 at $x = x_i$ to h_i at $x = x_i + h_i \cot\mu$. It remains constant to $x = x_f$, and then h decreases linearly to zero at $x = x_f + h_i \cot\mu$. This is illustrated in Figure 34.

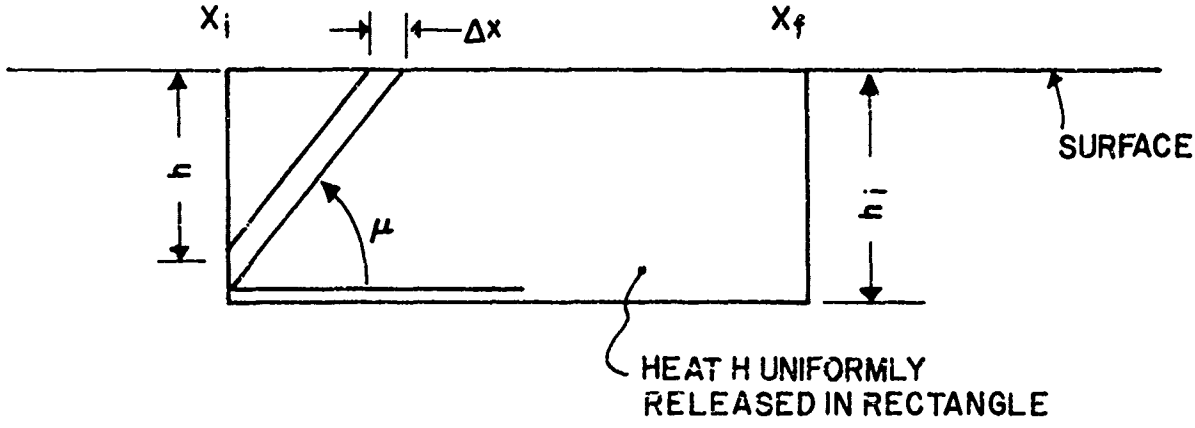

FIGURE 33. HEAT ADDITION ADJACENT TO A SURFACE IN SUPERSONIC FLOW.

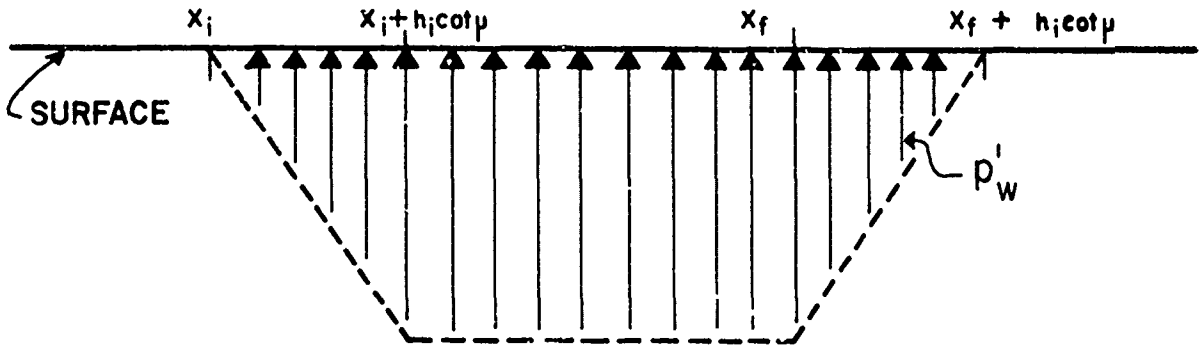

FIGURE 34. PRESSURE DISTRIBUTION DUE TO HEAT ADDITION ADJACENT TO A SURFACE.

It is of interest to examine streamlines near the surface in the region of heat addition; see Figure 35. The streamline passes along ABCD. It is shown dashed with an exaggerated slope below. The streamline is straight from the time it enters the heat addition region until it arrives at A. This is so since $\overline{aA} = \overline{a'A}$. From A to B the right-running characteristic grows in length relative to $\overline{aA}$. Hence the streamline is curved from A to B. From B to C the difference in length $\overline{b'B} - \overline{bB}$ is constant; hence the streamline is straight but at an angle to the mainstream. From C to D less and less of the right-running characteristic passes through the image heat addition region, and v' becomes smaller and smaller until finally the streamline is horizontal at D. From C to D the streamline is obviously curved.

When the streamline is moved closer to the surface, as is the case in the lower part of Figure 35, the deflection is considerably less. It is obvious that the streamline on the surface will not be deflected since $\overline{aA} = \overline{a'A} = \overline{cC} = \overline{c'C} = \overline{d'D} = \overline{dD}$ for this case.

Comparing Figures 25 and 35, one gains some insight to the quandry discussed in connection with Figure 25. When the heat addition is confined to a mathematical line, as in the top of Figure 25, one has difficulty because of streamline deflection near the source. However, when the heat is distributed as in Figure 35, there is no problem.

Based on Figure 34 and Equation (135), it is apparent that one has in hand the tools necessary to study the forces on bodies due to heat addition, at least in the linearized case. Refer to Mager's paper for performance of an airfoil with heat addition.

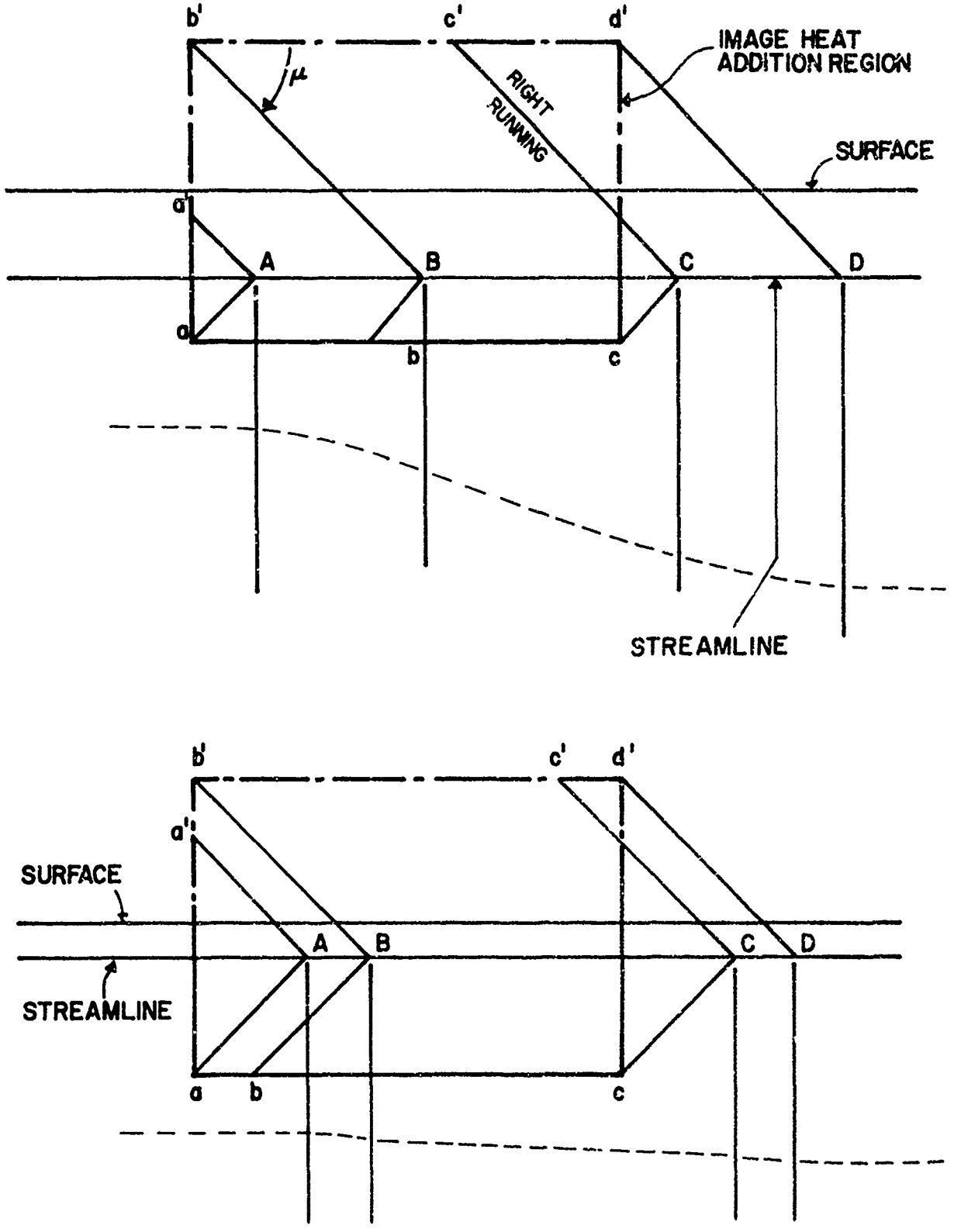

FIGURE 35. STREAMLINES IN REGION OF HEAT ADDITION.

Alleviation of Boattail Drag for a Plug Nozzle

In the Mach number range $0.8 \leqslant M_0 \leqslant 1.2$, which is the transonic regime, the nozzle gross thrust coefficient decreases significantly. A factor which makes this transonic dip all the more important is the corresponding increase in the transonic drag coefficient. Typical data for a plug nozzle are shown in Figure 36, which is copied from the NASA Memorandum by Harrington.[18] Part (a) is of interest here while part (b) is not. Two flow phenomena cause the dip in C_{fg}. One is the change in plug thrust. Figure 36(d) shows the behavior of plug thrust. Another influence is boattail drag identified in Figure 36(c) as primary flap drag. Plug thrust decreases and boattail drag increases in the transonic region.

Is there anything that can be done to correct the loss of the transonic C_{fg}?

Rabone[19] shows that by going to small plug angles, some of the loss of plug thrust can be recovered, although there is still a dip near M = 1.2. Harrington[18] uses a translating shroud that has a pronounced influence on the boattail drag; however, the loss of a plug thrust partially remains.

An alternate approach is to burn externally on the boattail. The direct thrust produced by high pressure on the boattail has very poor SFC. However, a flow interaction may occur which greatly increases thrust. This phenomenon has been termed "wave trapping" by Fuhs. Figure 37 illustrates some essential features of the interaction.

With heat addition on the boattail, the turning angle, θ, of the primary nozzle flow is less. See the angle θ in the region labelled (1) in Figure 37. At the slipstream between the external flow and the nozzle flow, the expansion

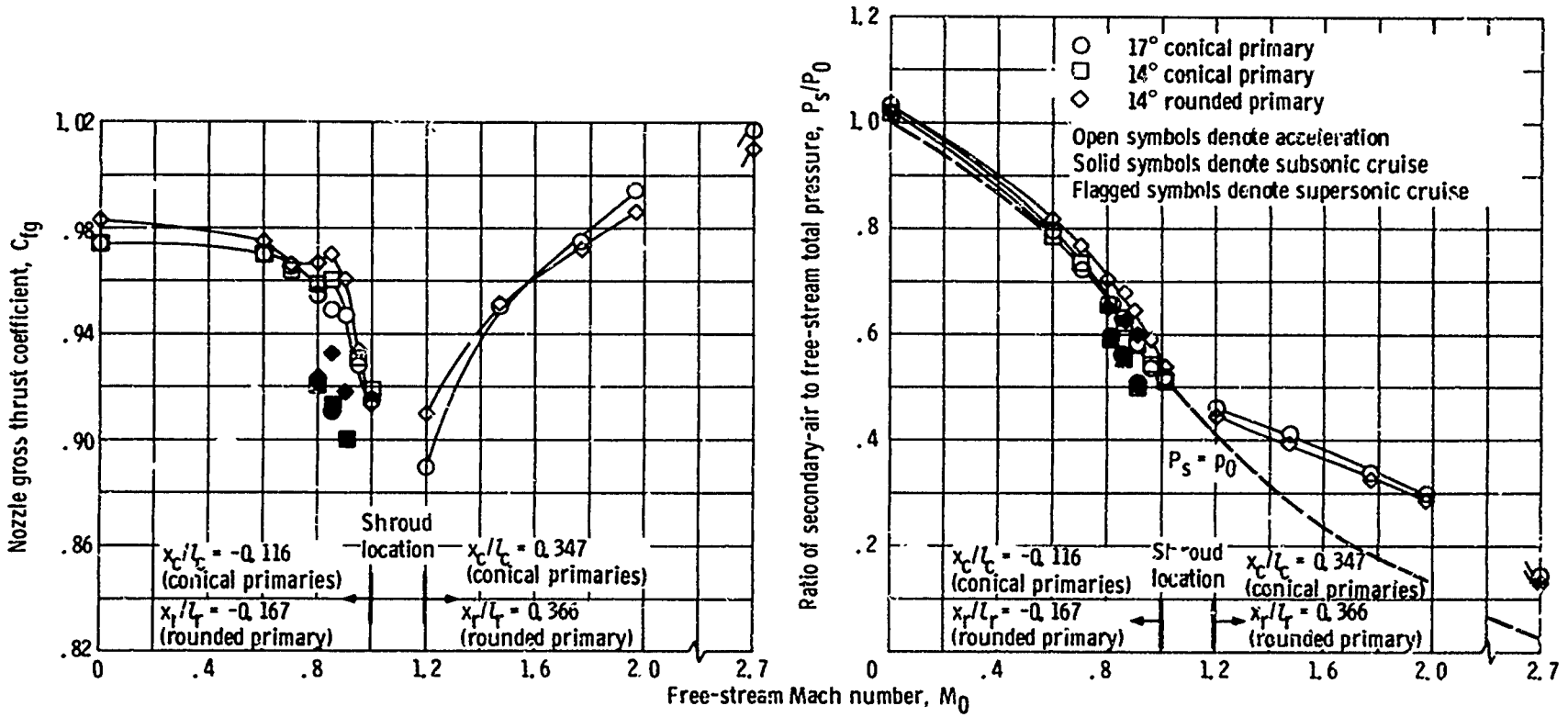

(a) Nozzle gross thrust coefficient.

(b) Secondary total-pressure recovery requirements.

Figure 36. - Comparison of nozzle characteristics. Full-length plug; corrected secondary weight flow ratio, $(w_s/w_p)\sqrt{T_s/T_p} = 0.04$.

(Reproduced from D. E. Harrington.[18])

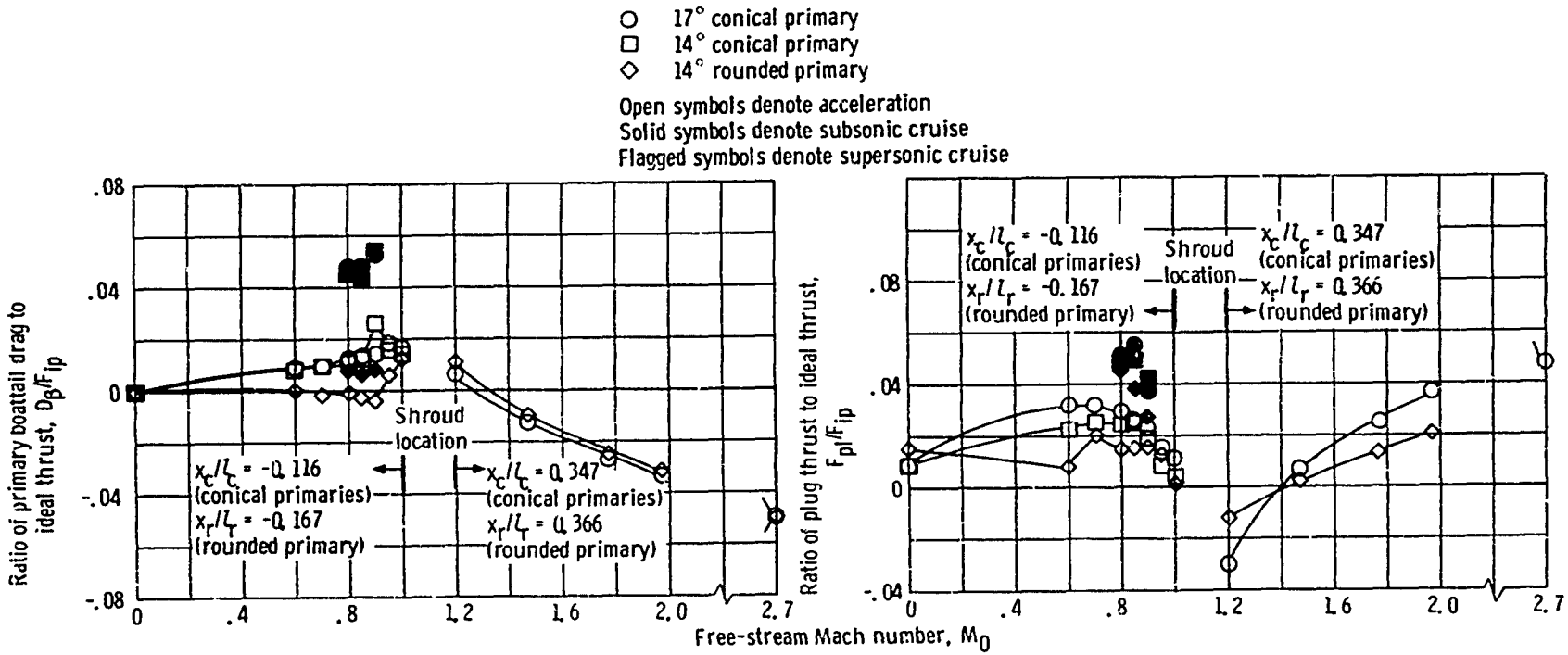

(c) Primary flap drag.

(d) Plug thrust.

Figure 36. - Concluded.

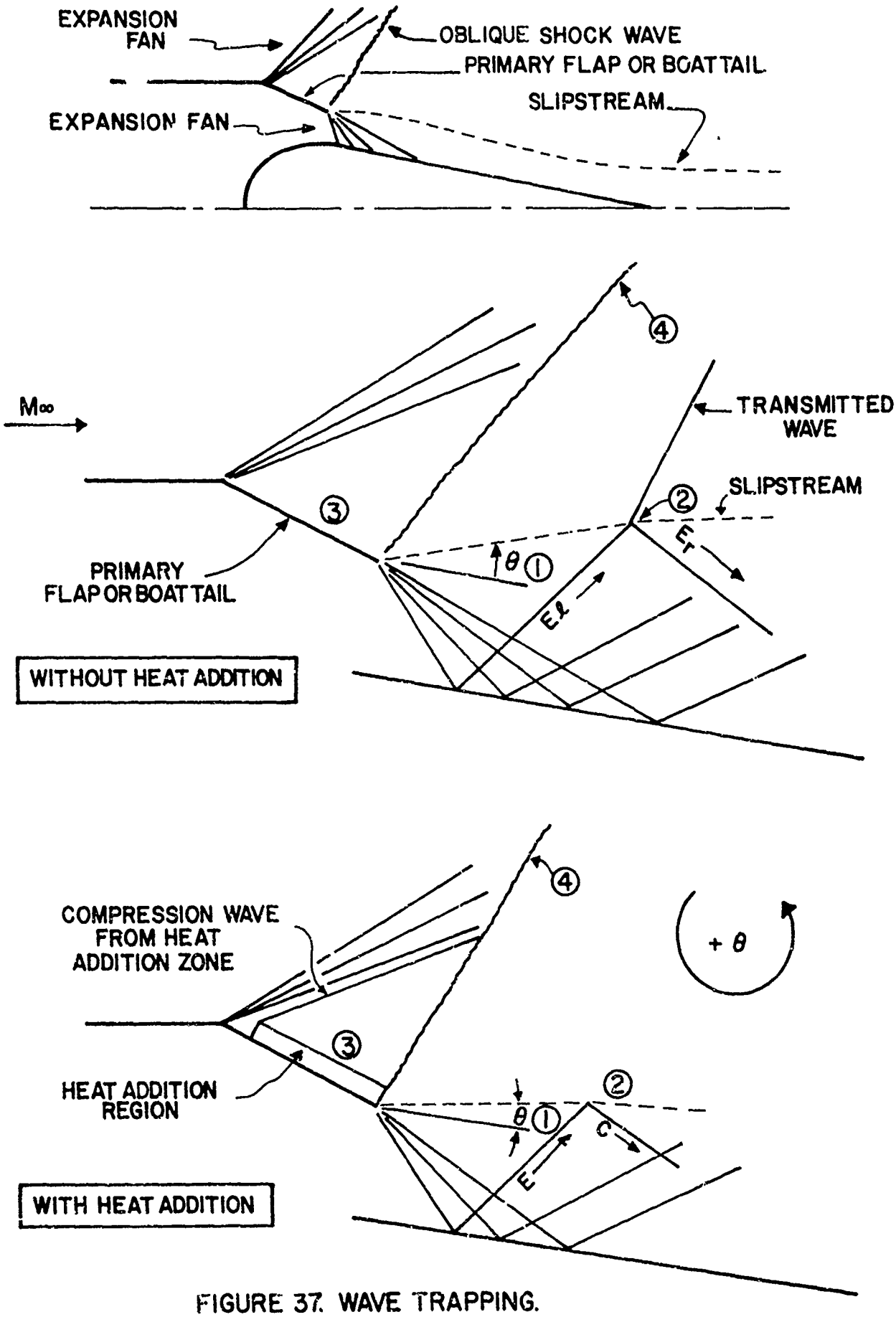

FIGURE 37. WAVE TRAPPING.

waves are flected as expansion waves without heat addition. These reflected expansion waves further reduce the pressure on the plug. The reflection is indicated point (2) in Figure 37. With heat addition, the expansion wave is reflect as a compression wave increasing pressure on the plug.

In region (3) without heat addition the pressure is low, and the Mach number is large. The oblique shock (4) has a shallow angle. It is necessary to match downstream pressure and flow direction for both the external and nozzle flow. At the match condition, the pressure rise across the oblique shock is small, giving large expansion of the nozzle primary flow.

With heat addition there are several changes to the flow in region (3). Pressure increased. The flow is deflected to larger values of θ. The Mach number is lowered in region (3) due to heat addition. Either a weak or a strong solution of the oblique shock occurs. When the strong shock solution occurs, the external flow downstream of the oblique shock is high subsonic. Expansion waves reflected off the plug surface are not transmitted into the external flow. Hence waves are trapped and are reflected as compression waves. The compression waves maintain a high plug pressure. Having looked at the interaction qualitatively, let us now examine the results of a sample quantitative calculation.

Wave Trapping; Quantitative Example

The same geometry plug nozzle was selected as that tested by Harrington.[18] The primary cap forming the boattail was turned inward at an angle of 17°. A freestream Mach number of 1.31 was chosen for the calculations; one reason for selecting the value of Mach number was to keep the external flow supersonic throughout when there was no heat addition. A nozzle pressure ratio of 6 was

chosen. According to Figure 5, at maximum thrust a higher NPR would be more appropriate for $M_0 = 1.31$. NPR of 6 is characteristic of cruise. In order that standard gas tables could be used, the ratio of heat capacities, γ, was set equal to 1.40.

To obtain the flow field, a planar, two-dimensional, finite, wave calculation procedure outlined in Section 12.9 of Liepmann and Roshko[15] was used. When the zone of influence, as defined by Oswatitsch[13] in Section 3.25 of his book, spans a distance small compared to flow radius, the two-dimensional planar procedure can give quite accurate answers for local values of flow. Near the plug nozzle throat, this procedure should give small errors; however, near the plug tip, sizeable error should be expected. In addition, the change in wave angle at the intersection of finite waves was neglected.

Results of the calculation are shown in Figures 38 and 39. Figure 38 shows the wave geometry. The dashed line is the slipstream between the external and the nozzle flows.

Consider the E_r wave* separating regions (1) and (2). It is reflected as an expansion wave from the plug, becoming an E_ℓ wave. The E_ℓ wave reflects from the slipstream immediately downstream of region (4). The value of the reflection coefficient is + 0.8. This means the reflected wave is E_r with a strength of 0.8 of that of the incident E_ℓ wave. At the next reflection from the slipstream, the coefficient is + 0.12, which means continued expansion. At the next reflection, the coefficient is - 0.08; there is an extremely weak compression wave reflected from the slipstream. As a consequence of the expansion,

*E means expansion, and C means a compression wave. Subscript r is for a right running wave, whereas subscript ℓ is for a left running wave.

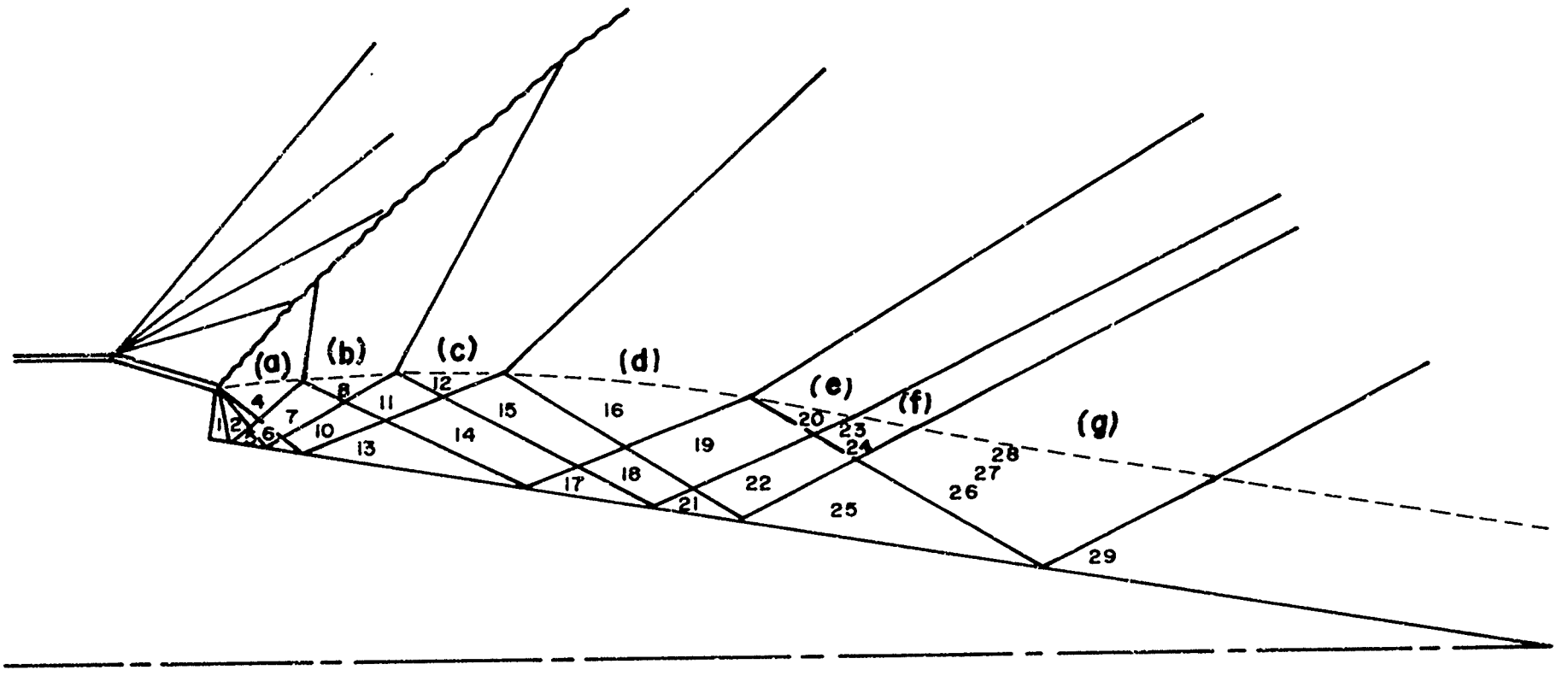

FIGURE 38. WAVE GEOMETRY FOR FLOW ALONG PLUG NOZZLE WITHOUT HEAT ADDITION.

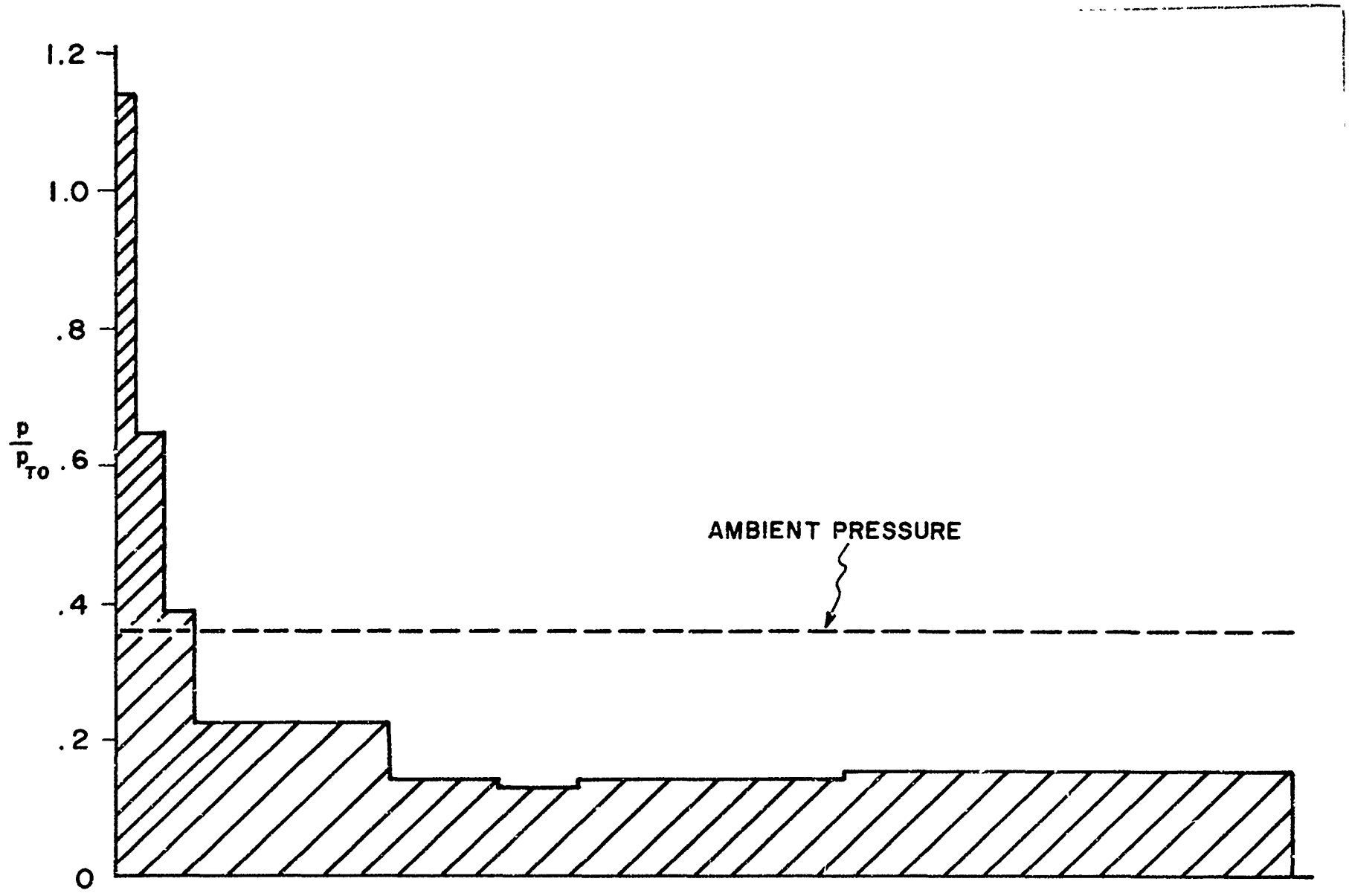

FIGURE 39. PRESSURE DISTRIBUTION ON PLUG.

the pressure along the plug drops below ambient as shown in Figure 39. Pressure below ambient on the plug results in a negative plug thrust. Integration of the curve shown in Figure 39 yields a value of the ratio, plug thrust to ideal nozzle thrust, equal to - 0.097. Direct comparison of this calculation with Harrington's data is not possible since all his tests at M = 1.31 were run with a shroud extending partially over the plug. However, the value of plug thrust has the correct algebraic sign and the correct order of magnitude. In fact, it is better than the correct order of magnitude; it is probably within 50 per cent of being correct.

Now let's add heat to the region near the boattail as shown in Figures 37 and 40. The length of the boattail is L. The thickness of the heat addition region is ℓ. The pressure increase due to heat addition is obtained from Equation (41). Evaluation of the integral yields

$$p' = \frac{(\gamma - 1)Mh\ell}{a\beta} \tag{136}$$

Equation (136) can be solved for the heat addition h, BTU/volume second, and then multiplied by $L\ell$.

$$L\ell h = \frac{a\beta p'L}{(\gamma - 1)M} \frac{BTU}{(length)(sec)} \tag{137}$$

Multiplication by $2\pi r$, i.e., the circumference of the boattail, leads to the time rate at which heat is released. Let H be the heating value of the fuel and $\dot{m}_f$, the fuel flow rate. The heat release rate is given by

$$\dot{m}_f H = \frac{2\pi r a\beta L p'}{(\gamma - 1)M} \tag{138}$$

The specific fuel consumption, SFC, is given by

$$SFC = \frac{3600\dot{m}_f}{\Delta D} \tag{139}$$

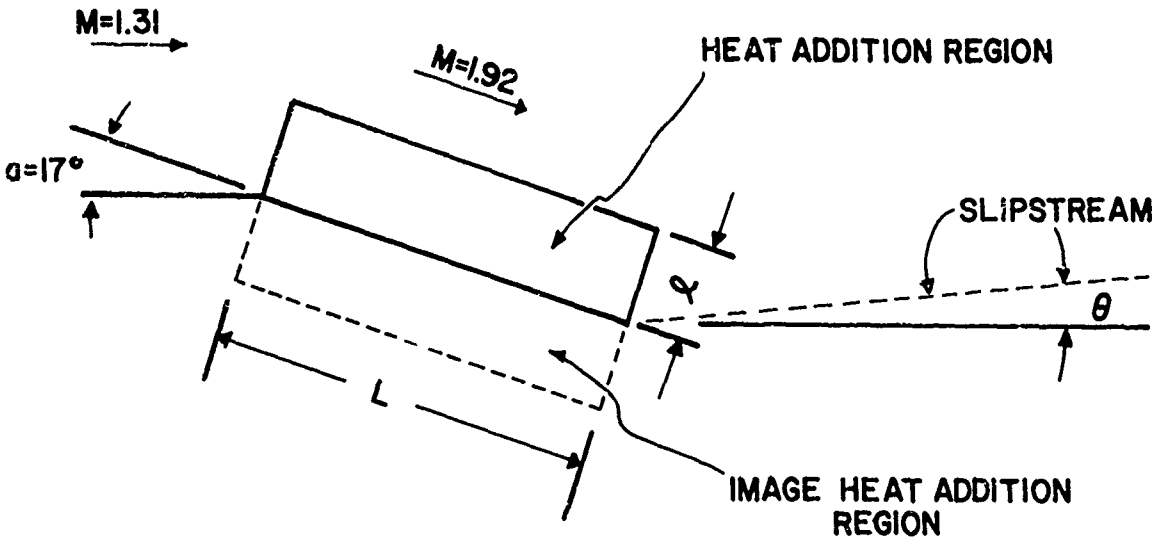

FIGURE 40. HEAT ADDITION REGION AT BOATTAIL.

when ΔD is the change in boattail drag. The change in boattail drag is $\Delta D = Lp' \sin \alpha$; the angle α is defined in Figure 40. Combining Equations (138) and (139) along with the expression for ΔD gives

$$SFC = \frac{3600a\beta}{(\gamma - 1)MH \sin \alpha} \tag{140}$$

Inserting numerical values, a = 1000 ft/sec, $\beta = \sqrt{M^2 - 1} = 1.615$, $\gamma = 1.4$, M = 1.92, H = 20,000 BTU/lb_m, and $\alpha = 17^o$, and dividing by 778 ft-lb_f/BTU leads to SFC = 1.685 per hour. This is not particularly an exciting value for SFC; however, for the strong solution the heat addition causes wave trapping and significantly increases plug thrust. Note that SFC is not dependent on the amount of heat added. Less heat gives less thrust; more heat gives proportionately more thrust.

Now let's look at the flow on the plug. To start the solution, the slipstream angle, θ, must be determined. Figure 41 is a plot of the curves showing pressure in the external flow as a function of θ and the pressure of the nozzle flow also as a function of θ. The ordinate is pressure behind the oblique shock (or downstream of the expansion fan for the nozzle flow) divided by freestream stagnation pressure. There are two possible solutions; the strong solution was chosen for this example. Values are $\theta = +0.3^o$, subsonic external flow, and a shock wave angle of 77^o. Knowing θ at the boattail-slipstream junction permits one to start the solution using finite waves.

The wave geometry along the plug is shown in Figure 42. Since the reflection coefficients at the slipstream have the value - 1.0, the flow becomes periodic. The pressure along the plug, which is shown in Figure 43, is everywhere larger than ambient pressure. Integration of the pressure gives

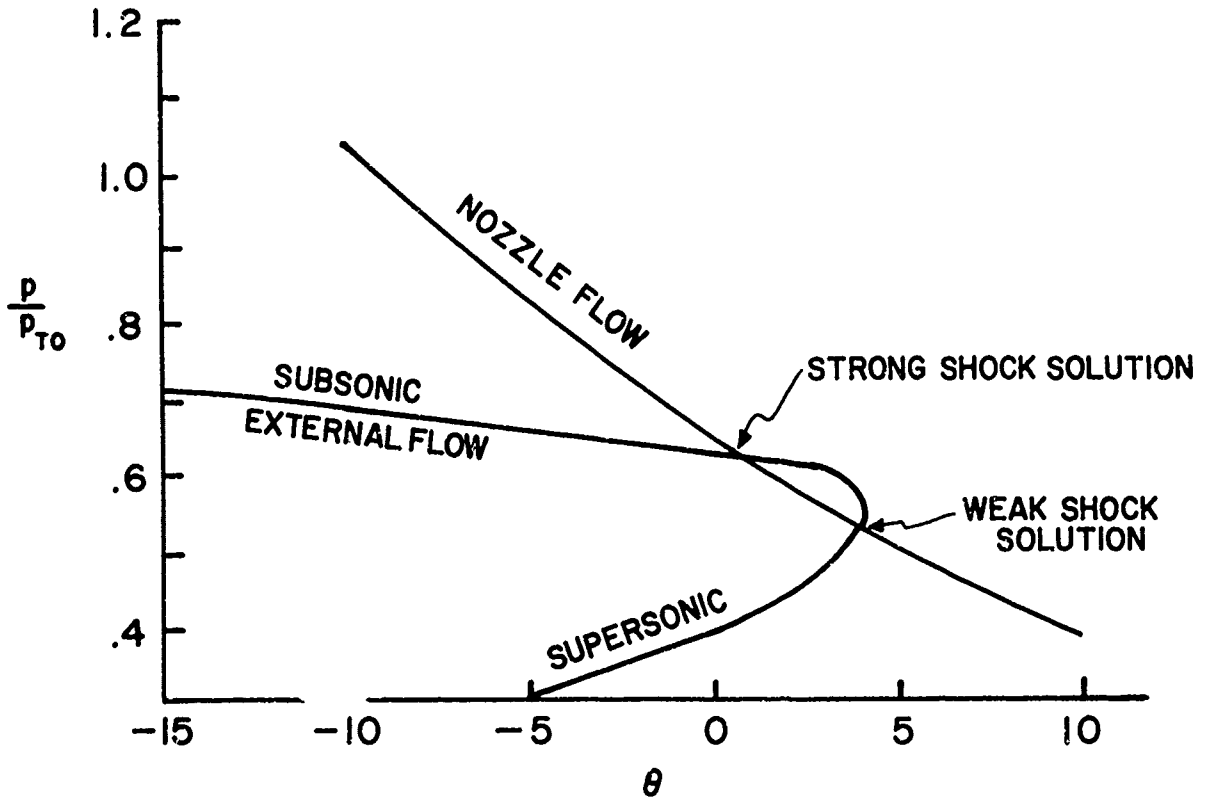

FIGURE 41. SOLUTIONS FOR INITIAL SLIPSTREAM FLOW ANGLE.

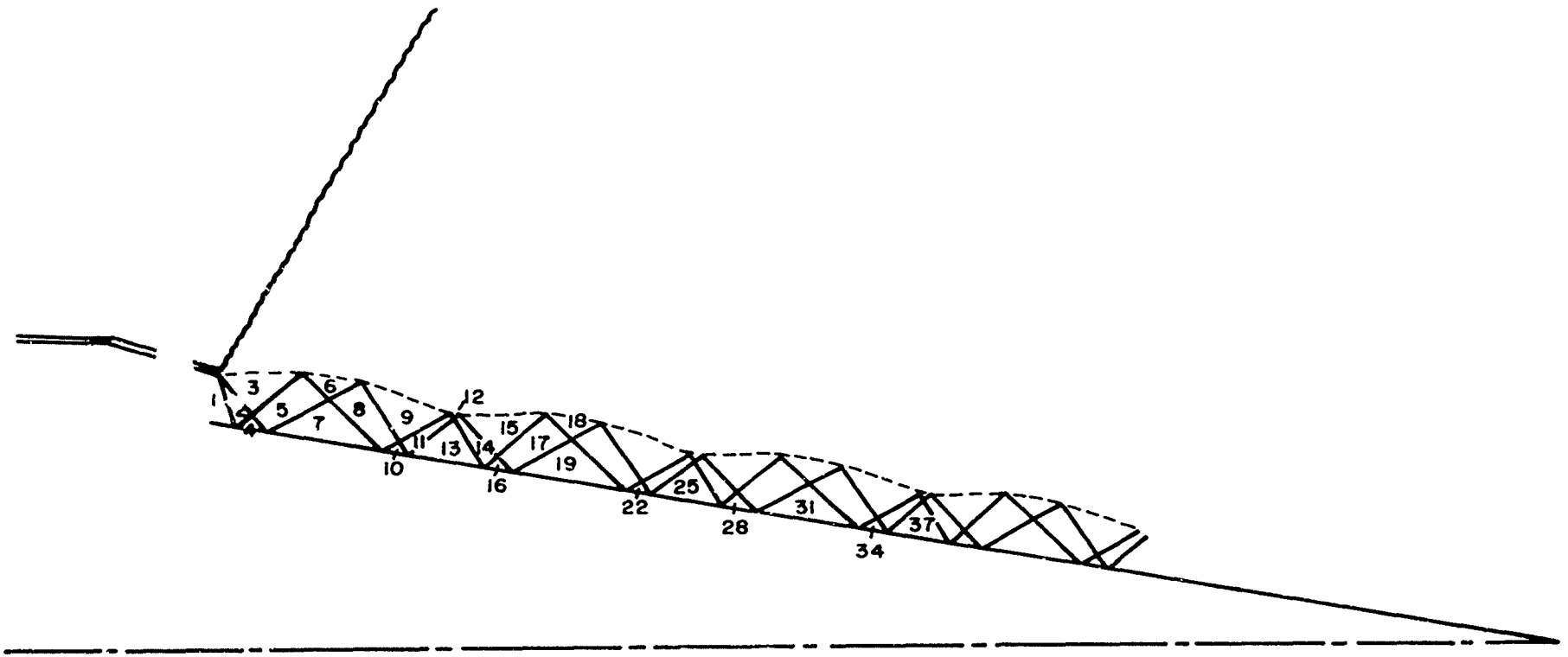

FIGURE 42. WAVE GEOMETRY FOR FLOW ALONG PLUG NOZZLE WITH HEAT ADDITION.

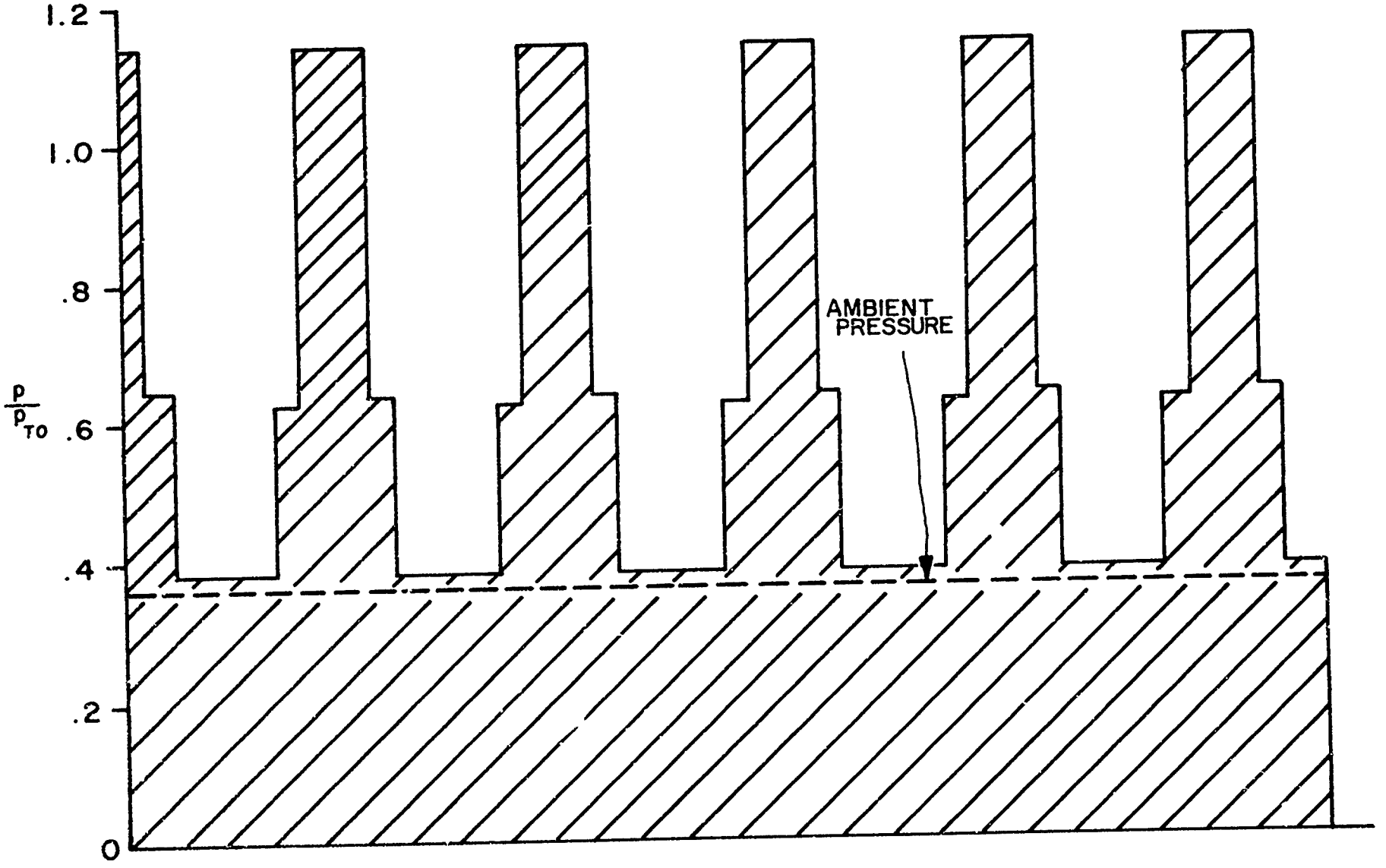

FIGURE. 43. PRESSURE DISTRIBUTION ON PLUG.

$$\frac{\text{plug thrust}}{\text{ideal nozzle thrust}} = 0.223$$

If heat is added so that $p'/p_{T0} = .027$ on the boattail, the value of SFC becomes less than 0.1 per hour ! In Equation (139), ΔD would now include both the decrease in boattail drag and the increase in plug thrust.

Wave Trapping; Discussion of Numerical Example

In the course of making a numerical experiment, there are numerous assumptions and decisions to make. Having completed this part of an analysis of the influence of heat addition, one has new perspective. The decrease in boattail drag and the corresponding SFC are fairly straightforward calculations, and the value of SFC = 1.685 is probably fairly accurate.

Considering the plug thrust increment due to heat addition, it is apparent that a crossroads occurs at the point of taking a weak or strong solution. See, once again, Figure 41. For this example, the strong solution was taken.

The strong solution gives a subsonic external flow at least initially. That fact, of course, is the basis for wave trapping. Somewhere along the plug, the external flow may accelerate from subsonic flow to supersonic flow. Once the external flow becomes supersonic, the waves are no longer trapped in the nozzle flow. Determination of the subsonic flow and the change to supersonic flow is extremely difficult.

If one had taken the weak solution instead of the strong solution, the pressure distribution along the plug, at least according to current estimates, would be qualitatively similar to Figure 39.

Changing NPR raises the curve labelled "NOZZLE FLOW" in Figure 41. As the nozzle-flow curve is raised, the weak and strong solutions converge to a

single solution at the point of tangency. See Figure 44(a) and 44(b). This single solution is a strong shock solution. Increasing NPR beyond the point of tangency raises the curve for "NOZZLE FLOW" so that an intersection of the nozzle flow curve and external flow curve does not occur. The oblique shock probably moves upstream to the point where the boattail is formed. This case is illustrated in Figure 44(c). This would give high pressure on the boattail but probably would give low plug thrust.

Adding heat on the boattail has two influences: (1) Due to change in θ, the curve for external flow in Figure 41 is shifted to the right; and (2) due to increased pressure ahead of the shock wave, the curve is moved vertically. This is illustrated in Figure 45(a). For large NPR and small heat addition, there may be a solution as shown in Figure 45(c). Additional heat release causes a shift in the curve making possible both weak and strong solutions. See Figure 45(d).

The validity of the flow shown in Figures 42 and 43 is doubtful due to the fact that the external flow probably accelerates from subsonic to supersonic. The strong solution may not occur. Consequently, one is skeptical of the SFC = 0.1. Additional analysis is necessary to obtain the plug pressure distribution with heat addition. Both the weak solution and refinement of the strong solution should be considered. One would expect the heat addition to have a favorable influence on plug thrust.

Base Flow Problem with Heat Addition; Planar Flow

One application of external burning which has been investigated both experimentally and theoretically is the modification of base pressure by heat addition. The heat may be added in the base recirculation zone, in the viscous

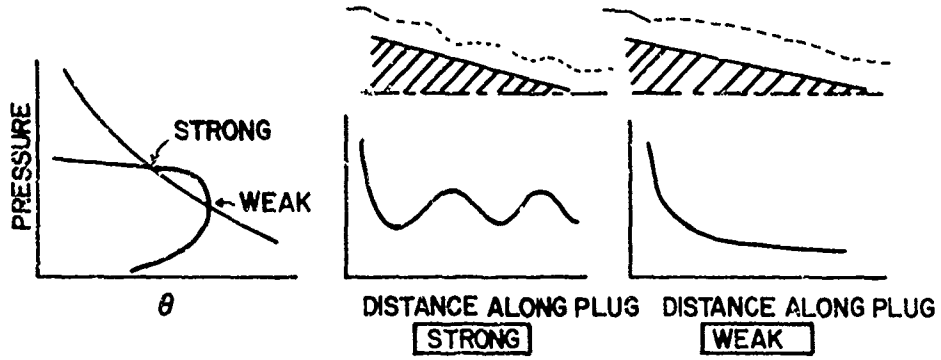

(a) TWO INTERSECTIONS; WEAK AND STRONG SOLUTIONS.

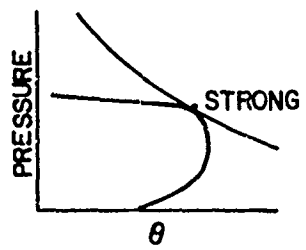

(STRONG SAME AS ILLUSTRATED ABOVE)

(b) TANGENT, STRONG SOLUTION.

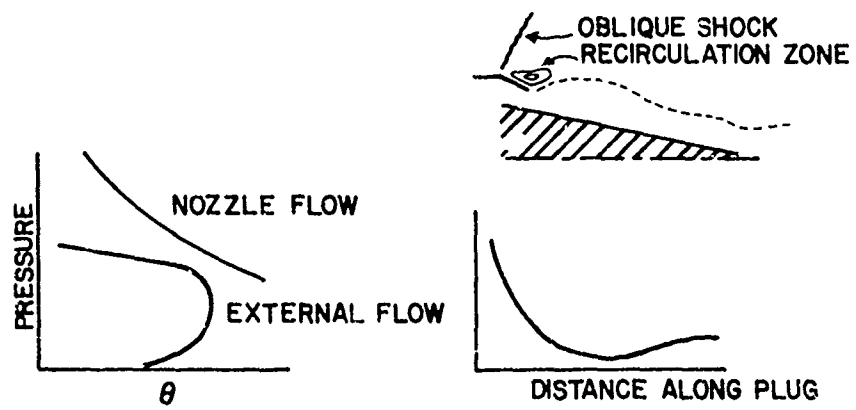

(c) NO INTERSECTION; SHOCK UPSTREAM OF BOATTAIL.

FIGURE 44.
INFLUENCE OF CHANGING NOZZLE PRESSURE RATIO WITH FIXED HEAT ADDITION.

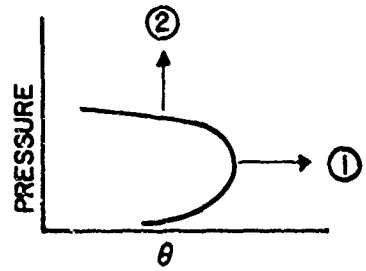

(a) INFLUENCE OF INCREASING HEAT ADDITION ON EXTERNAL FLOW.

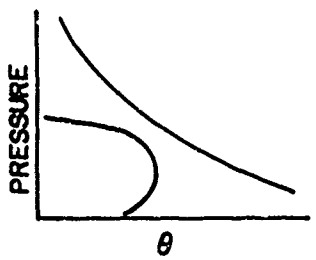

PRESSURE DISTRIBUTION AND FLOW SIMILAR TO FIGURE 44(c)

(b) NO INTERSECTION WITH SMALL HEAT ADDITION.

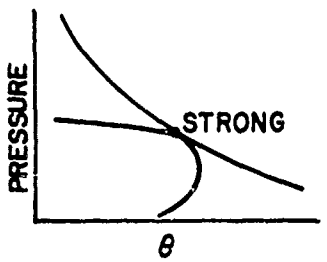

PRESSURE DISTRIBUTION AND FLOW SIMILAR TO FIGURE 44(b)

(c) TANGENT STRONG SOLUTION.

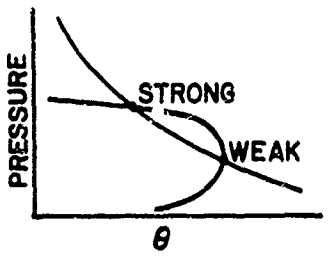

PRESSURE DISTRIBUTION AND FLOW SIMILAR TO FIGURE 44(a)

(d) TWO SOLUTIONS; WEAK AND STRONG.

FIGURE 45.
INFLUENCE OF CHANGING HEAT ADDITION WITH FIXED NOZZLE PRESSURE RATIO.

shear layer, or on the inviscid flow adjacent to the shear layer. In 1967, Billig[16] prepared an excellent summary of work to date. More recently, Roberts[20] has written a survey on the subject.

It is worthwhile to examine the base flow from an integral point of view. This is illustrated in Figure 46. The control volume for the momentum theorem is shown as dashed lines with various surfaces identified by a, b, c, ... Using notation of Chapter 7 of Liepmann and Roshko,[15] the momentum theorem is

$$\int \rho u_i (u_j n_j) dA + \int p n_i dA = 0 \tag{141}$$

One can add an integral of ambient pressure over the control volume. For base pressure i = 1.

$$\int \rho u_1 (u_1 n_1 + u_2 n_2) dA + \int (p - p_\infty) n_1 dA = 0 \tag{142}$$

For the control volume shown in Figure 46, there are four integrals.

$$\int_{ab} (p_b - p_\infty)(-1) dA + \int_{bc} \rho u_1^2 (-1) dA + \int_{cd} (p - p_\infty) n_1 dA + \int_{de} \rho u_1^2 dA = 0 \tag{143}$$

$$\int_{ab} (p_b - p_\infty) dA = \underbrace{\int_{de} \rho u_1^2 dA}_{(1)} + \underbrace{\int_{bc} - \rho u_1^2 dA}_{(2)} + \underbrace{\int_{cd} (p - p_\infty) n_1 dA}_{(3)} \tag{144}$$

Heat addition in the inviscid flow above the edge of the shear layer will alter the shape of the streamline from c to d. Changing streamline cd will not influence integral (2) above. It is not readily apparent how integral (1)

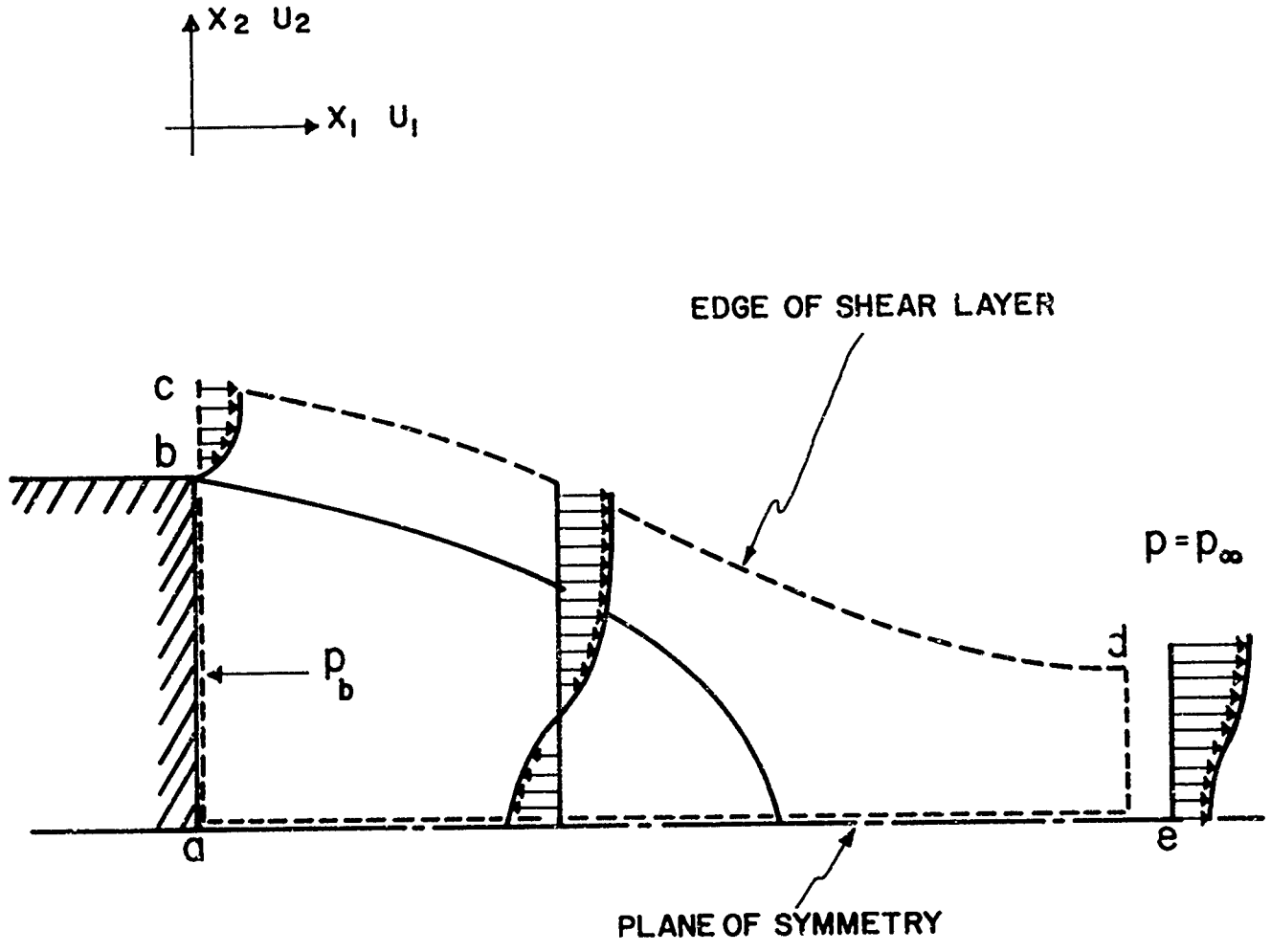

FIGURE 46. BASE FLOW.

changes due to modification of streamline cd. Of course integral (3) is directly influenced.

To gain some insight into the anticipated change in integral (1), one can use the continuity equation which is

$$\int_{bc} \rho u_1 dA = \int_{de} \rho u_1 dA \tag{145}$$

Since integral over surface bc doesn't change when streamline cd is changed, this means the integral over de does not change. Any variation in integral (1) of Equation (144) is due to variations in ρ and u_1^2; however, Equation (145) tells us any change in ρ is balanced by a compensating change in u_1.

If the flow above the edge of the shear layer illustrated in Figure 46 is inviscid and if only one family of characteristics is significant, then one can relate local streamline slope to pressure. To demonstrate the influence of the shape of streamline cd on base pressure, a sample problem was worked. This is illustrated by Figure 47. Streamline cd is used with the same lateral displacement but with large turning angle in the upper diagram. The pressure distribution along the streamline is shown in the graphs below each streamline. From the curves one can evaluate the integral or equivalent series

$$I = \int_{cd} \frac{p}{p_T} n_1 dA = \sum_j \frac{p_j}{p_T} \Delta A_j \tag{146}$$

where ΔA_j is the element of area projected in the x_1 direction. Numerical values for I are 12.8 for upper curve and 21.7 for lower curve. Relating Equation (146) to Equation (144) gives

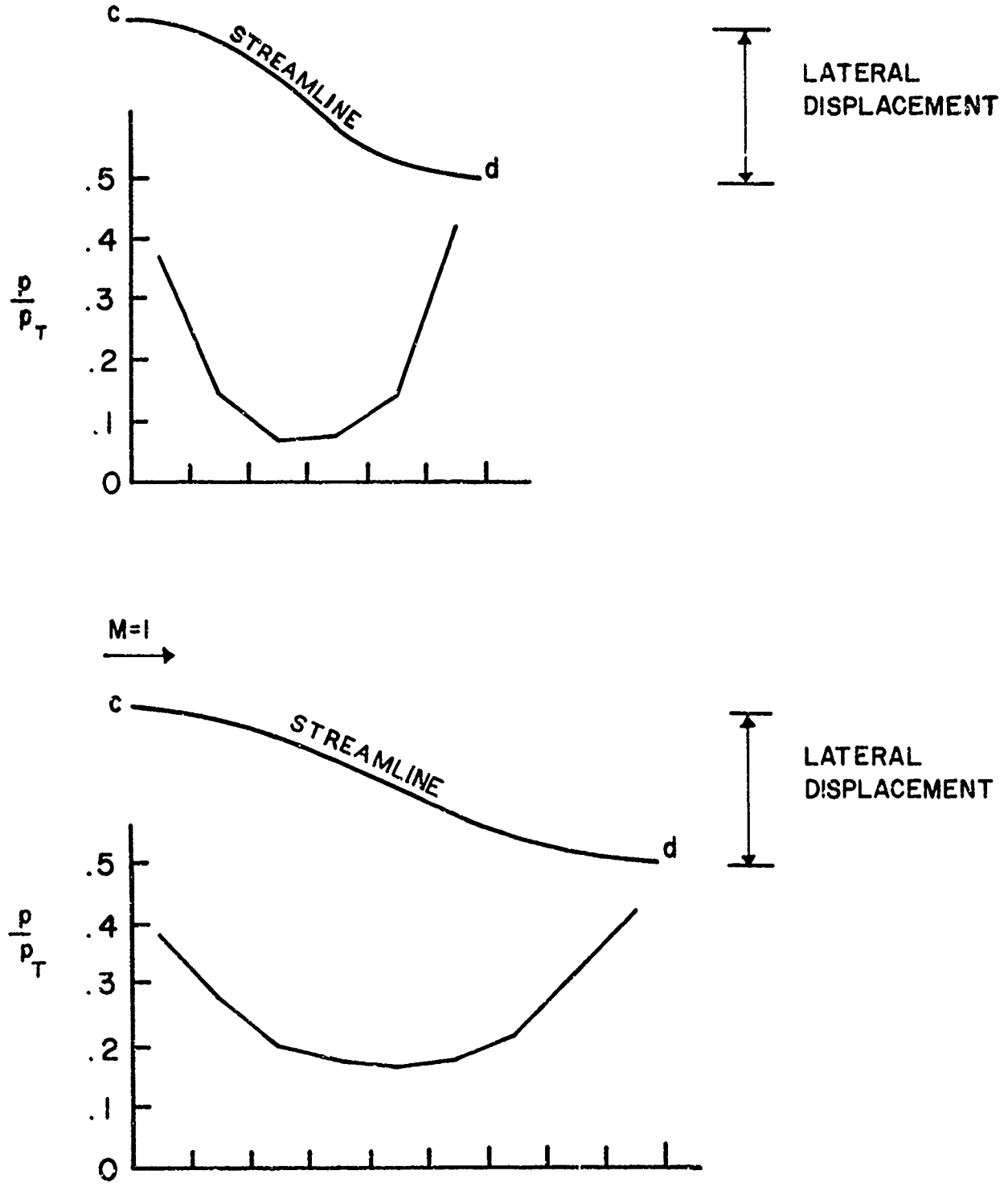

FIGURE 47. PRESSURE ON EDGE OF SHEAR LAYER.

$$p_T \int_{cd} \left(\frac{p}{p_T} - \frac{p_\infty}{p_T}\right) dA = \int_{cd} (p - p_\infty) n_1 dA = p_T(I - 52.8) \qquad (147)$$

The sharp turning curve gives a value of $-40p_T$ for integral (3) of Equation (144), whereas the gradual turning curve gives $-31.1p_T$. The base pressure would be greater with the gradual turning streamline cd. It is obvious from this analysis that one wants to maintain a high pressure on streamline cd to increase base pressure. The heat addition zone shown in Figure 48 will do that.

Now let's return to the problem of how much pressure increase results from the heat addition zone. Consider a heat addition zone located above a slipstream as shown in Figure 49. This is a model to represent the flow depicted in Figure 48. One replaces the lateral gradient in Mach number with a slipstream having supersonic flow above and subsonic flow below. With a lateral Mach number gradient, as in Figure 48, the characteristics reflect from the sonic line in the form of a cusp.

A paragraph will now be used to explain the notation E_r, C_r, E_ℓ, C_ℓ. The symbols E and C are for Expansion and Compression waves. The subscripts r and ℓ represent right running and left running waves respectively.

In Figure 49 the heat addition zone has a leading edge swept at angle μ. This gives a finite wave C_r. The pressure along the slipstream remains at pressure p_∞. The waves from the heat addition zone and the reflected waves turn the flow while keeping pressure constant. One way to describe this is to say that the compression waves from the heat addition zone have cancelled the expansion waves which would have originated due to kink in streamline at

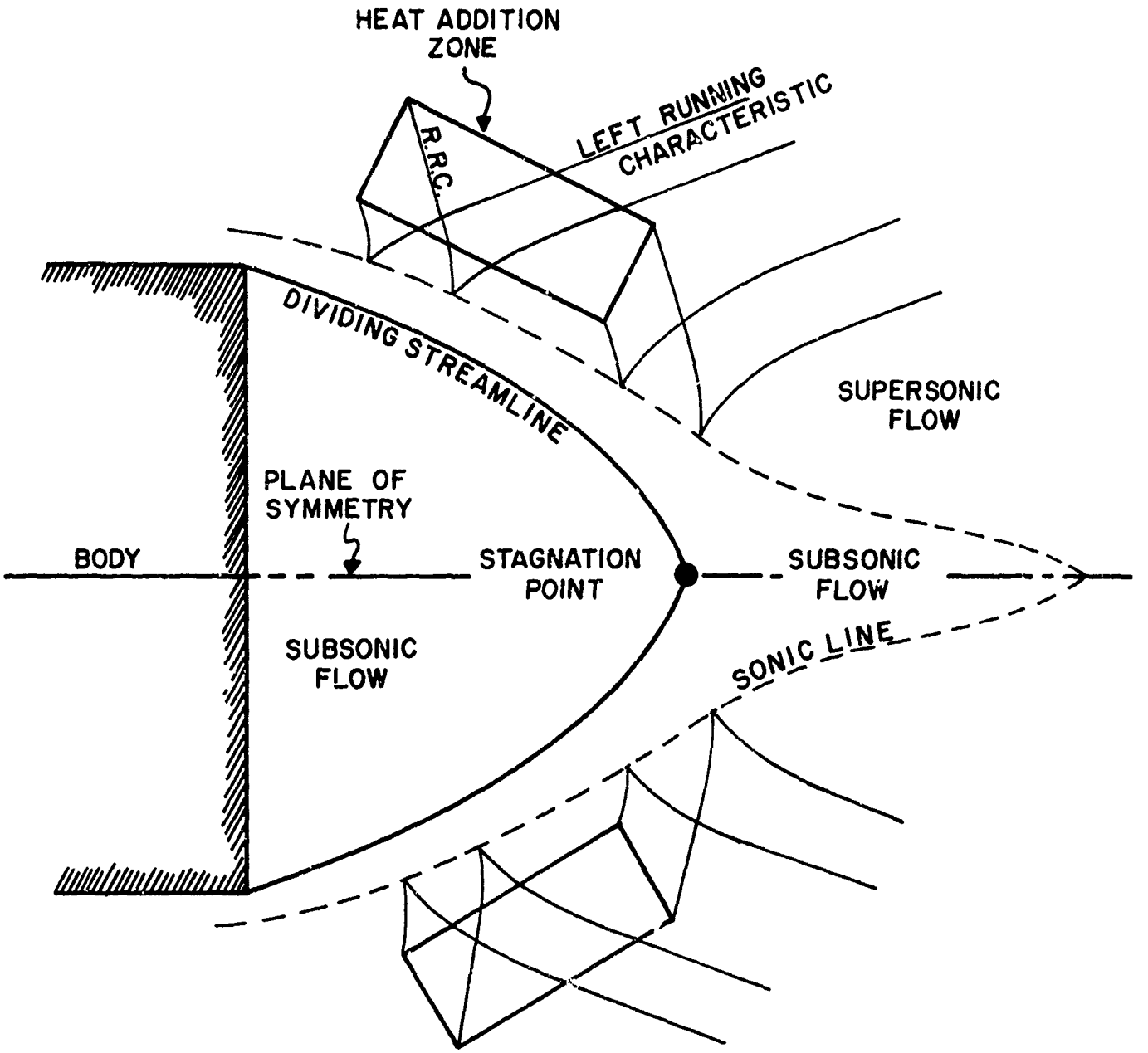

FIGURE 48.
INTERACTION OF HEAT ADDITION ZONES WITH BASE FLOW.

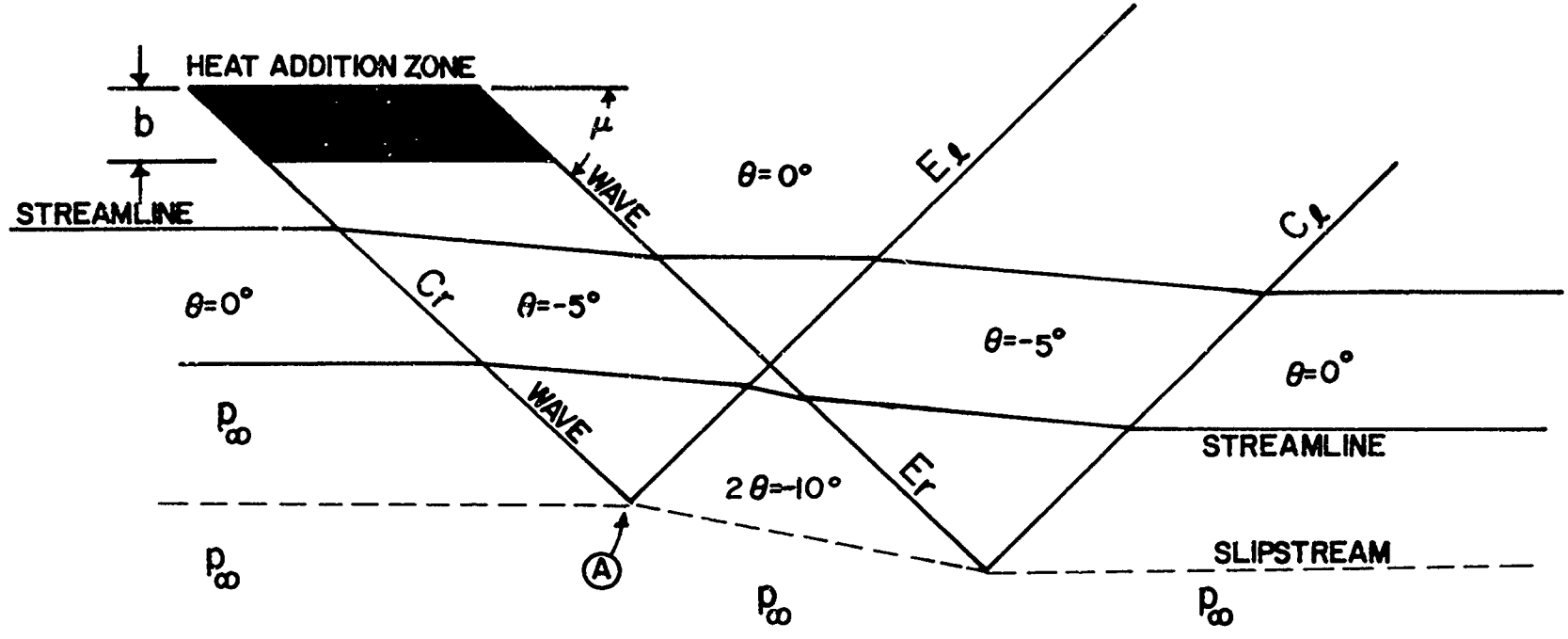

FIGURE 49. INTERACTION OF A HEAT ADDITION ZONE WITH A SLIPSTREAM.

point (A). The turning angle is 2θ at point (A) or twice the turning angle due to C_r. The reflection has effectively doubled the influence of the waves from the heat addition zone.

The doubling of effectiveness can be seen in the following analysis: In free unbounded space the turning angle is given by

$$\tan \theta = \theta = \frac{v'}{U + u'} = \frac{v'}{U} = \frac{(\gamma - 1)hb}{2\gamma pU} \tag{148}$$

Equation (148) is obtained from geometry and Equation (40). From Equation (41)

$$p' = \frac{(\gamma - 1)Mhb}{2a\beta} \tag{149}$$

where symbol b is defined by Figure 49. Due to turning of flow by an amount 2θ, the increment of pressure decrease would be

$$p'' = -\frac{2\gamma M^2 p\theta}{\beta} \tag{150}$$

From the flow field analysis illustrated in Figure 49, the following equation must be true

$$2p' + p'' = 0 \tag{151}$$

Combining Equations (148), (149), (150), and (151), one can verify that Equation (151) is in fact true.

The mechanism for altering base pressure by heat addition in the adjacent inviscid flow is apparent if one retraces the discussion associated with Figures 46, 47, and 48. To summarize, the streamline cd must turn inward toward the axis or plane of symmetry. Without heat addition, this turning causes the pressure to drop. Sharp turning gives low pressure and low base pressure; see Equation (144) and Figure 47. Heat addition allows this inward turning without loss of pressure as shown in Figures 48 and 49. Strahle's[21] analysis suggests a new way to overcome base drag.

Base Flow Problem with Heat Addition; Axisymmetric

The analysis of Fein[22] and Strahle[23] considered a two-dimensional planar geometry, i.e., wing-like objects. Projectiles are, of course, axisymmetric. This section examines some of the changes to be expected when the planar results are replaced by calculations for the axisymmetric case.

The method outlined in Liepmann and Roshko[15] was used to calculate the flow field for axisymmetric heat addition. To verify the procedure for handling the characteristics near the axis, a model of a spherical, radially expanding flow was used. The results of that calculation are shown in Figure 50. Since the flow is known, one knows Mach number at any radius R. The Mach number calculated from the characteristics solution is shown in the third column of the data summary in Figure 50. The Mach number based on the value of R and flow area is shown in the first column.

A planar radial flow has an area variation linear in R, whereas the axisymmetric radial flow has a R^2 dependence for area. This can be represented by

$$\underset{\text{Planar}}{\frac{\Delta A}{A} = \frac{\Delta R}{R}} \qquad \underset{\text{Axisymmetric}}{\frac{\Delta A}{A} = 2\frac{\Delta R}{R}} \tag{152}$$

Partial solutions of the flow field with heat addition were obtained for two cases. Both cases had an annular heat addition zone as illustrated in the lower left-hand corner of Figure 51. The heat addition was sufficient to cause a maximum turning angle of $\theta_{max} = -6^\circ$ at a radius of 6 inches. In the first case, the heat zone was bounded by $6 \leqslant r \leqslant 7$ and $0 \leqslant z \leqslant 3$. In the second case, it was $6 \leqslant r \leqslant 8$ and $0 \leqslant z \leqslant 3$. For the first case, shown in Figure 51, $M_0 = \sqrt{2}$.

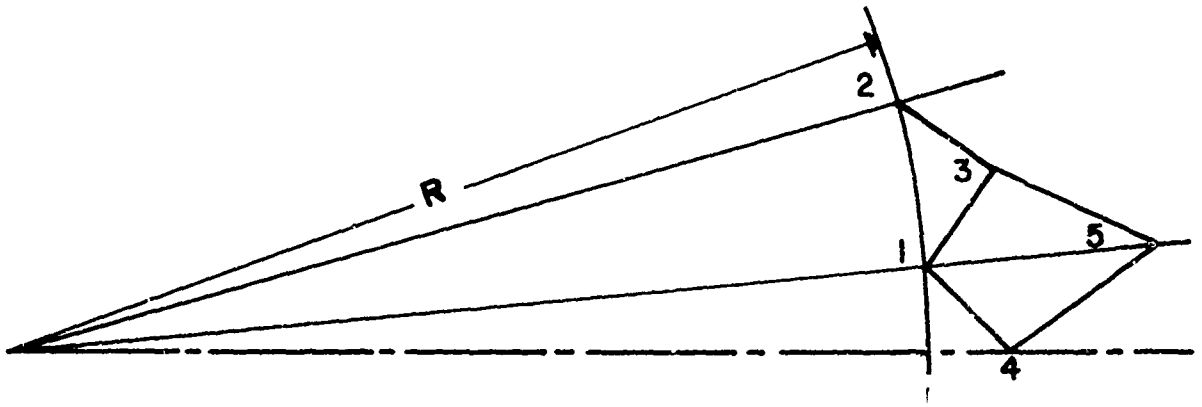

M Using Area	Point	M	ν	θ	μ	r	sin θ	$\frac{\sin\theta}{r}$	$\left(57.7 \sin\mu \frac{\sin\theta}{r}\right)$	sin μ
1.33	1	1.33	7.0	5	49	.44	.0872	.198	8.53	.751
1.33	2	1.33	7.0	15	49	1.32	.2585	.196	8.53	.751
1.65	3	1.68	17.46	10	34	.96	.173	.180	6.18	.595
1.65	4	1.68	17.46	0	34	0	0	.196	6.73	.595
2.05	5	2.09	28.91	5	28.6	.57	.0872	.153	4.22	.479

FIGURE 50. CHARACTERISTICS SOLUTION FOR AXISYMMETRIC RADIAL EXPANSION.

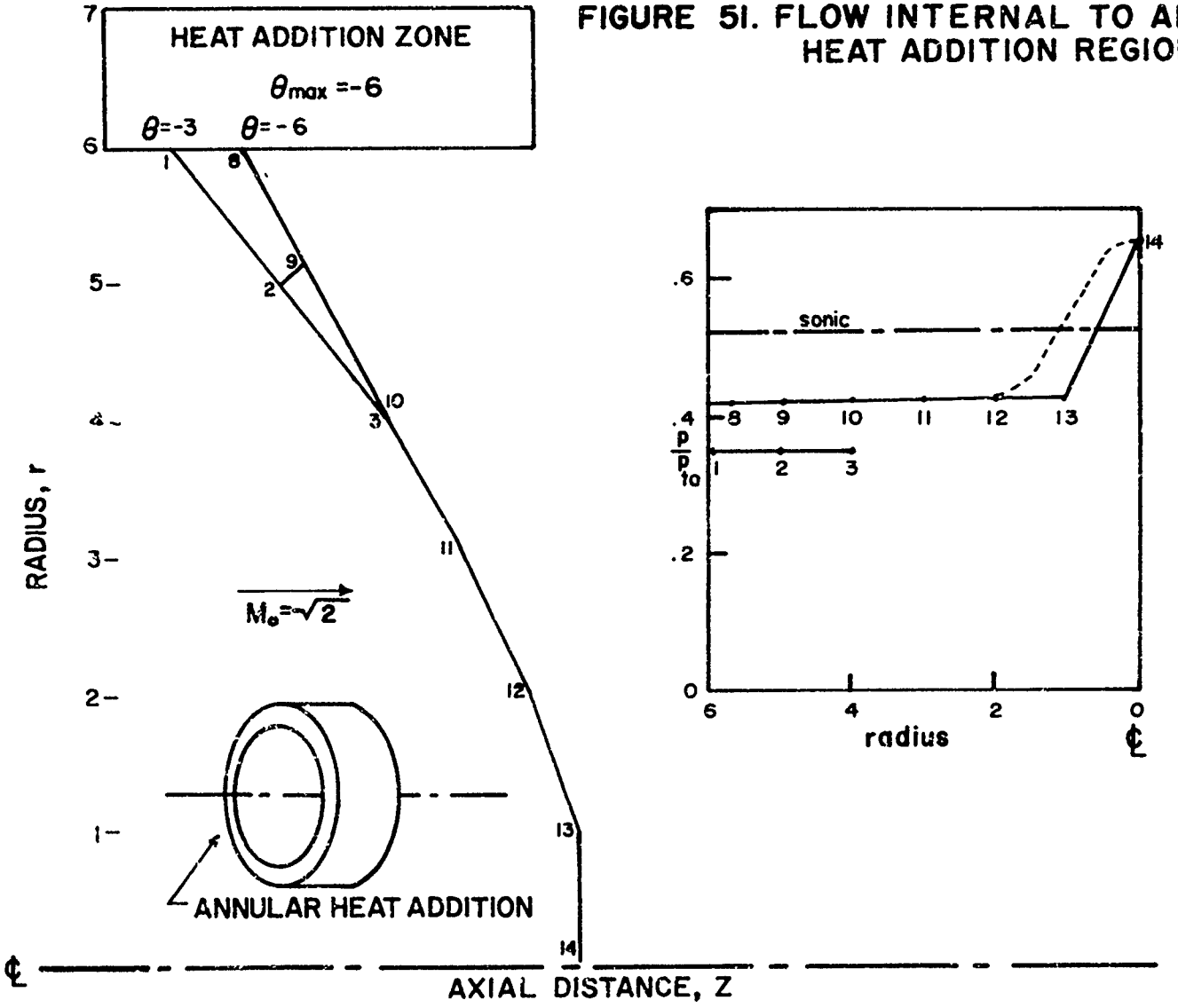

FIGURE 51. FLOW INTERNAL TO ANNULAR HEAT ADDITION REGION.

For the second case, M_0 was chosen as 2, and the radial extent of the heat addition zone was increased to spread out the waves. This was done to avoid merging of the characteristics to form a shock wave.

Pressure versus radius is plotted in Figure 51. The mid-characteristic, which has points 1, 2, and 3, has an imperceptible increase in pressure as radius decreases. The characteristics converge to form a shock wave. When this happens, the techniques outlined in the book[23] and NACA TN[24] by Ferri are applied.

Along the characteristic, which starts at r = 6" with $\theta_{max} = -6^{\circ}$, the pressure rises slightly to a radius of r = 2". Between $0 \leqslant r \leqslant 2$, the pressure increases rapidly. Due to the large mesh size, the pressure variation at points 12, 13, and 14 may not be correct. Certainly the end point, number 14, is correct. The dashed line represents the curve that would probably obtained with finer mesh size and a more accurate treatment of the shock waves. Note that for $M_0^2 = 2$, even a normal shock wave is nearly isentropic, which permits treatment of shock waves as finite isentropic compression waves.

The conclusions from Figure 51 are as follows:

(a) In the axisymmetric geometry, compression waves tend to merge more quickly.

(b) The increase of pressure with decreasing radius is very small until the axis is approached.

Now let's look at the second example which was chosen to avoid a shock wave.

The characteristics for the second case are shown in Figure 52. Increasing the spacing of the waves did not completely avoid a shock wave. A normal shock extends from points 13 and 14 to the axis.

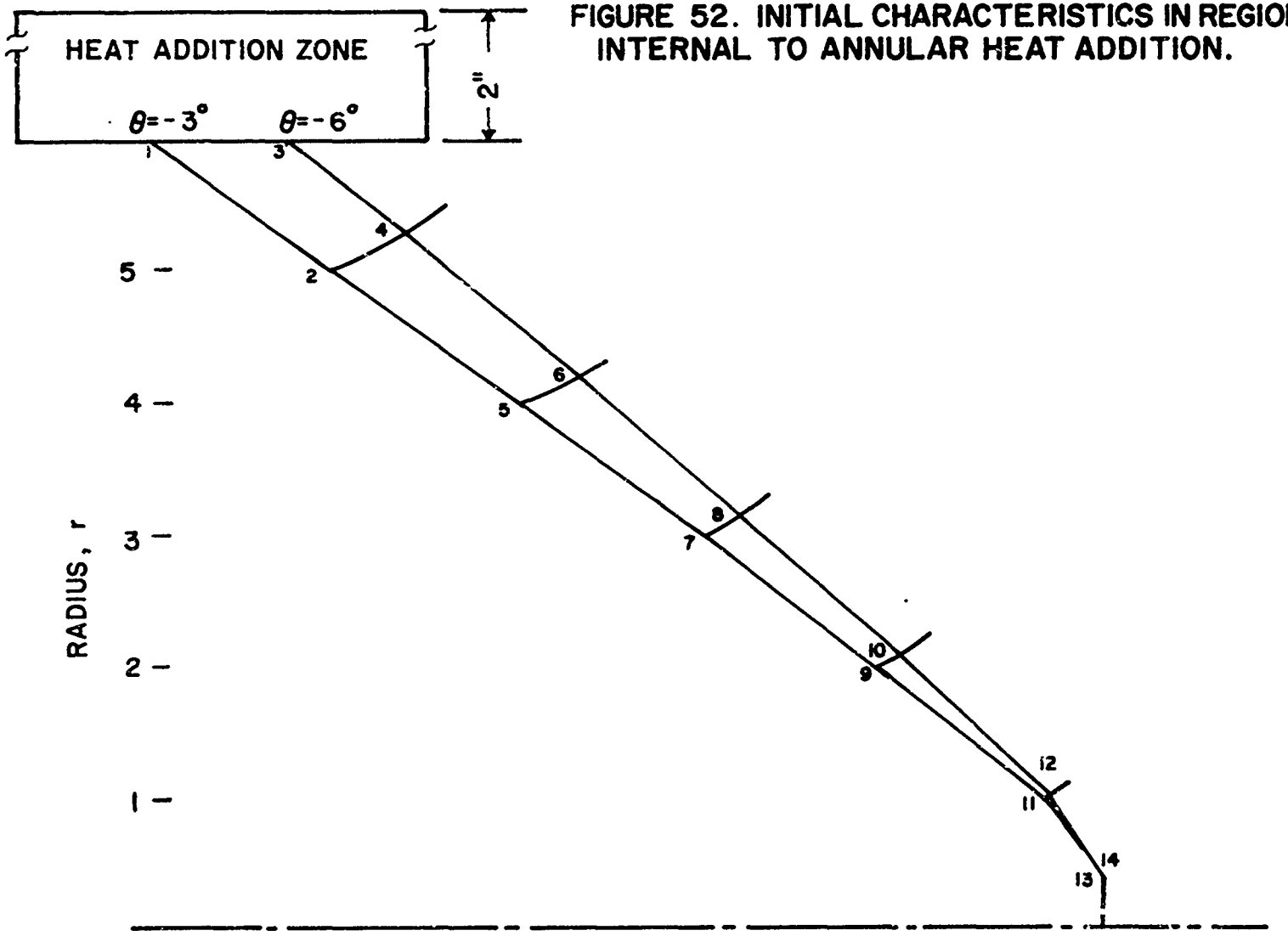

FIGURE 52. INITIAL CHARACTERISTICS IN REGION INTERNAL TO ANNULAR HEAT ADDITION.

The pressure as a function of radius is shown in Figure 53 for the mid-wave (wave starting at r = 6 with $\theta = -3^{\circ}$) and the terminal wave (wave starting at r = 6 with $\theta = -6^{\circ}$). As before in the previous example, the pressure does not increase significantly until very close to the axis. This is true for both the mid-wave and the terminal wave. The pressure is shown as a dash-dot-dash line between point 14 and the axis since this was not calculated in detail.

Figure 54 gives information about the streamlines and flow deflection. Right on the axis, of course, the streamline is the axis. There is large turning near the axis giving small radius of curvature for the streamline. This balances the large radial pressure gradient near the axis.

The conclusions from the second case are the same as the first case.

Preliminary Comments Based on a Cursory Look at Axisymmetric Case

The change in base drag is given by

$$\Delta D_b = \Delta p_b A_b \tag{153}$$

Each of the two terms, Δp_b and A_b, will now be discussed. The results shown in Figures 51, 52, and 53 suggest that Δp_b may not be increased significantly as a direct result of changing geometry from planar to axisymmetric. However, the results shown in Figures 51, 52, and 54 more closely apply to pressure at the dividing streamline and not to base pressure. The flow in the base region may magnify the pressure, just as the initial pressure due to heat addition at r = 6 is increased slightly due to axisymmetric geometry.

Compression originating with the heat addition will be reflected at the sonic line. See Figure 48 and point (A) of Figure 55. These compression waves will be reflected from the wake of the heat addition zone; see point (B) of Figure 55. The reflection may be negative, i.e., changing the compression waves to expansion waves. This negative reflection would not be favorable.

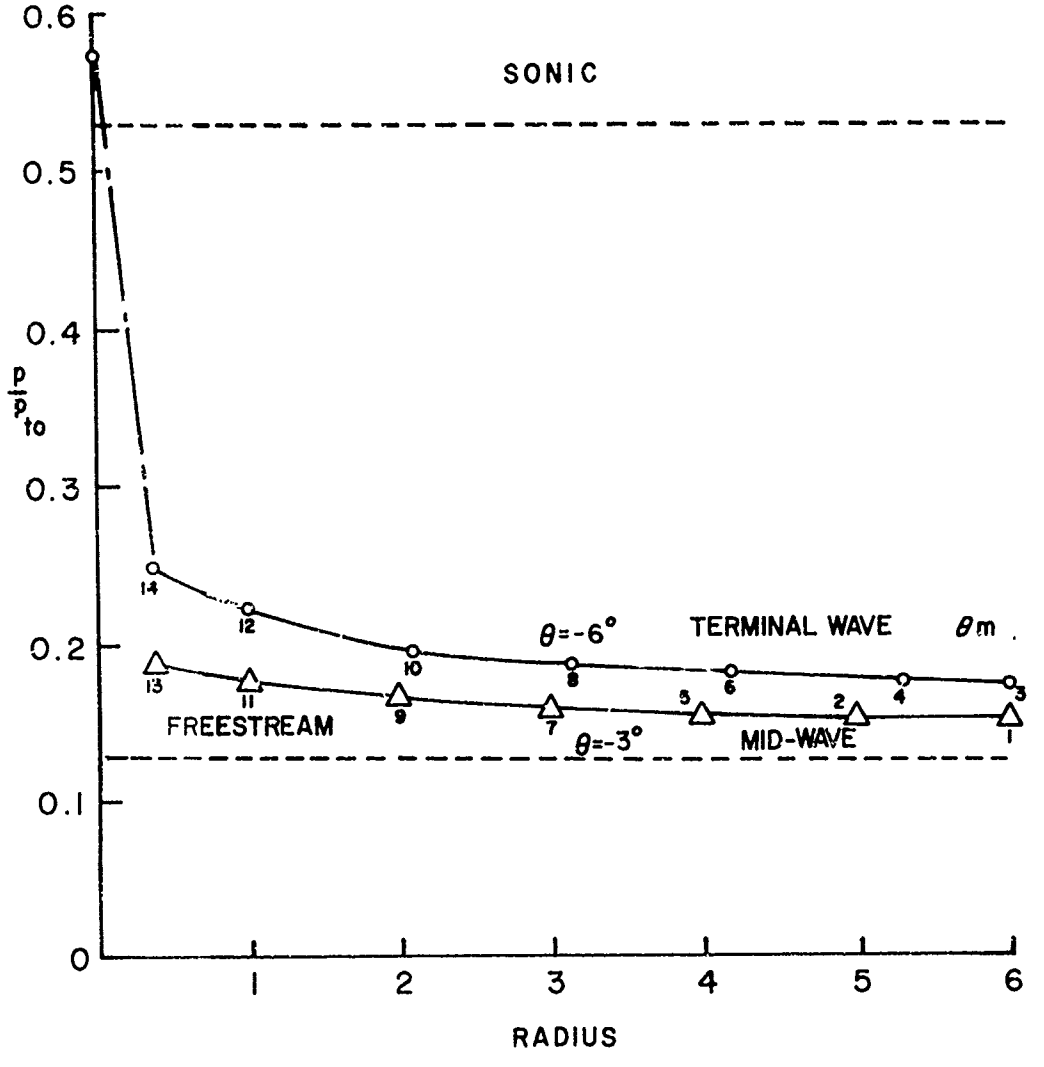

FIGURE 53. PRESSURE DISTRIBUTION ALONG CHARACTERISTICS OF FIGURE 52.

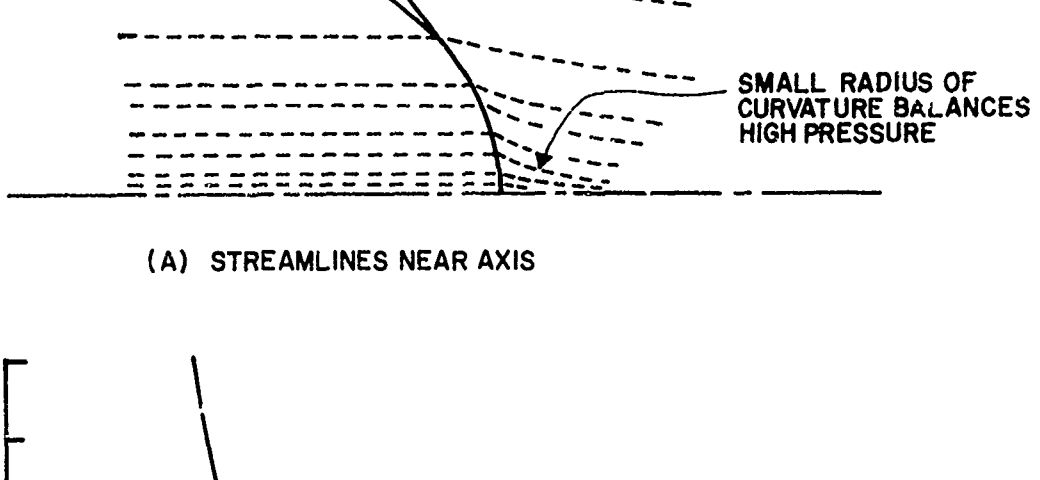

(A) STREAMLINES NEAR AXIS

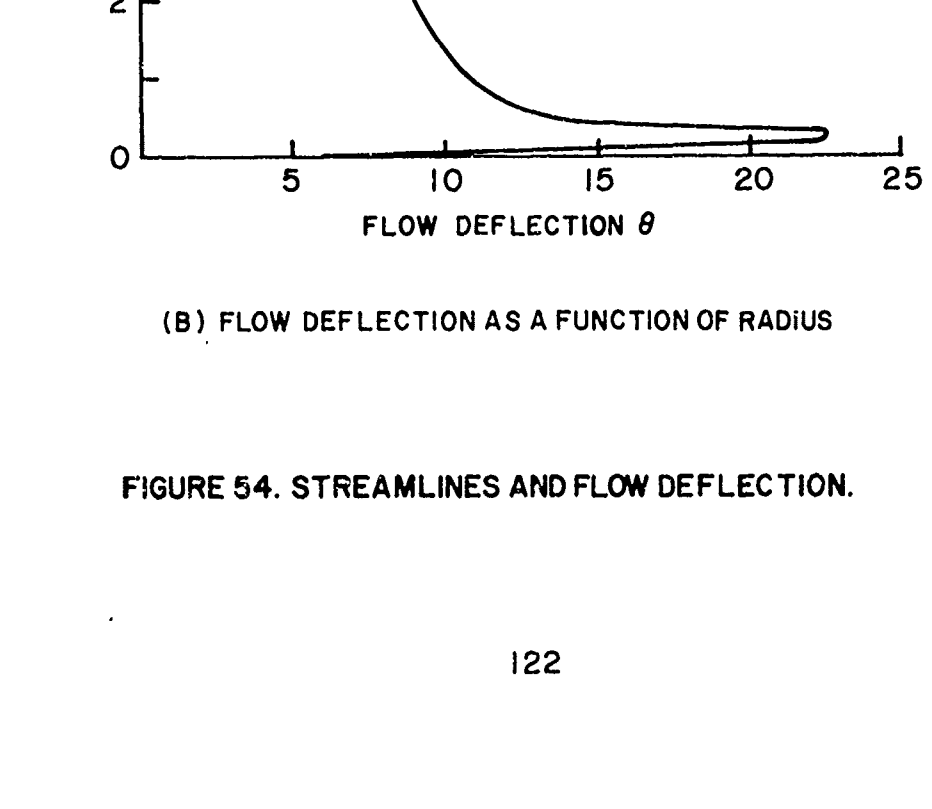

(B) FLOW DEFLECTION AS A FUNCTION OF RADIUS

FIGURE 54. STREAMLINES AND FLOW DEFLECTION.

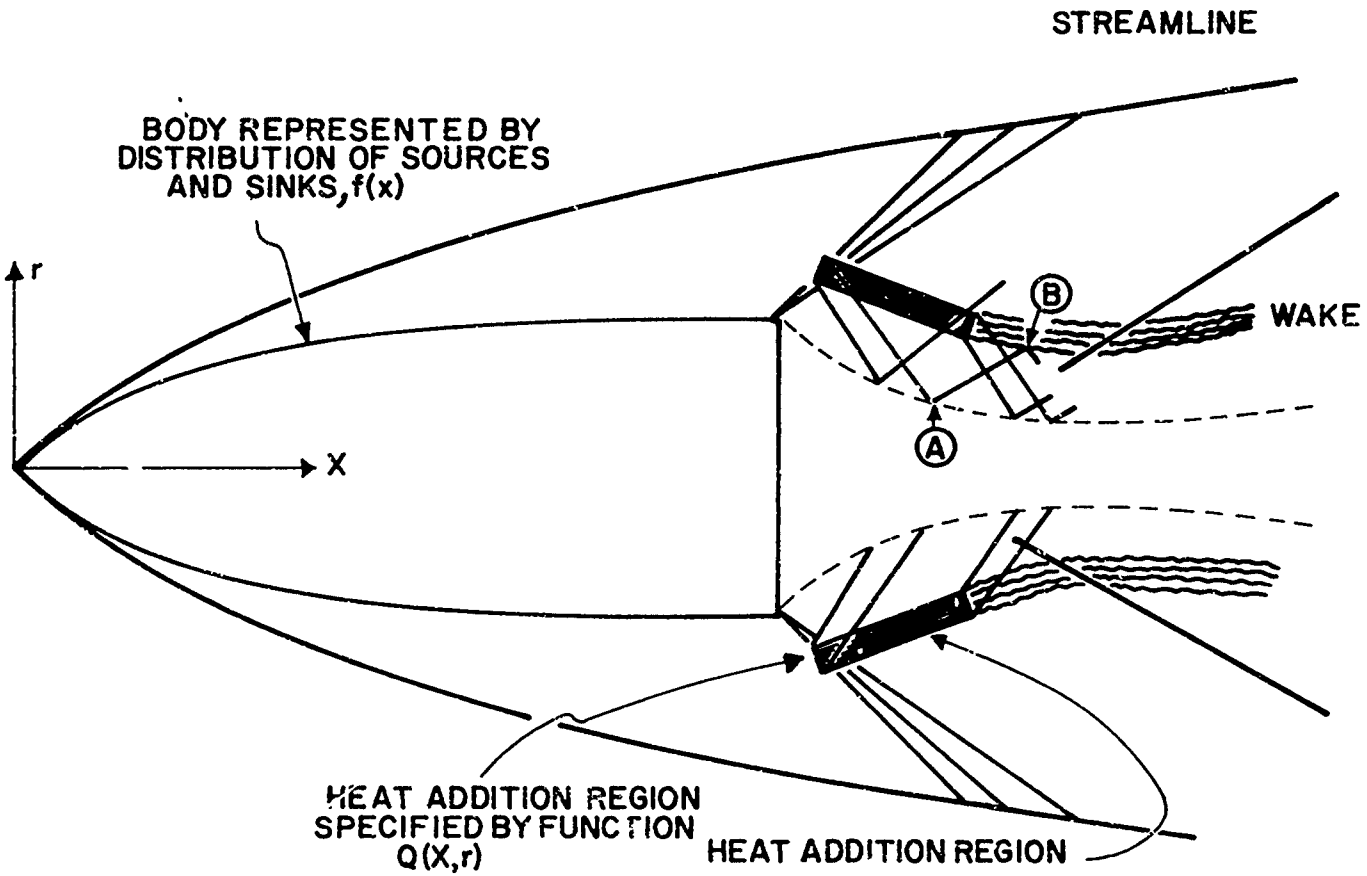

FIGURE 55. BASE PRESSURE INCREASE DUE TO HEAT ADDITION.

Now let's look at the area term. Consider the same amount of heat, Q, released in both planar and axisymmetric case. In the axisymmetric case, Q is distributed along a circle of radius r_2 giving $A/2\pi r_2$, BTU/length sec. In the planar case, Q is distributed along two lines of length πr_2. One line is at the top, and the other at the bottom. See Figure 56. For the planar case, the heat release is $Q/2\pi r_2$, BTU/length sec, which is identical to the axisymmetric case. The area influenced by the heat release is in the ratio

$$\frac{\text{base area; axisymmetric case}}{\text{base area; planar case}} = \frac{\pi r_1^2}{2\pi r_1 r_2} = \frac{r_1}{2r_2} \tag{154}$$

Making r_1/r_2 small helps increase pressure at r_1 due to heat addition; see Figure 56. Making r_1/r_2 large makes the base area very small in axisymmetric case as compared to the planar case. One factor helps; the other hurts.

As a final remark, it should be stated again that these are preliminary thoughts and conclusions.

Spin Recovery Wing Heat Addition

Some modern fighter and attack aircraft can be flown into spins of such nature that special equipment is needed for recovery. The drag parachute may be deployed to lift the aircraft tail. Before normal flight is restored, the parachute must be jettisoned. An alternate method of obtaining a torque on the aircraft would be heat addition. Figure 57 illustrates a modern fighter in a spin. The engines run normally and produce thrust. By spraying fuel into the exhaust stream, the heat addition deflects the jet downward. A torque is developed which tends to lift the tail. Let's compare a parachute recovery with heat addition.

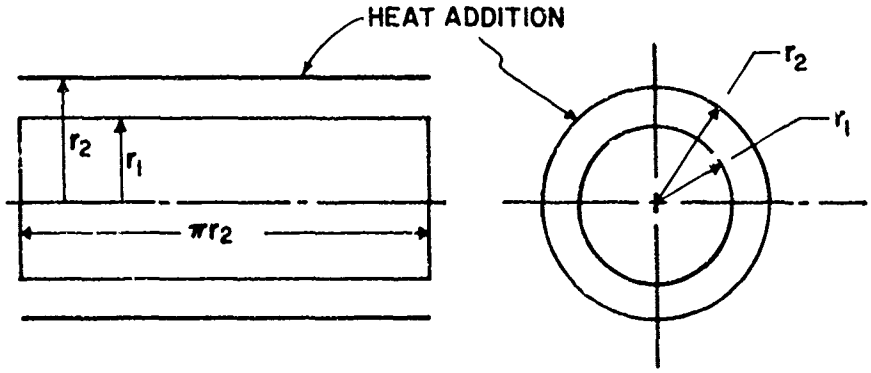

FIGURE 56. COMPARISON OF BASE AREA FOR PLANAR AND AXISYMMETRIC GEOMETRY.

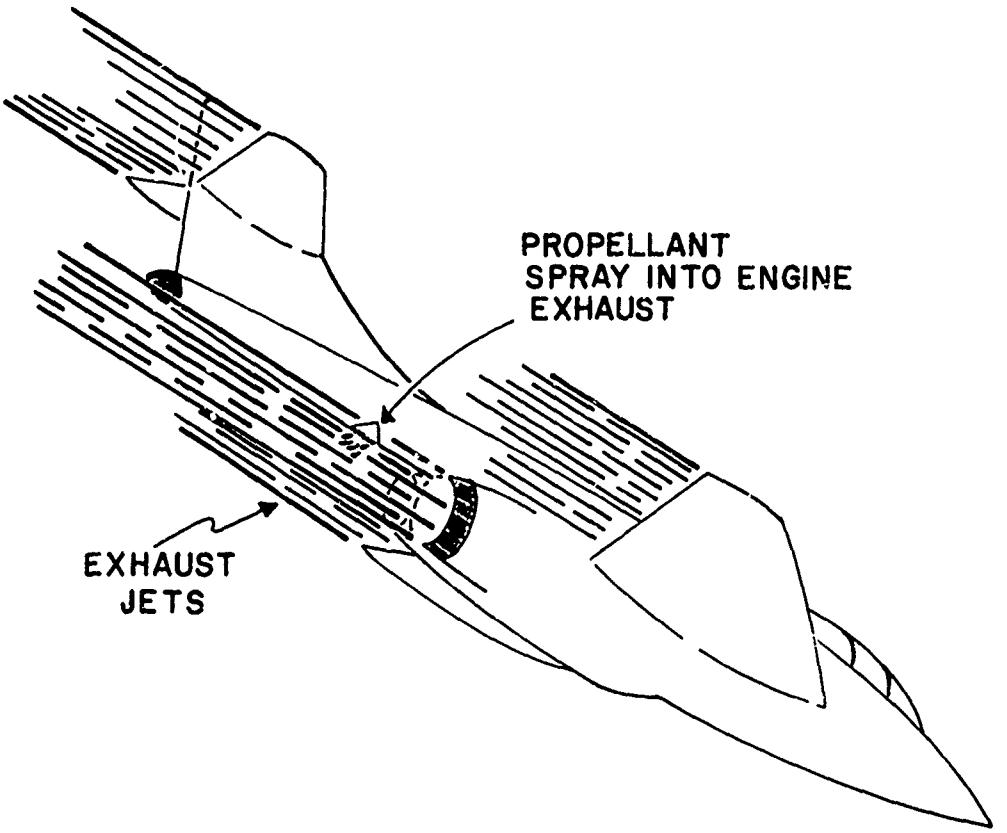

FIGURE 57. SPIN RECOVERY USING HEAT ADDITION.

Assume the aircraft has a moment of inertia of 6×10^6 lb ft^2 about the pitch axis. Assume the installed thrust is 35,000 lb with afterburner. If the flow can be deflected by 6° with heat addition, the force tending to lift the tail is 4000 lb. If the aircraft has a moment arm of 22 feet, the restoring torque is 8.8×10^4 lb ft. Time required to point the aircraft downward, i.e., turn 90° in pitch, is

$$t = \sqrt{\frac{\pi I}{T}} = 46 \text{ sec}$$

If the sink rate is 140 ft/sec, the recovery altitude is 6400 ft.

One can estimate the amount of heat to be added for a deflection of 6° using Equations (119) through (129). The temperature of exhaust must be increased by 30 per cent.

Now consider a parachute of 10 ft diameter with a drag coefficient of 2. The drag at a sink rate of 140 ft/sec will be

$$D = \frac{1}{2}\gamma p M^2 A C_D = 4200 \text{ lb}$$

This is comparable to the force due to thrust deflection. Performance of parachute and heat addition is comparable.

SUMMARY AND CONCLUDING DISCUSSION

Use of an area rule or quasi area rule implies optimization. The area rule can be used to translate an optimum axisymmetric body, e.g., von Karman ogive, to a three-dimensional body. The optimum axisymmetric body shape is found by application of the calculus of variations to the source distribution function, $f(x)$. When there is heat addition, there is a new function to optimize, $Q(x,r)$; see Figure 55. Both $f(x)$ and $Q(x,r)$ must be simultaneously optimized. The

axisymmetric, small perturbation, solution for heat addition has never been obtained; it is an essential building block of the quasi area rule.

When the body develops lift with aerodynamic circulation, there is another complexity to the analysis. Vorticity due to lift must be included in the analysis. There may be an optimum balance between lift generated aerodynamically and lift generated by heat addition.

To apply the optimization technique to turbojets, ramjets, or other internally burning, air breathing, engines, a different analytical technique is required. A combined thrust-drag technique was briefly introduced. This method uses an energy disc.

By discussing both one-dimensional and two-dimensional, planar, heat addition, the connection between heat fronts, combustion fans, and one-dimensional heat addition was demonstrated. Heat addition in the planar case may be represented either by line sources or by a volume distribution function, $Q(x,r)$. In several ways heat addition is similar to the flow generated by a solid body. The pressure on the flat plate of Figure 32 is the same as that caused by a wedge of angle θ. Pressure and velocity perturbations are identical for both solid body and heat addition. Differences exist between flow over solid bodies and flow through a region of heat addition. One difference is drag.

There are three approaches to calculate thrust minus drag in an inviscid flow: integration of pressure over the body surface, momentum control volume, and wave drag. Integration of pressure is the most direct of the methods. Figures 22 and 27 illustrate the wave energy and momentum approaches for a thrusting, lifting, planar airfoil. Figures 20, 23, and 26 illustrate the wave and momentum approaches for an isolated heat addition zone in an infinite medium. The merit of a particular method depends on the geometry.

Applications of external burning include lifting, thrusting airfoils, base or boattail pressure modification for an exhaust, development of base thrust for projectiles, and spin recovery. External burning for airfoils and projectiles has been studied extensively both theoretically and experimentally. A new phenomenon occurs for the exhaust problem; this is wave trapping. A preliminary analysis indicates heat addition for spin recovery is comparable to use of a parachute.

REFERENCES

1. H. Ashley and M. Landahl, Aerodynamics of Wings and Bodies, Addison-Wesley Pub., Reading, Mass., 1965.

2. T. von Karman, "The Problem of Resistance in Compressible Fluids," GALCIT Publication No. 75, 1936. Also Collected Works of T. von Karman, Pergamon Press.

3. W. R. Sears, "On Projectiles of Minimum Wave Drag," Quarterly Journal of Applied Mathematics, 4, pp. 361-366, Jan., 1947.

4. H. Lomax and M. A. Heaslet, "Recent Developments in the Theory of Wing-Body Wave Drag," J. Aero. Sci., 23, pp. 1061-1074, 1956.

5. R. T. Whitcomb, "A Study of the Zero-Lift Drag-Rise Characteristics of Wing-Body Combinations near the Speed of Sound," NACA Report 1273, 1956.

6. L. I. Sedov, Similarity and Dimensional Methods in Mechanics, Academic Press, New York, 1959.

7. A. H. Shapiro, The Dynamics and Thermodynamics of Compressible Fluid Flow, Ronald Press, New York, 1953.

8. W. R. Sears, Editor, General Theory of High Speed Aerodynamics, Volume VI, Princeton Series on High Speed Aerodynamics and Jet Propulsion, Princeton Univ. Press, 1954.

9. A. H. Shapiro and W. R. Hawthorne, "The Mechanics and Thermodynamics of Steady, One-Dimensional Gas Flow," Journal of Applied Mechanics, 14, pp. A317-338, 1947.

10. H. S. Tsien and M. Beilock, "Heat Source in a Uniform Flow," J. Aeronautical Sciences, 16, p. 756, 1949.

11. K. Oswatitsch, "Thrust and Drag with Heat Addition to a Supersonic Flow," R. A. E. Library Translation No. 1161, January 1967, Great Britain.

12. L. H. Townend, "An Analysis of Oblique and Normal Detonation Waves," R. A. E. Technical Report No. 66081, March 1966, Great Britain.

13. K. Oswatitsch, Gas Dynamics, Academic Press, New York, 1956.

14. M. A. Heaslet and H. Lomax, "Supersonic and Transonic Small Perturbation Theory," Princeton Series on High Speed Aerodynamics and Jet Propulsion, Volume VI, Princeton University Press, 1954, pp. 141-142.

15. H. W. Liepmann and A. Roshko, Elements of Gasdynamics, John Wiley, New York, 1957.

16. F. S. Billig, "External Burning in Supersonic Streams," Technical Memorandum, TG-912, May 1967, The Johns Hopkins University, Applied Physics Laboratory.

17. Artur Mager, "Supersonic Airfoil Performance with Small Heat Addition," 26, pp. 99-107, 1959.

18. D. E. Harrington, "Performance of a 10^{o} Conical Plug Nozzle with Various Primary Flap and Nacelle Configurations at Mach Numbers from 0 to 1.97," NASA TM X-2086, Dec. 1970.

19. G. R. Rabone, "Low Angle Flug Nozzle Performance Characteristics," AIAA Propulsion Joint Specialists Conference. Flight Propulsion Division, General Electric Company, Cincinnati, Ohio.

20. A. Roberts, "External Burning Propulsion: A Review (U)," Indian Head Special Publication 71-79, 25 May 1971, Naval Ordnance Station, Indian Head, Maryland.

21. Warren C. Strahle, "Theoretical Consideration of Combustion Effects on Base Pressure in Supersonic Flight," Twelfth Symposium on Combustion, Combustion Institute, Pittsburgh, Pa., pp. 1163-1173, 1969.

22. H. L. Fein, Personal Communication.

23. A. Ferri, Elements of Aerodynamics of Supersonic Flows, MacMillan Co., New York, 1949.

24. A. Ferri, "Application of the Method of Characteristics to Supersonic Rotational Flow," NACA TN 1135, 1946.

BIBLIOGRAPHY

1. A. L. Addy, "Experimental-Theoretical Correlation of Supersonic Jet-on Base Pressure for Cylindrical Afterbodies," J. of Aircraft, 1, pp. 474-477, 1970.

2. G. Maise, "Wave Drag of Optimum and Other Boat Tails," J. of Aircraft, 7, pp. 477-478, 1970.

3. B. T. Chu, "Pressure Waves Generated by Addition of Heat in a Gaseous Medium," NACA, TN 3411, June 1955.

4. B. T. Chu, "Mechanism of Generation of Pressure Waves at Flame Fronts," NACA TN 3683.

5. J. Zierep, "On the Influence of the Addition of Heat to Hypersonic Flow," RAE Lib. Trans. No. 1222, 1967 April.

6. E. G. Broadbent and L. H. Townend, "Shockless Flows with Heat Addition in Two Dimensions," RAE TR 69284, Dec. 1969.

7. E. G. Broadbent, "A Class of Two Dimensional Flows with Heat Addition," RAE TR 68005, Jan. 1968.

8. L. H. Townend, "An Analysis of Oblique and Normal Detonation Waves," RAE TR 66081, March 1966.

9. I. I. Pinkel and J. S. Serafini, "Graphical Method for Obtaining Flow Field in 2D SFS Stream to Which Heat Is Added," NACA TN 2206, Nov. 1950.

10. J. Zierep, "The Ackeret-Formula for Supersonic Flows with Heat Addition," Unpublished Notes.

11. D. Rues, "Three-Front Configurations with Energy Addition," RAE Lib. Trans. No. 1260, Nov. 1967.

12. E. R. Whittley and H. Barrow, "A Study of the Effect of Space Variable Heat Release on Fluid Flow in a Duct," Paper 7, Thermodynamics and Fluid Mechanics Convention, Cambridge, 1964.

13. F. Bartlma, "Boundary Conditions in the Presence of Oblique Reaction Waves in Supersonic Flow," RAE Lib. Trans. No. 1358, April 1969.

14. G. G. Cheryni, "Supersonic Flow Past Bodies with Formation of Detonation and Combustion Fronts."

15. B. S. Baldwin, Jr., "An Optimization Study of Effects on Aircraft Performance of Various Forms of Heat Addition," NASA TN D-74, March 1960.

16. D. Rues, "Concerning the Equivalence Between Heat- Force- and Mass-Sources," RAE Lib. Trans, No. 1119, July 1965.

17. R. G. Dorsch, J. S. Serafini, E. A. Fletcher, and I. I. Pinkel, "Exp. Investigation of Aerodynamics Effects of External Combustion in Airstream below 2D SPS Wing at Mach 2.5 and 3.0," NASA Memo 1-11-59E.

18. J. Pike, "A Design Method for Aircraft Basic Shapes with Fully Attached Shock Waves Using Known Axisymmetric Flow Fields," RAE TR 66069, March 1966.

19. J. Zierep, "Transonic Flow with Heat Input," RAE Lib. Trans. No. 1452, Feb, 1970.

20. J. Zierep, "Similarity Laws for Flows Past Aerofoils with Heat Addition," RAE Lib. Trans. No. 1114, June 1965.

21. F. Lane, "Linearized Supersonic Theoretical Approximation to 3D Combustor Flow," GASL TR No. 544, July 1965.

APPENDIX - PROPERTIES OF DELTA FUNCTION

I $$\delta(x) = \begin{cases} 1 & x = 0 \\ 0 & x \neq 0 \end{cases}$$

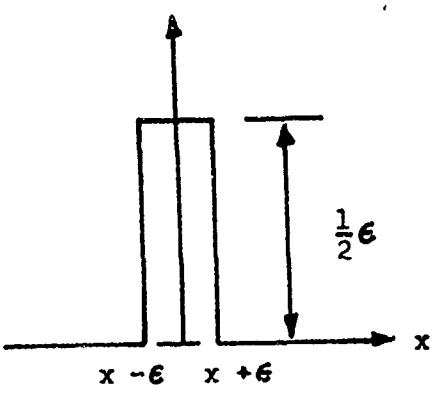

$$\int_{-\infty}^{\infty} \delta(x)dx = \lim_{\epsilon \to 0} \int_{x-\epsilon}^{x+\epsilon} \frac{1}{2\epsilon}\, dx$$

$$= \lim_{\epsilon \to 0} \frac{x+\epsilon}{2\epsilon} - \frac{(x-\epsilon)}{2\epsilon} = 1$$

II $$\int_{-\infty}^{\infty} f(x)\delta(x)dx = f(0)$$

$$\int_{-\infty}^{\infty} f(x)\delta(x-a)dx = f(a)$$

III Derivative of unit function

$$I(x) = \begin{cases} 1 & x > 0 \\ 0 & x < 0 \end{cases}$$

$$\frac{dI}{dx} = \delta$$

Proof g_1 and g_2 = positive number

$$d(fI) = fdI + Idf$$

$$FdI = d(fI) - Idf$$

$$\int_{-g_2}^{g_1} f(x)\frac{dI}{dx}dx = f(x)I(x)\Big|_{-g_2}^{g_1} - \int_{-g_2}^{g_1} I(x)f'(x)dx$$

$$= f(g_1) - \int_{0}^{g_1} f'(x)dx = f(g_1) - f(g_1) + f(0) = f(0)$$

IV $\quad \delta(x) = \delta(-x)$

V $\quad x\delta(x) = 0$

VI $\quad \delta(ax) = \frac{1}{a}\delta(x)$

Proof

$z = ax \qquad dz = adx$

$$\int_{-\infty}^{\infty} f(x)\delta(ax)dx = \frac{1}{a}\int_{-\infty}^{\infty} f(\frac{z}{a}\delta(z)dz = \frac{1}{a}f(0)$$

VII $\quad \left[\delta(x^2 - a^2)\right] = \frac{1}{2a}\left[\delta(x + a) + \delta(x - a)\right]$

Proof

$$\delta\left[f(x)\right] = \frac{1}{\left|\frac{df}{dx}\right|}\left[\delta(x - x_0) + \delta(x - x_1) + \delta(x - x_2) + \ldots\right]$$

$$\delta(x^2 - a^2) = \frac{1}{2x}\left[\delta(x + a) + \delta(x - a)\right]$$

$x_0, x_1, x_2 \ldots$ are roots of $f(x)$

VIII

$$\left[\delta(a - x)dx\right]\delta(x - b) = \delta(a - b)$$

Proof

$$\int f(a)\int\delta(a - x)dx\ \delta(x - b)da = \iint f(a)\delta(a - x)\delta(x - b)dadx =$$

$$= \int f(x)\delta(x - b)dx = f(b)$$

$$\int f(a)\delta(a - b)da = f(b)$$

Second Proof

$$\int f(b)\int\delta(a - x)dx\ \delta(x - b)db = \iint f(b)\delta(a - x)\delta(x - b)dbdx =$$

$$\int f(x)\delta(x - a)dx = f(a)$$

$$\int f(b)\delta(a - b)db = f(a)$$

IX $\quad f(x)\delta(x - a) = f(a)\delta(x - a)$

$$\int f(x)\delta(x - a)dx = \int f(a)\delta(x - a)dx = f(a)\int\delta(x - a)dx = f(a)$$

$$\int f(x)\delta(x-a)da = \int f(a)\delta(x-a)da = f(x)$$

X

$$\frac{df}{dx} = \int_{-\infty}^{\infty} \frac{d\delta(x-y)}{dx} f(y)dy$$

XI

$$\delta(x-x') = \frac{1}{2\pi}\int_{-\infty}^{\infty} e^{i\omega(x-x')}d\omega$$

XII 3D Delta Function

$$\delta(\vec{r}) = \delta(x)\delta(y)\delta(z) = \frac{1}{8\pi^3}\int e^{i\vec{k}\cdot\vec{r}}\, d^3k$$

$$\vec{r} = \vec{e}_x x + \vec{e}_y y + \vec{e}_z z$$

XIII $\nabla^2\left(\frac{1}{r}\right) = -4\pi\delta(r)$

$$\int \delta(r)dxdydz = 1 \qquad \delta(r) = \begin{cases} 0 & r \neq 0 \\ 1 & r = 0 \end{cases}$$

$$r = \sqrt{(x-x')^2 + (y-y')^2 + (z-z')^2}$$

XIV

$$\int_{-\infty}^{\infty} \cos\omega x d\omega = 2\pi\delta(x)$$

Equal in sense both behave same as factors in an integrand.

XV Generalized 2D δ-function

$$\int \delta(r - a)\delta(\phi - \alpha) r\,dr\,d\phi = 1$$

XVI $$\delta[f(x)] = \frac{1}{\left|\frac{df}{dx}\right|}\,\delta(x - x_0)$$

where $f(x_0) = 0$. Note $\delta(f)df = \delta(x)dx$

XVII Ways to represent δ function

$$\delta_\epsilon(x) = \begin{cases} \frac{1}{2\epsilon} & |x| \leq \epsilon \\ 0 & x > \epsilon \end{cases}$$

$$\delta_n(x) = \sqrt{\frac{n}{\pi}}\, e^{-nx^2}$$

XVIII

$$\delta[\phi(x)] = \sum_i \frac{1}{\phi'(a_i)}\,\delta(x - a_i)$$

$\phi(x) = 0$: a_i are roots of $\phi(x) = 0$. $\phi' = \frac{d\phi}{dx}$.

XIX $$\int_a^b \int_a^b \delta(x - y)\,dx\,dy = b - a$$

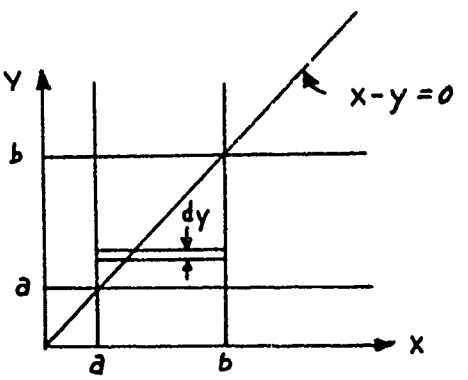

Proof

$$\int_a^b \delta(x - y)\,dx = 1$$

$$\int_a^b dy = b - a$$

XX
$$\int_c^d \int_a^b \delta(x - y)dxdy = \begin{cases} b - c & b > y > c \\ 0 & d > y > b \end{cases}$$

Proof

See diagram.

$$\int_c^d \delta(x - y)dy = 1 \quad \text{if} \quad b > y > c$$

$$\int_c^d \delta(x - y)dy = 0 \quad \text{if} \quad d > y > b$$

$$\int_c^d \int_a^b \delta(x - y)dxdy = \int_a^b dx = (b - c)$$